ELECTRIC POWER RESEARCH INSTITUTE

2010-009 BWR Vessel & Internals Project (BWRVIP)

January 12, 2010

Document Control Desk
U. S. Nuclear Regulatory Commission
11555 Rockville Pike
Rockville, MD 20852

Attention: Michael McCoppin

Subject: Project No. 704 – BWRVIP-216NP: BWR Vessel and Internals Project, BWR Reactor Pressure Vessel Embrittlement Correlation Studies

Enclosed are five (5) copies of the report "BWRVIP-216NP: BWR Vessel and Internals Project, BWR Reactor Pressure Vessel Embrittlement Correlation Studies," EPRI Technical Report 1019056, May 2009. This report is provided to the NRC for information only.

The enclosed report examines two candidate reactor pressure vessel (RPV) embrittlement correlations (developed through the U. S. Nuclear Regulatory Commission Office of Nuclear Regulatory Research) with special reference to their applicability to BWR surveillance data.

Please note that the enclosed report is non-proprietary and is available to the public.

If you have any questions on this subject please call Randy Schmidt (PSEG Nuclear, BWRVIP Assessment Committee Technical Chairman) at 856.339.3740.

Sincerely,

Rick Libra

Rick Libra
Exelon
Chairman, BWR Vessel and Internals Project

Together . . . Shaping the Future of Electricity

G004
NRR

Add'l copies sent to PM

ELECTRIC POWER
RESEARCH INSTITUTE

BWRVIP-216NP: BWR Vessel and Internals Project

BWR Reactor Pressure Vessel Embrittlement Correlation Studies

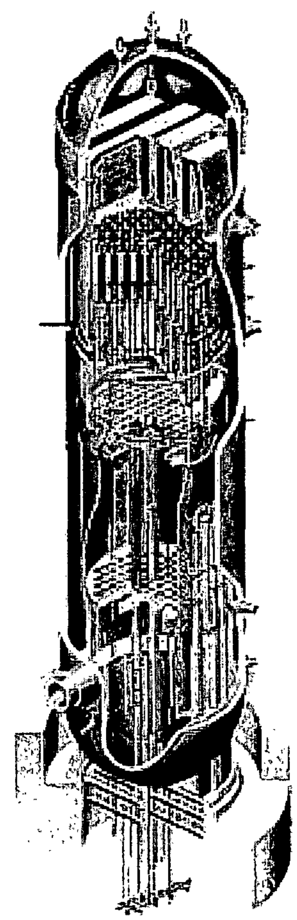

BWRVIP-216NP: BWR Vessel and Internals Project

BWR Reactor Pressure Vessel Embrittlement Correlation Studies

1019056

Final Report, May 2009

EPRI Project Manager
R. Carter

ELECTRIC POWER RESEARCH INSTITUTE
3420 Hillview Avenue, Palo Alto, California 94304-1338 · PO Box 10412, Palo Alto, California 94303-0813 · USA
800.313.3774 · 650.855.2121 · askepri@epri.com · www.epri.com

DISCLAIMER OF WARRANTIES AND LIMITATION OF LIABILITIES

ORGANIZATION(S) THAT PREPARED THIS DOCUMENT

National Nuclear Laboratory

ATI Consulting

NOTE

For further information about EPRI, call the EPRI Customer Assistance Center at 800.313.3774 or e-mail askepri@epri.com.

CITATIONS

This report was prepared by

National Nuclear Laboratory
168 Harwell International Business Center
Didcot, Oxon. OX11 0QJ
U.K.

Principal Investigators
S. Ortner
A. Fellerman
C. English

ATI Consulting
P.O. Box 5769
Pinehurst, NC 28374

Principal Investigator
W. Server

This report describes research sponsored by the Electric Power Research Institute (EPRI) and its BWRVIP participating members.

The report is a corporate document that should be cited in the literature in the following manner:

BWRVIP-216NP: BWR Vessel and Internals Project, BWR Reactor Pressure Vessel Embrittlement Correlation Studies. EPRI, Palo Alto, CA: 2009. 1019056.

REPORT SUMMARY

This report examines two candidate reactor pressure vessel (RPV) embrittlement correlations (developed through the U.S. Nuclear Regulatory Commission [NRC] Office of Research) with special reference to their applicability to BWR surveillance data.

Background

The structural integrity of RPVs in U.S. light water reactors (LWRs) is assessed with input from NRC Regulatory Guide (RG) 1.99, Revision 2, "Radiation Embrittlement of Reactor Vessel Materials." This RG includes an embrittlement correlation describing the rate of increase of the ductile-to-brittle transition temperature of an RPV steel as a function of irradiation conditions (such as neutron fluence and irradiation temperature) and material properties (such as composition and product form). The NRC is planning to issue a new revision of RG 1.99. Since the publication of Revision 2, there has been an increase in the mechanistic understanding of RPV embrittlement and a large increase in the amount of LWR surveillance data. The revision will, therefore, contain a better-informed embrittlement correlation than the current version. At present, two main candidate correlations are being considered for inclusion, and both have been found to describe the data in the U.S. LWR surveillance database well. These two correlations were derived as input for probabilistic fracture mechanics work focused on PWR pressurized thermal shock concerns. The database is, however, dominated by data from PWRs, and it appeared possible to the Electric Power Research Institute (EPRI) that data from BWRs might be less well described than data from PWRs.

Objectives

- To compare and contrast two candidate RPV embrittlement correlations from a mechanistic and statistical perspective
- To identify potential improvements to the embrittlement correlations through statistical analyses

Approach

The project team assessed the candidate embrittlement correlations based on a mechanistic understanding of the embrittlement process derived from information in the literature and on key information gained in the EPRI-Central Research Institute of the Electric Power Industry (CRIEPI) jointly-funded research program into microstructural effects in RPV embrittlement. The team used the U.S. LWR reactor embrittlement database as input to the evaluation. Statistical analysis of the surveillance data was conducted using modifications to the candidate embrittlement correlations to ascertain whether improvements in the fits to the data could be achieved. The error surface may contain many local minima or regions of minimal slope, making it difficult to reach the global minimum in error space.

Results

When the database is considered as a whole, the correlations examined provide good descriptions of the U.S. LWR surveillance database. However, they under-predict the data at low fluxes or low levels of copper precipitation. Because these are the conditions of typical BWR surveillance data, the correlations are not optimal for assessing the condition of BWR RPVs. The causes of biases were investigated and are most likely related both to the presence of a dose rate term in the matrix damage or matrix feature components of the correlations and to an absence of a dose rate term in the copper precipitation components. It might be useful to replace the current symmetric fluence functions with an asymmetric function. These premises require further investigation; statistical analysis shows that the candidate correlations are equations with complex distributions of errors.

EPRI Perspective

The results from this study reveal that the candidate correlations provide good descriptions of the U.S. LWR surveillance database—when the database is considered as a whole. However, these correlations are limited in accurately predicting BWR embrittlement trends. This highlights the importance of using the most up-to-date microstructural understanding to provide the starting conditions and the most suitable statistical techniques to optimize the embrittlement correlations. It is recommended that a new correlation, with adjusted flux functions, be attempted. Such a correlation should be applicable to both BWR and PWR data and be more likely to permit extrapolation to higher fluences. In addition, given the complex nature of the equations, it is also recommended that more sophisticated statistical fitting methods be used.

Keywords

Radiation embrittlement
Reactor pressure vessel integrity
Reactor vessel surveillance program
Embrittlement correlation models
Dose rate effects

ABSTRACT

The forms of two recent radiation embrittlement correlations (developed through the NRC Office of Research) have been examined. The two correlations (termed Eason et al. and EricksonKirk) are slightly different but each appeared generally well-justified on mechanistic grounds. There were minor characteristics of each correlation which appeared only weakly justified, such as flux terms in both the matrix damage (MD) and Cu-rich precipitation (CRP) components of embrittlement, the form and location of the temperature dependence, and the reduced number of product form terms in one of the correlations. From a mechanistic point of view, none of these aspects are strongly problematic, and it appeared likely that they were statistically justifiable on the grounds of the particular characteristics of the LWR surveillance database (i.e. small ranges of certain parameters such as irradiation temperature, or correlations between parameters related to Cu and P contents).

Comparison between the measured and predicted shifts, and statistical refitting of the data revealed the following:

- Both correlations provide good descriptions of the U.S. LWR surveillance database, when the database is considered as a whole. When the database is broken down into sub-sets according to the flux or to the CRP fluence function (i.e. to the fraction of CRPs precipitated), then sub-sets are observed in which the correlations provide less accurate predictions of the data.
- The correlations under-predict the data at low fluxes or low levels of precipitation.
- The database as a whole, and the PWR sub-set of the data, are dominated by data at medium-to-high fluxes, or high values of the fluence functions. The effect of the under-predictions of the low-flux or low-precipitation data is to increase the scatter observed in the predictions of these data.
- Since the typical BWR surveillance data correspond to low fluxes and low CRP generation levels, none of the correlations are optimal for assessing the condition of BWR RPVs.
- The assessment showed little intrinsic difference between BWR and PWR surveillance data in the applicability of the correlations. Where PWR and BWR data fall in the same flux-fluence ranges, the bias tends to be similar for the two reactor types.
- The causes of the biases were investigated, and it is most likely that they are related to the presence of a dose rate term in the MD or matrix feature components of the correlations, and an absence of a dose rate term in the Cu precipitation components. It is also possible that it would be useful to replace the current symmetric fluence functions with an asymmetric function. These premises require further investigation.

- Statistical analysis shows that the candidate correlations are equations with complex distributions of errors. The error surface may contain many local minima or regions of minimal slope, so that reaching the global minimum in error space is difficult. The local minimum to which a statistical analysis tends depends strongly on the starting values chosen for different parameters and functions, and on the algorithms used to minimize the errors.
- If an inappropriate term is introduced, then the depth of the local minimum may be such that it is not straightforward to remove the term.
- This highlights the importance of using the most up-to-date microstructural understanding to provide the starting conditions, and the most suitable statistical techniques to optimize the embrittlement correlations.

It is possible to re-parameterize the correlations such that they describe the BWR data better. Such re-parameterized correlations do not describe the PWR data well, and do not address the flux problem. Since no difference was observed between BWR and PWR data, re-parameterization is not the preferred way forward. It is recommended that a new correlation be attempted, with adjusted flux functions. Such a correlation should be applicable to both BWR and PWR data, and be more likely to permit (moderate) extrapolation to higher fluences. In addition, given the complex nature of the equations it is also recommended that the use of more sophisticated statistical fitting methods be used.

CONTENTS

LIST OF FIGURES

LIST OF TABLES

1 INTRODUCTION

The integrity of the reactor pressure vessel (RPV) is vital for the safety of nuclear power plant. Exposure of RPV steels to neutron radiation, however, degrades their fracture resistance. As a consequence, surveillance programs are put in place whereby samples of RPV steel are exposed to a similar neutron flux to that experienced by the RPV itself. Selections of samples are then withdrawn periodically and their mechanical properties tested. In the absence of any other information, the mechanical properties of the surveillance samples would be compared with the properties required for structural integrity, plus a safety margin, and the vessel assessed for continued operation. Such direct comparisons require a very large amount of surveillance material or a large safety margin. It is preferable to compare the measured embrittlement with that predicted by a well-founded model, or with the rate of embrittlement shown by similar materials in the past. The correlations between embrittlement and neutron exposure may then be used to assess the remaining safe operational life of the RPV.

In the case of pressurized water reactors (PWRs) and boiling water reactors (BWRs), the similarity of construction of a large number of vessels has permitted the accumulation of a large amount of related surveillance data, the statistical analysis of which has been used to develop embrittlement correlations suited to the condition monitoring of their RPVs. Over the period of operation of these light water reactors (LWRs), the understanding of the mechanisms of radiation embrittlement of RPV steels has developed such that the correlations may be mechanistically-informed rather than purely statistical in nature. This aspect of the correlations is of particular value when they must be used to extrapolate to conditions beyond the maximum and minimum values of the database (e.g. high fluences and low fluxes). A number of different mechanistically-guided correlations have been developed, based on statistical analysis of the LWR surveillance databases existing at different times.

A short overview, summarizing the historical development of such correlations within the U.S., is given in Section 1.1. At present, two new correlations have been proposed for use in U.S. RPV safety assessments. The aim of the work described in this report is to evaluate the applicability of these correlations to BWR safety assessments. The methods used to consider the candidate correlations are described in Section 1.2.

1.1 Historical Overview of U.S. Embrittlement Correlations

The radiation embrittlement of RPV beltline materials is currently assessed according to the U.S. Nuclear Regulatory Commission (NRC) Regulatory Guide 1.99, Revision 2 [1] (RG1.99, Rev. 2), which dates back to the 1980s. This Guide presents methods for estimating the shift in the ductile-to-brittle transition temperature (DBTT) and the drop in the Charpy upper shelf energy (USE). It incorporates a correlation between the Charpy shift (DT) and the irradiation fluence (ϕt, as defined for neutron energies greater than 1 MeV), which was derived statistically from a database containing fewer than 170 surveillance data points. The embrittlement correlation in RG1.99, Rev.2 allows for three material parameters to affect the rate of embrittlement with neutron fluence: material type (base metal or weld), copper (Cu) content and nickel (Ni) content. The same equation for estimating the mean shift in irradiated Charpy properties was historically used in the ASTM Standard Guide for Predicting Neutron Radiation Damage to Reactor Vessel Materials (E 900-87) [2].

Significant additional Charpy V-notch DBTT shift data have been generated since RG1.99, Rev. 2 and ASTM E 900-87 were issued. In addition, much information has been published from materials test programs which have enhanced mechanistic understanding of the microstructural changes leading to embrittlement. As a result, a number of newer correlations have been developed and proposed as improvements to RG1.99, Rev. 2. An embrittlement correlation (Eason, Wright and Odette, EWO) was developed under NRC sponsorship, and published in 1998 as NRC report NUREG/CR-6551 [3]. This correlation is based on a mechanistically-guided, statistical regression analysis of the database consisting of 752 shift measurements of which 80 to 90 were from BWR surveillance capsules. The EWO model was then used as the basis for further updated and/or simplified models by its own authors [4] (referred to as the draft NRC2000 model, since it was not formally published as an NRC report) and by workers sponsored by the Electric Power Research Institute (EPRI) [5]. The EPRI simplified model was approved by ASTM E10 and published as an ASTM Standard (E900-02) [6, 7].

The databases used to develop correlations subsequent to RG1.99 comprised surveillance data acquired up to 2000, and contained far more data from PWRs than from BWRs. The correlations were, naturally therefore, optimized against predominantly PWR data. In 2003, the BWR Integrated Surveillance Program (ISP) [8] produced 62 additional BWR data points. These points included low-flux, low-fluence data from the EPRI-Central Research Institute of the Electric Power Industry (CRIEPI) jointly-funded research program [9] which expanded the BWR database sufficiently that it became possible to assess whether the BWR surveillance data were as well-predicted by the (old and new) correlations as the PWR data. Assessments [10, 11, 12] showed that the BWR data were not predicted well by the correlations based on PWR-dominated data. In particular, the embrittlement shifts of the BWR materials tended to be under-predicted by both E900-02 and the draft NRC2000 models, especially at high measured shifts (DT>~50°C) and high Cu contents. The concurrent expansion of the PWR surveillance database showed that the embrittlement of the low-fluence PWR materials also was not well-predicted.

As a result, the NRC funded additional work to produce improved correlations, which was intended to describe both PWR and BWR data more effectively. One correlation has been published by workers at Oak Ridge National Laboratory [13] (Simplified NRC2006 or sNRC2006), and another has been drafted by EricksonKirk at the NRC [14] (RM6-2 and RM9). The database used for these correlations contained the additional BWR data as indicated above and additional PWR data obtained through about 2004.

The work described in this report uses the same database as sNRC2006 and EricksonKirk with the addition of 24 ISP BWR data values and updated fluxes and fluences for some of the other ISP BWR data sets.

1.2 Objective of this Report

The object of this report is to evaluate the latest embrittlement correlations (sNRC2006 [13] and RM6-2 [14]). The evaluation is in two parts: First the forms of the correlations are considered relative to our best understanding of embrittlement mechanisms; then the quantitative agreement between the correlations and surveillance data is assessed.

The mechanistic evaluation (Chapter 4) will make particular use of the insights into RPV embrittlement mechanisms derived from the EPRI-CRIEPI jointly-funded research program [9, 15, 16, 17, 18, 19, 20, 21, 22, 23, 24, 25, 26] (summarized in Chapter 3). The data used for the statistical assessment will include the PWR-BWR surveillance database published within [13], and also more recently-acquired BWR data (described in Chapter 2). The expansion of the surveillance database and production of this BWR-only database forms part of the assessment program. The statistical assessment (Chapters 5 and 6) is carried out with respect to both the expanded PWR-BWR database and the BWR-only data set.

The report then clarifies the extent to which the latest models require modification to improve their mechanistic plausibility and their applicability to BWR surveillance data. Recommendations for future progress are given in Chapter 7.

1.3 Implementation Requirements

This report is provided for information only. Therefore, the implementation requirements of Nuclear Energy Institute (NEI) 03-08, Guideline for the Management of Materials Issues, are not applicable.

2 DESCRIPTION OF DATABASE

The data used in this assessment comprise mainly those described in Appendix C (Analysis Data Base) in [13], in which the Excel spreadsheet containing the data is described as "TTSDatabase8_04R1.xls"[1]. The development and history of this database is described in detail in [13]. It contains 704 data points from PWR surveillance schemes and 151 points from BWR schemes. Of the BWR surveillance samples, most were irradiated in typical surveillance positions, but some were irradiated in atypical locations, such as within the core shroud, giving higher (and less well characterized) irradiation temperatures and fluxes. In accordance with the usage developed in [13], the BWR data discussed in this report will be divided into the typical and atypical categories, with the atypical data being further subdivided into BWRa and BWRb categories. The BWRa samples come from the Big Rock reactor, in which they were irradiated at ~299°C (570F), while the BWRb samples come from Dresden-2 and -3 and Quad Cities-1 and -2 plants, in which they were irradiated at 286°C (546F). Typical BWR samples were irradiated at 275-279°C (527-534F).

Of the typical BWR specimens in TTS8-04R1, 60 were irradiated at Oyster Creek as part of the BWRVIP SSP program (Capsules D, E, F, G, H and I). During the present assessment, the neutron flux and fluence values for these specimens were updated. This involved only minor changes to the values in the database. The database used in the present assessment was also expanded by the inclusion of 24 additional typical BWR data points from specimens irradiated in the Cooper plant (Capsules A, B and C) as part of the BWRVIP ISP program.

Figure 2-1 shows the flux and fluence distributions in the database used in the current assessment. (There is some superposition of points in these graphs as some irradiation capsules contained a variety of steel compositions or product forms.) It shows that the BWR SSP data from Cooper plant generally increase the number of typical BWR data points, while the SSP data from Oyster Creek also extend the range of the typical BWR data so that there is some overlap with the lowest fluence PWR data. In general, however, the typical BWR data lie to lower fluxes and fluences than the PWR data. There is also overlap between the atypical BWRa and BWRb data and the PWR data, this time at the highest fluxes and fluences. The BWRa data include the highest fluxes and fluences of the entire data set.

Figure 2-2 shows the fluence and irradiation temperature distributions in the database. The typical BWR data lie at the low end of the temperature range shown by the PWR samples. The BWRb data lie within the PWR temperature range and the BWRa data lie within and above the PWR range.

[1] This database will be referred to as TTS8-04R1 in the remainder of the report.

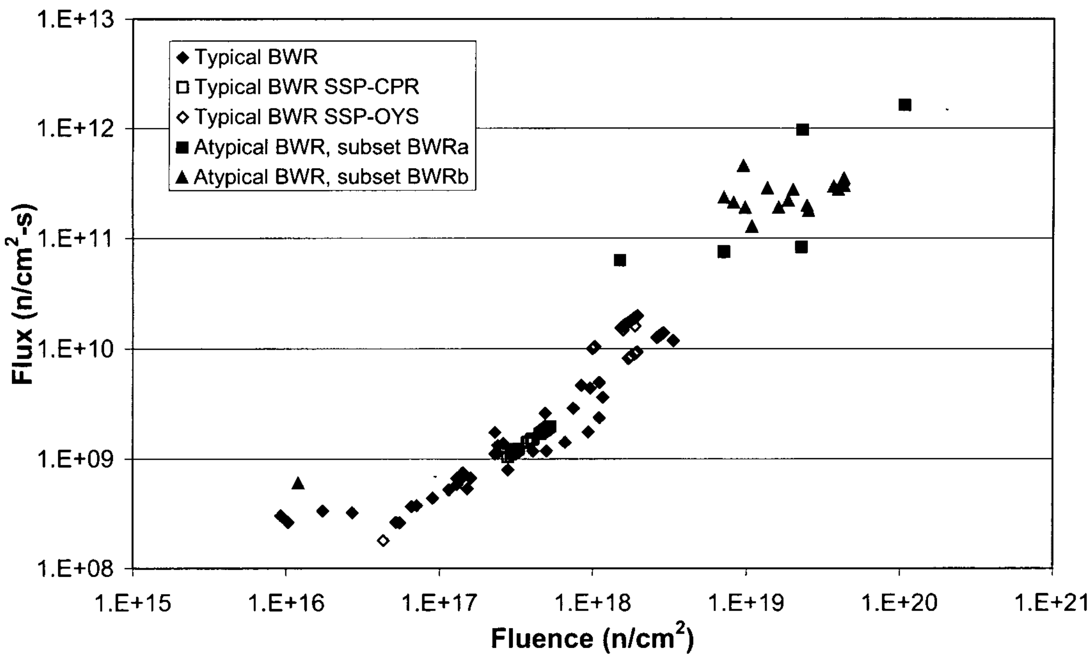

a) BWR data

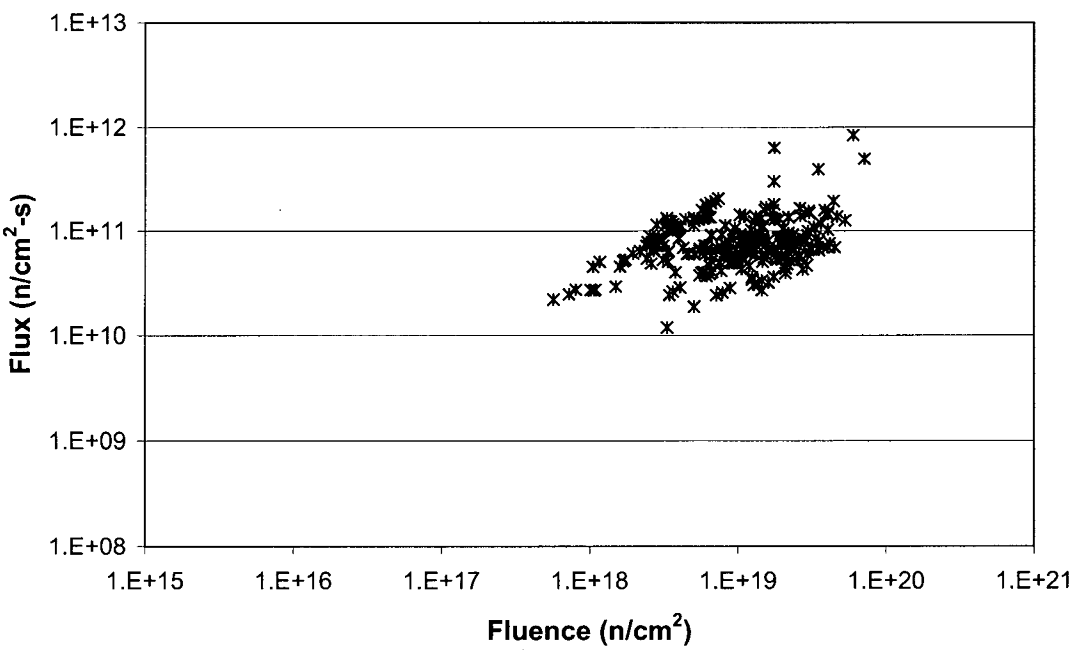

b) PWR data

Figure 2-1
Flux and fluence distributions in database used in this assessment

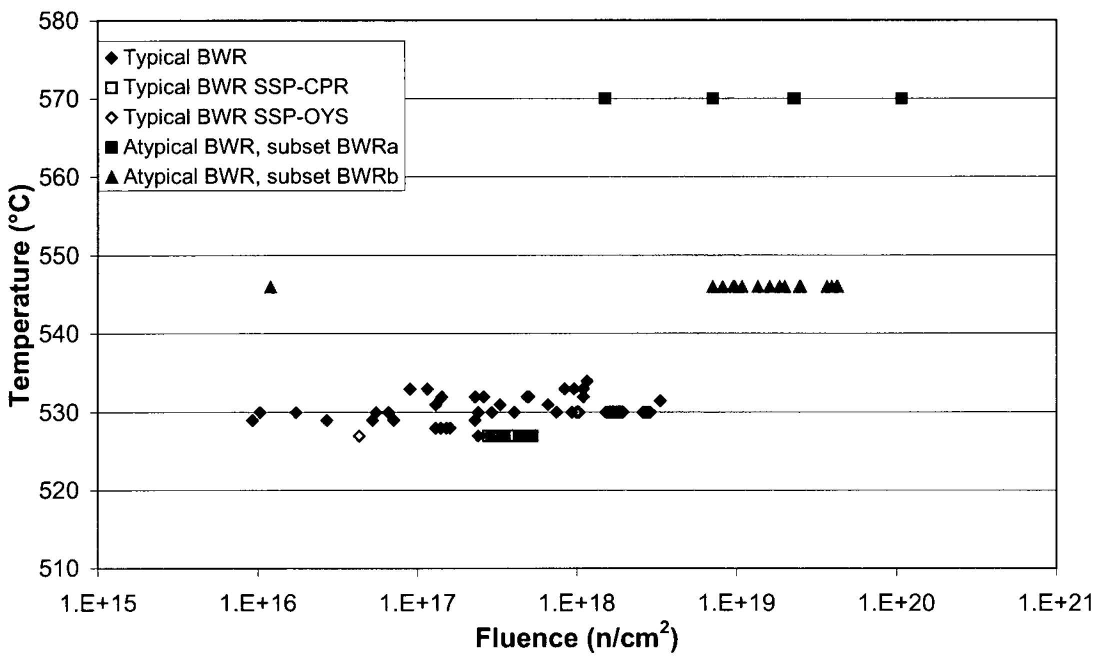

a) BWR data

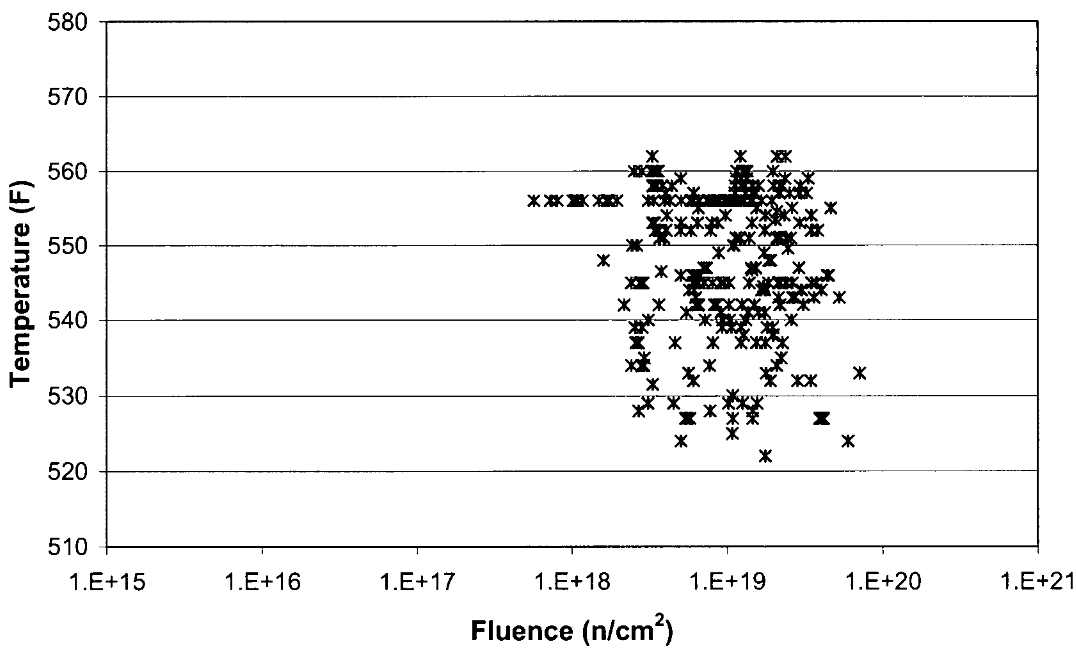

b) PWR data

Figure 2-2
Temperature and fluence distributions in database used in this assessment

The overall data distributions are plotted in Figure 2-3.

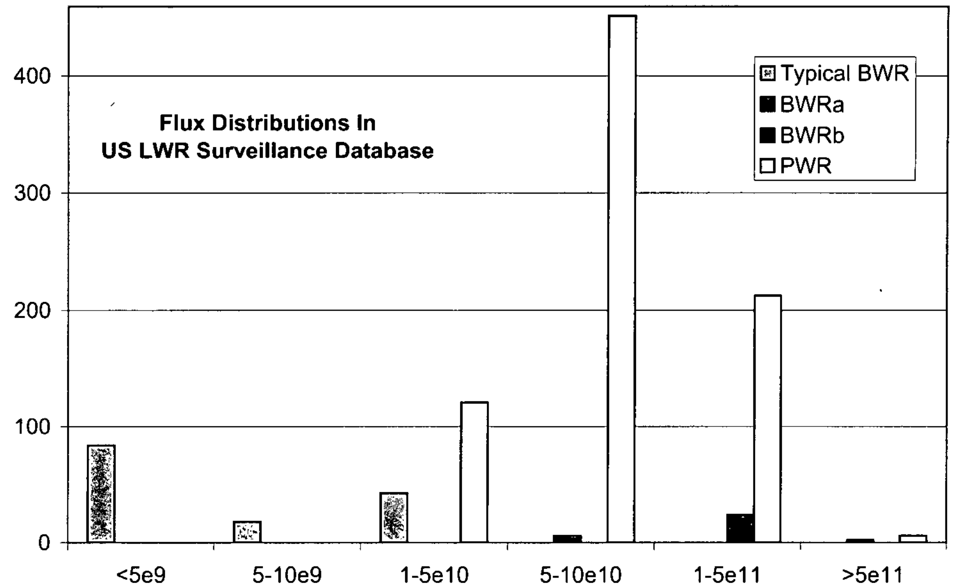

a) Flux (n/cm^2-sec)

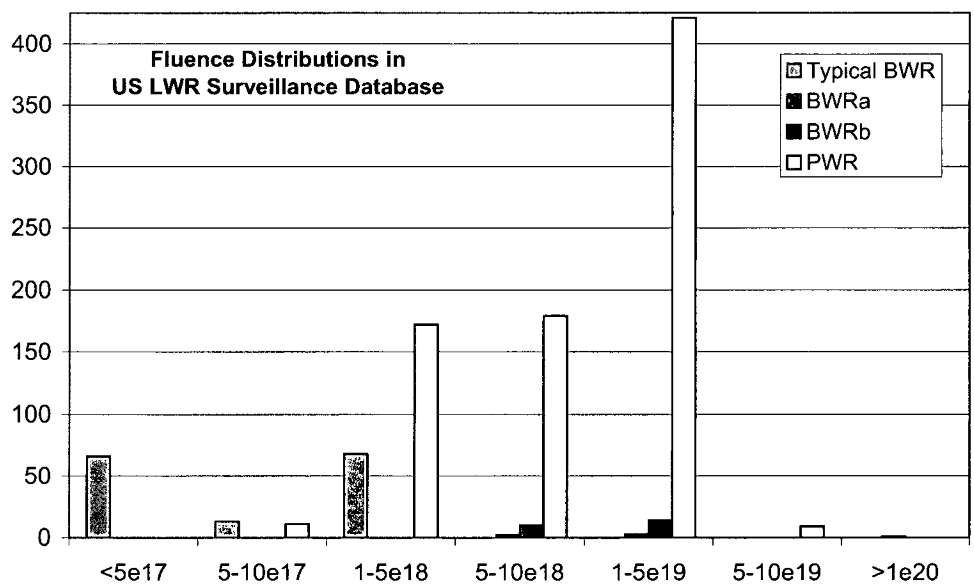

b) Fluence (n/cm^2)

Figure 2-3
Proportions of samples of different kinds exposed to a) different fluxes b) different fluences

Figure 2-3 shows clearly the dominance of the PWR data within the database. The typical BWR data are fairly evenly distributed in the ranges flux<$5x10^{10}$n/cm^2-s and fluence <$1x10^{19}$n/cm^2. The PWR data, however are peaked in the ranges $5x10^{10}$-$1x10^{11}$n/cm^2-s and 1-$5x10^{19}$n/cm^2.

3
MECHANISTIC BACKGROUND TO ASSESSMENT OF NEW CORRELATIONS

3.1 Basic Mechanisms of Radiation Embrittlement in RPV Steels

During the neutron irradiation of a component, collisions between the incident neutron and constituent atoms result in momentum transfer to the lattice atoms. If the transfer is sufficiently energetic, atoms can be permanently displaced from their lattice sites resulting in a vacant lattice site (a vacancy) and a lattice atom in an interstitial site in the lattice (a self interstitial atom, SIA). Individual vacancies and SIAs are described as point defects. At RPV operating temperatures both vacancies and SIAs are mobile. Microstructural development under irradiation depends on both the migration and clustering of the point defects themselves, and on interactions between the point defects and solute atoms. There are three basic micromechanisms which, historically, have been generally accepted to control RPV embrittlement:

- The formation of point defects, and their grouping together into clusters and dislocation loops.
  These individual defects and their groupings are described as matrix defects. They interfere with the free movement of dislocations, such that an increased stress is required to induce plastic deformation of the steel. This component of radiation-induced hardening is referred to as matrix hardening, or matrix damage.
- The precipitation of solute atoms.
  In RPV steels, the solute atoms involved are generally those which would precipitate under thermal conditions (i.e. their precipitation is thermodynamically favored), but the rate of precipitation is much enhanced in the presence of radiation. This is because the radiation-induced point defects assist both solute diffusion and precipitate nucleation. The main solute element involved in irradiation-enhanced precipitation in RPV steels has been found to be copper, thus the features were originally described as copper-rich precipitates, CRPs. Further examination has shown that many elements may be involved in the features, of which Ni, Mn and Fe are most commonly found; Si tends to be incorporated at higher fluences; P is often found within the precipitates, or enhanced in the regions around them; minor alloying elements such as Cr appear occasionally at very low concentrations. As a rough guide, the levels of Cu, Ni and Mn in the precipitates reflect the levels of these elements in solution prior to irradiation, and the actual Cu content may be very low in low-Cu steels. The dilute nature of the features has led to them being referred to as clusters rather than classical precipitates (copper-enriched clusters, CECs) and, more generally, as solute clusters. Solute clusters also interfere with the free movement of dislocations. The subsequent hardening has been described as the Cu component of hardening, or as the solute-related component of hardening.

With either cause of hardening, the hardening results in embrittlement of the steel. This is shown most characteristically by an increase in the temperature of the steel's ductile-to-brittle transition (DBT). The third embrittlement mechanism does not involve hardening:

- The irradiation induced or enhanced segregation of elements to grain boundaries.
  Some of the elements which segregate to the boundaries (e.g. phosphorus) reduce the grain boundary cohesion, encouraging intergranular failure and embrittlement.

In association with the increases in the DBTT, embrittlement is manifest as a decrease in the Charpy upper shelf energy or the fracture toughness at temperatures above the DBTT.

The anticipated development of the embrittlement produced by the first two mechanisms summarized above is often shown schematically as in Figure 3-1. The matrix damage component alone of embrittlement has been found to be (approximately) dependent on the square root of neutron fluence, though the exact proportionality may differ from one class of material to another. The transition temperature shift due to irradiation-produced CECs initially rises slowly, then at an increasing rate, before once again slowing. It has generally been considered that the CEC component of embrittlement reaches a maximum level, and then saturates, producing an embrittlement *versus* fluence curve with a plateau, as illustrated in Figure 3-1. The magnitude of the plateau level of embrittlement depends on the available Cu (i.e. the Cu in solution prior to irradiation), and has been assumed to correlate with the precipitation of all the available Cu. The analysis of data from the EPRI-CRIEPI jointly funded research program, however, suggested that, at long times/high fluences, the hardening would decrease as the CECs coarsened (i.e. increased in size while decreasing in number, as is found during thermal ageing in the absence of irradiation). The use of a curve with a plateau rather than a maximum to predict hardening may be considered to be conservative [27, 28] as no "advantage" is taken from the possible softening.

With either cause of hardening, the change in Charpy impact properties is directly proportional to the change of yield strength. Non-hardening embrittlement is sometimes considered to have a relationship of its own to fluence, but sometimes is considered to modify the matrix damage component.

This division of radiation-induced hardening into a pure matrix damage term and a copper-dependent term is known to be simplistic. Solute atoms (particularly the interstitial solutes C and N, but also the substitutional solutes such as Cu, Ni etc.) are known to interact with the point defects and point defect clusters, affecting their stability and the hardening produced by the (point defect dominated) complex. In their turn, the CECs may incorporate some point defects. In addition, if only very low levels of copper (say <~0.05 wt. %) are present, then solute clustering can still occur, but at a much lower rate, and involving predominantly Ni, Mn and Si (in which case the features are sometimes described as MNPs – Mn-Ni-rich precipitates). The slow rate of this process means that the development of hardening caused by such minimal-Cu solute clusters has been studied less than that due to clusters in higher-Cu steels, and it is not known, for example, whether a maximum/plateau in this form of hardening can be expected at extremely high fluences (say $>10^{20}$n/cm^2). There is also evidence that, even in steels with higher levels of Cu, at high fluences, when the precipitation of CECs has reduced significantly the level of dissolved Cu, the formation of distinct Cu-free, Mn-Ni-Si solute clusters will occur [29]. Hardening from these late-blooming MNPs could produce a distinct secondary hardening peak, or a peak which merges with the CEC hardening peak to enhance the appearance of a plateau in solute cluster hardening.

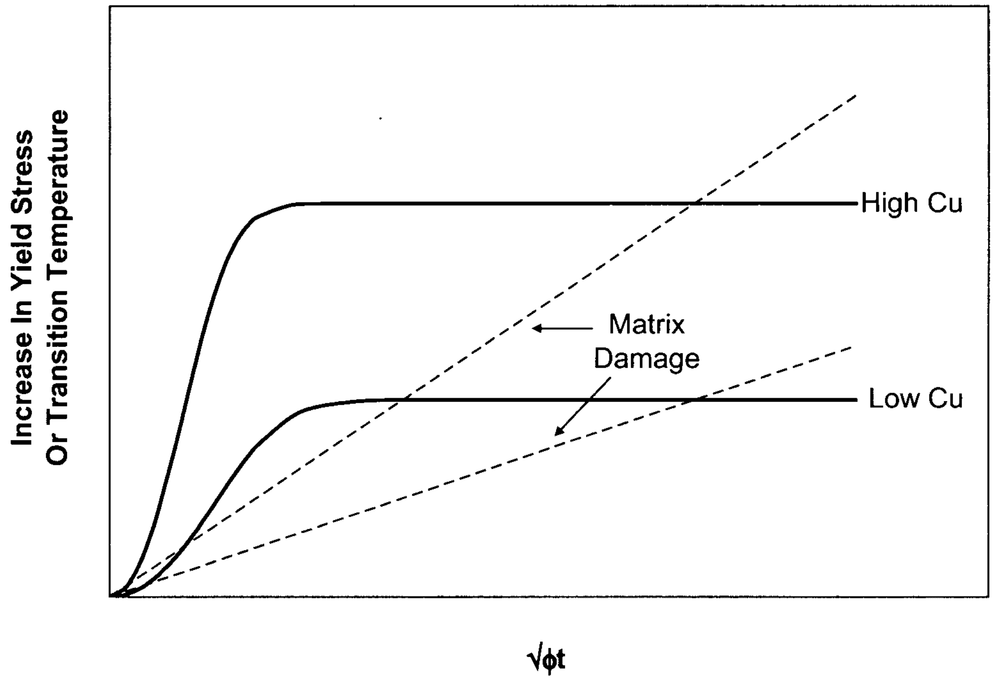

Figure 3-1
Increase in yield strength as a function of neutron fluence

There is some evidence that MNPs (whether late-blooming or not) are more diffuse (contain more Fe) than CECs [38], and may not be strictly precipitates, but "clouds" of solutes attracted to the strain fields around point defect clusters or small dislocation loops. In this case, the observation of MNPs will indicate that the hardening associated with matrix defects is changing. The hardening due to matrix defects is known to be affected strongly by the presence of C and N. These interstitial solutes appear to be absorbed into MDs at very low fluences ($<5x10^{17}$ n/cm^2 in [30]). It is not clear by how much the hardening from C-N-complexed MDs would be increased by their later association with clouds of substitutional solutes.

Despite these complexities, the framework shown in Figure 3-1 is generally convenient to use, is familiar to workers in the field of radiation damage, and affects the form of many embrittlement correlations.

3.2 Summary of Mechanistic Insights from the EPRI-CRIEPI Jointly-Funded Research Program Relevant to Forms of Embrittlement Correlations

3.2.1 Segregation

The irradiation-induced segregation of various elements to grain boundaries was measured in many RPV steels during the EPRI-CRIEPI jointly-funded research program. The rate of increase of the main embrittling segregant (P) was low, making it unlikely that non-hardening embrittlement would occur in the steels/irradiation conditions studied.

3.2.2 Hardening-Related Embrittlement in Steels with Cu<0.07wt.%

The low-Cu steels in the EPRI-CRIEPI jointly-funded research program [9, 15-26] contained 0.060 or 0.063wt.% Cu.

The combination of mechanical property measurements and different microstructural analyses carried out during the EPRI-CRIEPI jointly-funded research program indicated that the defects responsible for matrix damage (the point defect dominated component of radiation hardening and embrittlement) were predominantly SIAs, SIA clusters and dislocation loops (probably in association with solute atoms). The numbers of both this type of defect and the vacancy-type defects increased with increasing fluence, although the latter did not significantly contribute to hardening. The possibility that MNPs also contributed to the hardening of the low-Cu steels could not be ignored, although their existence under the conditions of irradiation fluence, flux and irradiation temperature used could not be shown unambiguously. The results do not, therefore, provide direct insight on how embrittlement from such features should be incorporated into an embrittlement correlation.

Observations from other sources [31] have indicated that the introduction of unstable matrix defects (i.e. those which could be annealed out at the irradiation temperature) increases the matrix damage at very high fluxes. The flux at which unstable matrix defects (UMDs) become influential was not clear. The flux at which UMD damage became evident was probably affected by the irradiation temperature and the fluence of observation. Fluxes of between $1x10^{12}n/cm^2$-s and $5x10^{12}n/cm^2$-s have been suggested [32]. Data from the EPRI-CRIEPI jointly-funded research program indicated that the upper limit is at least greater than $5.4x10^{12}$ n/cm^2-s (at 10^{18} n/cm^2).

In accordance with previous observations, the hardening/embrittlement from matrix defects was found to be affected by product form. This observation was thought to support the assumption that matrix defects are generally complexed with solute atoms. The combination of hardening and positron annihilation data could be interpreted as indicating that the most relevant solute was C, although other options were still considered possible.

3.2.3 Embrittlement in Steels with Cu>0.15wt.%

The steels which contained >0.07wt.% Cu (and could therefore be expected to exhibit Cu precipitation) all contained Cu>0.15wt.%. Analysis of the compositions, sizes and volume fractions of solute clusters measured during the program, and of the levels of dissolved solutes, taken altogether, showed that the processes of cluster nucleation, growth and coarsening, characteristic of age hardening under thermal conditions, all occurred during CEC formation under irradiation. This permitted the rationalization of the influences of some of the material/environmental variables on CEC development and hardening/embrittlement.

It is generally accepted that increasing flux increases the vacancy concentration in the higher-Cu steels, as well as in the lower-Cu steels [e.g. 28, 34]. The increase in vacancy concentration increases the diffusion rate of substitutional solutes (such as Cu, Ni and Mn) so, in the higher-Cu steels, flux has an opportunity to affect hardening. Increasing the diffusion rate increases the volume fraction of CECs produced at a given time. This was the main effect of flux on CEC precipitation observed.

The extent to which flux affects the diffusion rate has been discussed in detail by [e.g. 28, 34]. It is relatively easy to show that a flux-dependence of diffusion will affect the fluence required to precipitate out a given fraction of solute. If the relation is of the form $D \alpha\ flux^p$ then, if $p<1$, although the time for a given level of precipitation will decrease with increasing flux, the fluence to a given level of precipitation will increase. Similarly if $p=1$, the precipitation rate with respect to fluence will be flux-independent. The value of p will itself be dependent on flux, as it varies according to the mechanism governing the availability of point defects. At very low fluxes, the vacancy distribution is dominated by equilibrium, thermal processes; at intermediate fluxes, irradiation-induced point defects are thought to annihilate predominantly at fixed sinks such as dislocations and grain boundaries; at higher fluxes, the point defects annihilate at solute traps, or as a result of random encounters between vacancies and SIAs in the matrix. The limits to these flux regimes are not known in detail, but Figure 3-2 shows the rough estimates of the regimes of relevance to reactor operation according to [32, 33] in terms of the fluence required to reach the plateau in CEC hardening. In either the low-flux or the high-flux portions of this figure, the volume fraction of Cu precipitated at a given fluence will decrease with increasing flux.

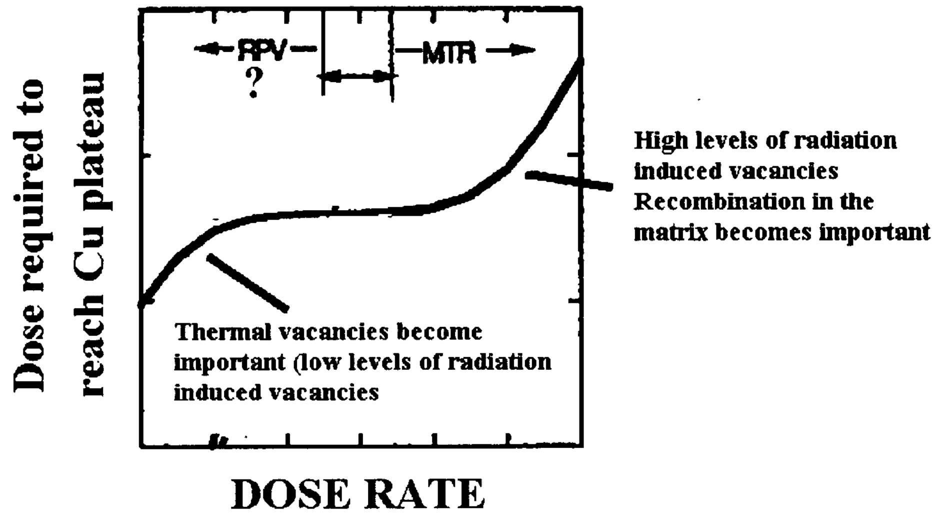

Figure 3-2
Sketch illustrating effect of flux (dose rate) on the fluence (dose) required to reach the plateau in Cu-related hardening [33]

In slight contrast to Figure 3-2, Figure 3-3 shows the scheme proposed by Odette et al in 2005 [34], which contains a point of inflection rather than a flat region in the intermediate-flux region. This is caused by the greater importance ascribed to point defect annihilation at solute traps rather than at fixed sinks.

Within the EPRI-CRIEPI program [9, 15-26], an effect of flux on precipitation rates was observed when comparing irradiations at around 10^{10} n/cm^2-s (typical of BWRs) with those around 6.45×10^{10} n/cm^2-s (typical of PWRs), and when comparing irradiations around 6.45×10^{10} n/cm^2-s with those around 5.4×10^{12} n/cm^2-s (typical of MTRs). This led to the conclusion that the region of fixed sink dominance (in which the fluence to reach a given level of precipitation would be independent of flux) was either at $<10^{10}$ n/cm^2-s, or confined fairly closely to PWR fluxes. In the latter case, the flux-dependence between the BWR and PWR irradiations would be related to the increasing importance of thermal vacancies in permitting substitutional solute diffusion. This assessment of the onset of thermal effects is in fair agreement with the analysis shown in Figure 3-3, in which the thermal regime appears below about 10^{10} n/cm^2-s.

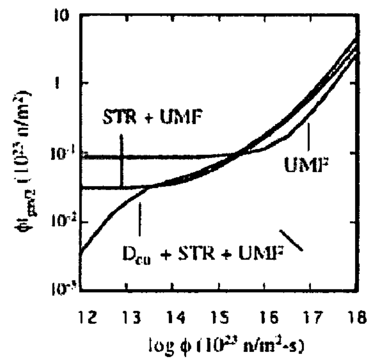

Figure 3-3
Sketch illustrating effect of flux (dose rate) on the fluence (dose) required to reach half the plateau in Cu-related hardening, according to Odette et al [34]

An additional effect of flux on CEC nucleation was observed during the EPRI-CRIEPI program , in that the sizes of clusters produced at a given volume fraction were lower at higher fluxes. This was interpreted as showing that matrix defects could act as nucleation sites for CECs, and that the CECs produced under irradiation were likely to incorporate point defects. Examination of the literature showed that this was a common (if small, and not always acknowledged) effect, as illustrated in Figure 3-4, which plots data from [35 and 36].

This association of microstructural refinement with an increase in hardening/embrittlement at a given volume fraction of CECs, is illustrated in Figure 3-5a for the materials in the EPRI-CRIEPI program, and in Figure 3-5b for the Rolls-Royce lower-Ni welds of Figure 3-4b. Although the effect is small, it appears that irradiations which produce large numbers of small clusters do indeed result in higher shifts at a given volume fraction of clusters than irradiations which produce smaller numbers of large clusters. i.e. a given level (volume fraction) of precipitation produces more hardening in a higher flux irradiation. This is also consistent with observations of CEC-induced hardening in (minimal-Ni) CMn submerged-arc welds irradiated at the relatively high temperatures found in some Magnox surveillance locations as shown in Figure 3.5c. (The high irradiation temperatures led to larger CECs, and greater variations in CEC diameter than are usually found in lower-temperature irradiations.)

Increasing the bulk level of Cu was observed to increase precipitation during fabrication heat treatments. In addition, higher dissolved Cu and Ni levels prior to irradiation increased the volume fraction of clusters produced under given irradiation conditions. This is consistent with increasing solute supersaturation increasing the driving force for cluster precipitation, for precipitation during both thermal ageing and precipitation. An increased driving force is generally observed to increase initial precipitation/hardening rates in an age hardening system. The rate at which Cu was removed from solution was, however, observed to be slower in the presence of higher Ni. (This is consistent with the increased total volume fraction of cluster at a given fluence, since the clusters contained additional Ni and Mn.) This could suggest that Ni affected the solubility of Cu.

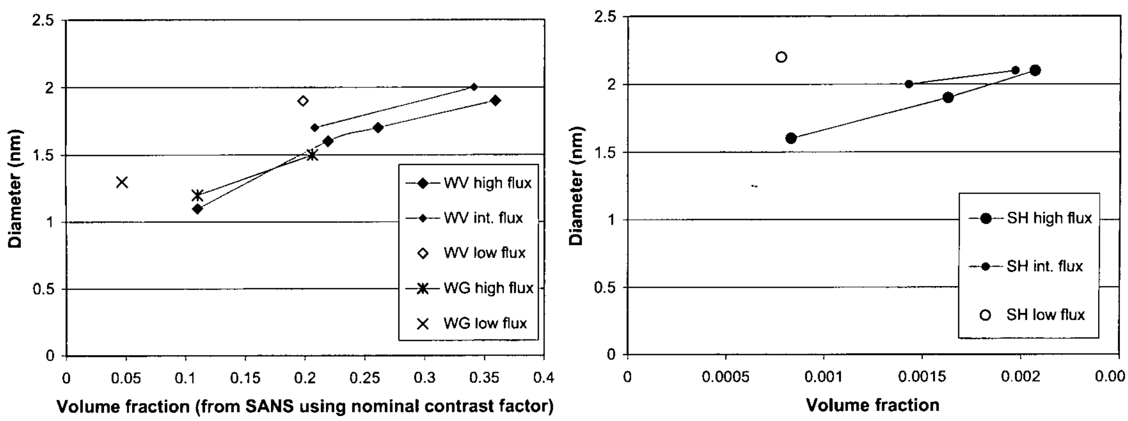

a) High Ni SAWs

b) Medium-Ni SAWs

Figure 3-4
Effect of flux on solute cluster diameters found at given volume fractions[2] of CRPs in MnMoNi submerged-arc welds with a) ~1.6wt. %Ni and b) ~0.8wt.%Ni [35, 36]

Ni was found in increasing amounts in CECs as the bulk Ni level increased (at least up to 0.6%Ni in the steel). The solute clusters in RPV steels tended to be enriched in Cu towards the centre, with Ni and Mn enhanced towards the outer regions. This was interpreted as being associated with a lower cluster-matrix interfacial energy. Lowering the interfacial energy also causes more rapid cluster nucleation. Thus this interpretation was also consistent with the observation that in the early stages of precipitation, the dominant effect of adding Ni to a RPV steel is the production of more, smaller clusters at a given volume fraction of CECs, and the production of higher volume fraction of CECs at a given fluence. This was observed within the EPRI-CRIEPI program. A reduced interfacial energy delays precipitate coarsening in an age hardening system. The range of fluxes and fluence applied during the Program did not permit this aspect to be observed, but investigation of the literature indicates that the addition of Ni does increase the volume fraction of clusters produced before coarsening sets in. (For a given flux and Cu level, this is equivalent to delaying coarsening to higher fluences.)

A summary of the effects of various material and environmental factors on the time/fluence to peak hardening from CECs, and the peak level of hardening is given in Table 3-1 and Table 3-2.[3]

[2] Note that, in SANS analyses, the conversion of signal intensity to volume fraction requires the use of a contrast factor. In [36] a nominal contrast factor was used (the same factor for both WV and WG), while in [35] the contrast factor for SH was not discussed. The absolute values of the volume fractions in Figure 3-4a and b may not be strictly comparable, but the relative volume fractions in each figure are comparable.

[3] The irradiation conditions used within the EPRI-CRIEPI program on microstructural effects were such that the influence of irradiation temperature could not be examined. This does not imply that such an influence is absent.

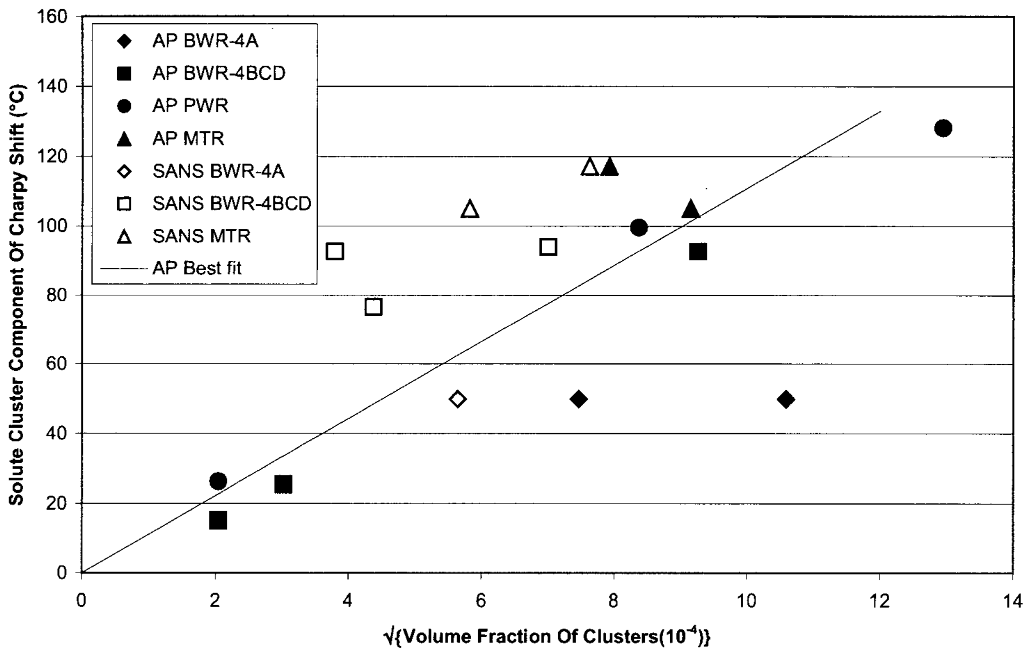

a) EPRI-CRIEPI data

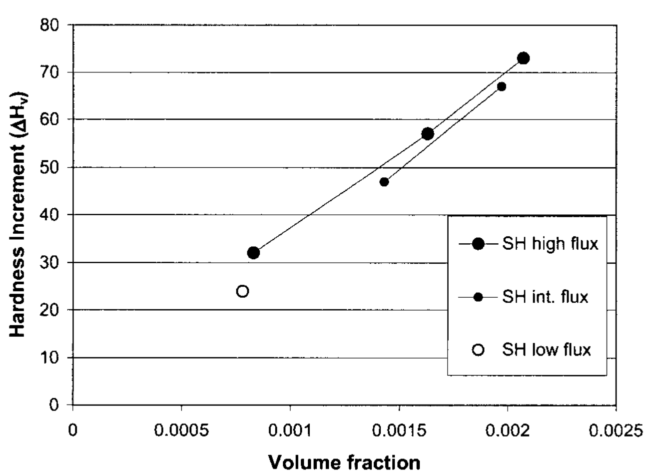

b) Rolls-Royce data [35, 36]

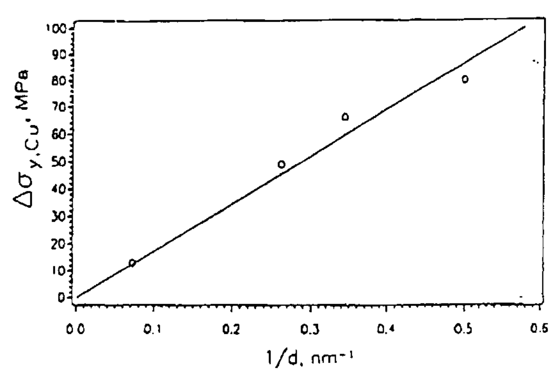

c) Magnox Electric data [37]

Figure 3-5
Dependence on volume fraction of a) CEC component of shift measured in steels irradiated at high flux (in MTR), intermediate flux (in PWR) and low flux (in BWR), b) hardness increment observed in low-Ni weld irradiated at different fluxes, and hardening due to a given volume fraction of CRPs during high-temperature surveillance irradiation of CMn SAWs [37]

Table 3-1
Summary of effects of changing properties on the behavior of an age hardening curve, correlated with the influence of the variables examined within EPRI-CRIEPI jointly-funded research program

Property Change	Effect on		Caused under Irradiation by:
	Time to Peak Hardness, t_p	Peak Hardness	
Decrease in hardening per particle	→	↓	Ni↑
Increase in solute diffusion rate	↓	→	Flux↑
Nucleation rate increased	↓	↑	Fluence↑, Ni↑, Cu↑
Diffusion distance decreased	↓	↑	Ni↑, Cu↑
Interfacial energy decreased	↑	↑	Ni↑

↓=feature decreases, ↑=feature increases, →=feature is unchanged.

Table 3-2
Effect of variables on hardening due to CECs (as a function of fluence)

Variable Increasing	Effect of this Increase on		Comment
	Fluence to Peak Hardness	Peak Hardness	
Flux	↑	↑	Related to the effect of flux on the diffusion rate (and hence on time to peak hardness t_p), and to the effect of fluence on the number of available nucleation sites produced within t_p.
Cu*	↓	↑	Related to the effect of Cu on supersaturation (nucleation rate and diffusion distance).
Ni	↑	↑	Related to the effect of Ni on hardening per particle, supersaturation and interfacial energy. The effect of interfacial energy is assumed to outweigh the effect of supersaturation in determining the time/fluence to peak hardening; the effects of supersaturation and interfacial energy are assumed to outweigh the effect of hardening per particle in determining the peak hardening level.

* This refers to the Cu level remaining in solution at the start of irradiation, which may be less than the bulk Cu level if the bulk Cu level is high, and depending on the pre-irradiation heat treatment.

3.2.4 Resulting Expectation of Embrittlement Correlation

In terms of the components of embrittlement correlations, the effects described in this Section may be considered to support (or not) the inclusion of certain dependences, as summarized in Table 3-3.

Table 3-3
Support provided by results of EPRI-CRIEPI program for the inclusion in embrittlement correlations of dependences on different properties

Feature	Dependences Suggested in Various Current Embrittlement Correlations [1-5, 13, 14]	Support from EPRI-CRIEPI Program
Matrix damage	Dependence on flux and product form	a) No support for flux. b) Limited support for product form.
Pre Plateau embrittlement from CECs	Dependence on flux and composition	c) Support for a dependence on flux. d) Support for dependence on composition.
Plateau Onset Fluence	Dependence on flux and Cu and Ni	e) Support for fluence for the onset of the plateau decreasing with decreasing flux, decreasing Ni, and increasing Cu.
Post Plateau embrittlement from CECs	Dependence on fluence and composition	f) Support for a plateau being a conservative approach, and for the level of the "plateau" increasing with increasing Cu and Ni levels. g) No evidence for late blooming phases under the conditions examined.

Table 3-1 – Table 3-3 provide part of the basis of the mechanistic evaluations of sNRC2006 and RM-6 (2) described in Sections 4 and 5. The evaluations will, necessarily, also be based on data from the extensive literature on microstructural and mechanical property development in RPV steels and related alloys exposed to radiation.

4

MECHANISTIC ASSESSMENT OF CANDIDATE CORRELATIONS

4.1 Mechanistic Assessment of the Simplified 2006 NRC Correlations (sNRC2006)

4.1.1 Description of sNRC2006 Correlation

The derivation of this correlation is described in [13]. It has the form:

TTS=MF+CRP **Equation 4-1**

where TTS = predicted irradiation-induced shift in Charpy 30ft lb transition temperature(in °F)
MF = component of shift attributed to matrix features
CRP = component of shift attributed to CRPs[4]

In Equation 4-1:

$$MF = A(1-0.001718T_i)(1+6.13PMn^{2.47})\sqrt{(\phi t_e)}$$ **Equation 4-2**

where A = $1.140x10^{-7}$ for forgings
$1.561x10^{-7}$ for plates
$1.417x10^{-7}$ for welds
T_i = irradiation temperature
P = bulk P (wt.%)
Mn = bulk Mn (wt.%)

$$(\phi t)_e = \left\{ \begin{array}{ll} \phi t \text{ for } \phi \geq 4.39x10^{10}\ \text{n/cm}^2\text{-s} & \\ \phi t\left(\dfrac{4.39x10^{10}}{\phi}\right)^{0.259} & \text{for } \phi < 4.39x10^{10}\ \text{n/cm}^2-\text{s} \end{array} \right\} = \text{effective (flux-corrected) fluence}$$

Equation 4-3

[4] Although the solute clusters have been referred to elsewhere as CECs, the sNRC2006 and RM correlations refer to the hardening from Cu-enriched solute clusters as CRP hardening. This terminology is retained within the report when the correlations, rather than the mechanisms, are discussed.

where ϕ = flux (n/cm^2-s)
t = irradiation time (s)

$$CRP = B\left(1+3.77Ni^{1.191}\right)f(Cu_e,P)g(Cu_e,Ni,\phi t_e) \quad \textbf{Equation 4-4}$$

where B = 102.3 for forgings
135.2 for plates in vessels manufactured by Combustion Engineering (CE)
102.5 for non-CE plates
155.0 for welds
128.2 for plates of the standard reference materials (SRMs)
Ni = bulk Ni (wt.%)

$$Cu_e = \begin{Bmatrix} 0 \text{ for Cu} < 0.072 \text{ wt.\%} \\ \min\left[\text{Cu}_{\text{actual}}, Cu_{\max}\right] \text{for Cu} > 0.072\text{wt.\%} \end{Bmatrix} = \text{effective Cu level} \quad \textbf{Equation 4-5}$$

where Cu_{actual} = bulk Cu level (wt.%)
Cu_{max} 0.243 for typical (Ni>0.5) Linde 80 welds
0.301 for all other materials.

$$f(Cu_e,P) = \begin{Bmatrix} 0 \text{ for Cu} \le 0.072 \\ \left[\text{Cu}_e - 0.072\right]^{0.668} \text{ for Cu} > 0.072 \text{ and P} \le 0.008 \\ \left[\text{Cu - }0.072 + 1.359(\text{P - }0.008)\right]^{0.668} \text{ for Cu} > 0.072 \text{ and P} > 0.008 \end{Bmatrix} \quad \textbf{Equation 4-6}$$

$$g(Cu_e, Ni, \phi t_e) = \frac{1}{2} + \frac{1}{2}\tanh\left[\frac{\log_{10}(\phi t)_e + 1.139Cu_e - 0.448Ni - 18.120}{0.629}\right] \quad \textbf{Equation 4-7}$$

(The "simplification" refers mainly to the removal of a temperature-dependence in the CRP component which was mechanistically-justified, but not strongly observed in the surveillance database. In addition, a separate value of Cu_{max} was originally defined for Linde 1092 welds, but this did not affect sufficient data points for its retention to be deemed valuable.)

4.1.2 Assessment of CRP Component

4.1.2.1 General Comments

The CRP component of sNRC2006 (Equation 4-4) describes the embrittlement due to Cu-related clustering as increasing with fluence, and then saturating. As mentioned earlier, the results of EPRI-CRIEPI jointly-funded research program indicated that the Cu-related hardening would probably reach a peak rather than a plateau. Since they also indicated that overageing would only occur at high fluences, it seemed that using a plateau to describe the hardening would lead to a very similar description at most fluences, and be conservative once the two descriptions deviated (assuming that the plateau level of hardness did not underestimate the peak hardening). The plateau form in sNRC2006 is therefore supported by its similarity to other correlations, and by the results of EPRI-CRIEPI jointly-funded research program.

The CRP component may be considered in two parts; the tanh term, g(Cu_e, Ni, ϕt_e), and the remainder. The tanh term describes the rate at which the plateau is reached, while the pre-tanh terms describe the "height" of the plateau (i.e. the maximum level of hardening to be associated with Cu clustering). Clearly, it is difficult to distinguish between a more-rapidly approached maximum and a higher maximum approached at a constant rate, unless there are sufficient data at fluences higher than that corresponding to maximum hardening. The database used in this assessment (i.e. the combination of TTS8-04R1 with BWR VIP ISP data as described in Chapter 2) contains 45BWR and 128PWR data points for which the value of g(Cu_e, Ni, ϕt_e) is between 0.75 and 1.0. Although these points refer to materials of a variety of compositions, fluences and fluxes, it is possible that the data are sufficient to make the distinction.

The results of EPRI-CRIEPI jointly-funded research program, summarized in Table 3-1 and Table 3-2 lead to an expectation that there should be:

- inverse or negative coefficients for an Ni term within g, and a positive coefficient for Ni outside g;
- positive Cu coefficients for Cu both within and outside g;
- inverse or negative coefficients for a flux term within g, and a positive coefficient for flux outside g.

Most of these expectations are met by sNRC2006; only the expectation of a flux term outside g is not met. Since this term is expected to be small, it may have been difficult to extract from the database analysis with statistical significance.

The overall appearance of the CRP term of sNRC2006 is thus supported by the mechanistic understanding of CEC hardening developed in the EPRI-CRIEPI jointly-funded research program. Beyond this, it is worth considering the individual terms in more detail.

4.1.2.2 Effective Copper (Cu)

The use of an "effective Cu" term is historically supported, and relates to two aspects; a solubility limit and precipitation during fabrication heat treatments prior to irradiation. From general considerations of precipitation, one would expect there to be a level of Cu at which the solid solution is saturated, and above which precipitation is encouraged. On the basis of modeling and microstructural studies, it is likely that the saturation level of Cu in solution at 270-290°C will be below the 0.072wt.% used here. (Auger et al put the solubility limit at around 0.007at.% [38].) It is more probable that the 0.072wt.% represents the Cu level above which the level of precipitation induces a degree of hardening which is measurably distinguishable from MD hardening at the surveillance fluences [39]. Since precipitation rates decrease with decreasing supersaturation, the degree of hardening which will be distinguishable from the (continuously increasing) MD hardening, will actually be higher as the solubility limit is approached. It is thus reasonable that Cu_e' goes to zero at a level above the actual solubility limit for Cu.

The upper limit for the Cu_e term is generally considered to reflect precipitation of Cu during vessel (or specimen) fabrication. It is not strictly accurate to assign a generally-applicable value to the amount of Cu which will precipitate out during fabrication, as the rate of precipitation increases with increasing bulk Cu and decreasing bulk Ni levels, as well as with increasing temperature. The dissolved Cu level will, however, approach the solubility limit at the stress relief heat treatment temperature more slowly for steels with smaller supersaturations of Cu (and similar relative rates of precipitation will occur during subsequent vessel cooling). It is, therefore, not unreasonable to analyze the database to derive a single value of Cu_e for all materials of a given product form (which may correspond to similar concentrations of elements other than Cu) with differing bulk Cu levels. The value will, however, be associated with considerable scatter. In addition to the effects of composition, the thermal histories of different vessels/components will vary, even if a common specification is used. Thus there will be some variability in the amount of Cu pre-precipitation between vessels/components.

The effect of pre-precipitation is probably incorporated within the B term as well as the Cu_{max} term. If, for example, the difference between CE plates (B=135.2) and non-CE plates (B=102.5) is due to a difference in heat treatment, then this should also affect the B values in the welds, since Linde 80 welds only appear in non-CE vessels (and ~2/3 of the PWR non-CE welds are Linde 80), and only CE vessels use Linde 1092 or Linde 0091 welds. There is no effect of vessel manufacturer in the B value for welds in sNRC2006, but Cu_{max} for the Linde 80 welds is lower than for other materials. (A low value for the Cu in solution in Linde 80 welds at the start of life was reported by McElroy and Lowe, who found that this explained the difference between embrittlement rates in these and other welds [40].) Reductions in Cu_{max} or B will have similar effects on the maximum embrittlement.

It is worth noting that the correlation between Linde 80 flux welds and non-CE manufacturers may not be the same in BWRs and PWRs. There is less information in the BWR surveillance database to correlate weld flux type with manufacturer. However, it may be observed that the most common non-CE PWR manufacturer was Babcock and Wilcox (B&W), and they used Linde 80 welds in their PWRs. In contrast, B&W are not the most common non-CE manufacturer for typical BWR surveillance samples and, in the BWRs which B&W did manufacture, not all the identified fluxes were Linde 80. This alone might lead to different correlations between CE/non-CE and thermal history (i.e. B and Cu_{max}) in BWR and PWR vessels. In addition, the RPV dimensions differ for BWRs and PWRs, thus even when the manufacturer and weld type are the same, the thermo-mechanical histories of BWR and PWR RPVs need not be the same. Thus, if the surveillance specimens have exactly the same thermal histories as the vessels, the balance between Cu_{max} and B found for different product forms in the PWR surveillance database need not be reproduced in the BWR surveillance database. (Unless the surveillance specimens are produced as e.g. cutouts for nozzle penetrations, they may not actually have the same thermal histories as the vessels. This may account for the difference in B values for the SRM plates and the other plates.)

Overall, then, the use of an upper cut-off for the effective Cu content contributing to radiation embrittlement has mechanistic support. Using a combination of Cu_{max} and B to account for pre-irradiation precipitation of Cu is an approximation but, given the number of unknowns associated with the vessel thermo-mechanical histories, and the influence of various minor elements on the precipitation rate of Cu during vessel/specimen fabrication, this is unavoidable.

4.1.2.3 Phosphorous (P)

In itself, the presence of a P term in the CRP component may be justified mechanistically in that P is observed within or around Cu-enriched solute clusters [e.g. 41]. There is, however, a P term in the MF component of sNRC2006 also. Thus the effect of a given level of P (above 0.008wt.%) is predicted to be greater in a steel with Cu>0.072wt.% than in one with Cu<0.072wt.%. This is in contradiction to data in the literature.

It is well-known that the effect of P on hardening/embrittlement is generally lower in steels with higher Cu [42, 43]. This is illustrated in Figure 4-1a and b, in which the dependence of DT on wt.% P is seen to be stronger in MnMoNi steel of 0.002wt.% Cu than in steel of 0.30-0.33wt.%Cu [42]. In Figure 4-1c [43], additional data were collated to show that the effect was probably not progressive with increasing Cu, but showed a step-change when the Cu level was high enough for CRPs to form.

Since a P term is present in the MF component of sNRC2006, it is not clear how well a positive P term in the CRP component will produce an optimum combination of effects.

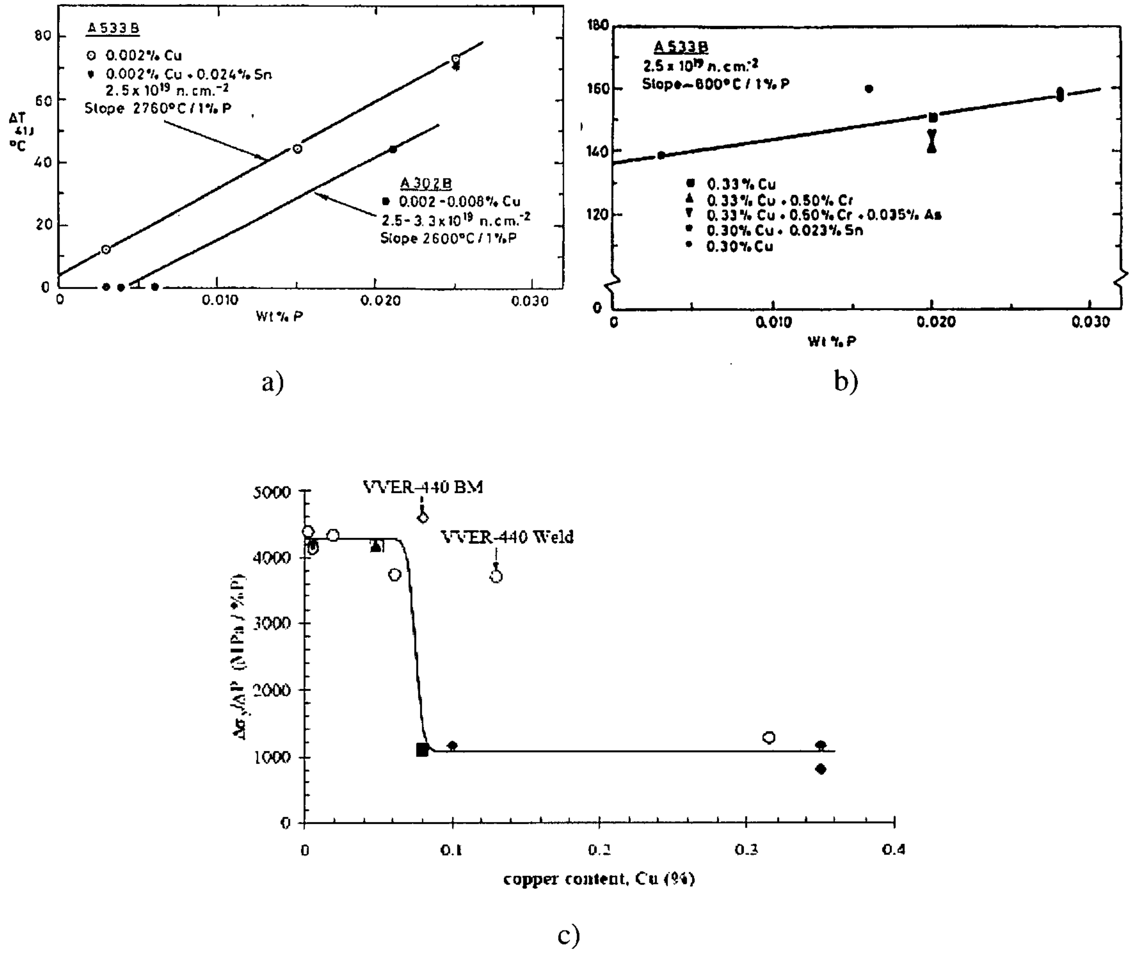

Figure 4-1
Effect of P on increasing irradiation embrittlement in a), b) low and high-A533B [42] and c) RPV steels (steels not otherwise identified are MnMoNi steels) with a range of Cu levels [43]

4.1.2.4 Flux

The CRP term in sNRC2006 differs significantly from that in E900-02 in its inclusion of a flux term. As has been mentioned, it is plausible that there should be a flux contribution to the tanh term, g(Cu_e, Ni, ϕt_e), due to the effect of flux on the substitutional solute diffusion rate. The flux term is set to unity at fluxes above 4.39×10^{10}n/cm^2-s (see Equation 4-3), i.e. for most of the PWR range. A flux-independent regime (or at least a regime of minimal flux-dependence) between 4.39×10^{10}n/cm^2-s and 1.63×10^{12}n/cm^2-s (the highest flux in TTS8-04R1) is consistent with Figure 3-2, with the observations made in EPRI-CRIEPI jointly-funded research program [9, 15-26] and with observations reported elsewhere in the literature (e.g. McElroy et al [44] put the flux-independent regime between 10^{10} and 10^{12} n/cm^2-sec.). This supports the postulate that thermal vacancies become increasingly relevant at BWR fluxes.

The flux term within g(Cu_e, Ni, ϕt_e) has the form $\phi^{-0.259}$. The power law form is plausible according to [34 and 13]. These references consider that the exponent will be -1 when thermal vacancies dominate, but 0 in the fixed sink regime. If the BWR fluxes are those at which thermal vacancies begin to be influential, then an exponent between 0 and -1 seems appropriate. This is, however, a wide range.

In EPRI-CRIEPI jointly-funded research program, flux was found to affect not only the rate of substitutional solute diffusion, but also the extent of heterogeneous nucleation of solute clusters on irradiation-induced defects. As a result, a given volume fraction of solute clusters would be produced by a larger number of smaller clusters at higher fluxes. This, in turn, affected the hardening/embrittlement induced by a given volume fraction of solute clusters. Subsequent examination of the data available in the literature (as described in Section 3.2.3) confirms this to be a general observation. Such an effect should be described by a flux term outside the tanh function.

The absence of a flux term outside the tanh function in the development of sNRC2006 could have been justified mechanistically because of the long-held view that hardening from CECs should be described by the Russell-Brown [45] model of modulus hardening. In this analysis, the particle strength changes in such a way that, the hardening produced by a given volume fraction of particles increases as the particle diameter increases up to diameters of ~2.5nm, then decreases. As a result, for particle diameters around 2-4nm, there is little effect of particle size on the hardening produced by a given volume fraction of clusters. This is illustrated in Figure 4-2a. Since CECs observed in even test reactor-irradiated samples are generally >1.5 nm, and the range of sizes observed in BWR and PWR irradiations tend to be around 2 – 3 nm, hardening by the Russell-Brown mechanism would result in radiation hardening which was particle-size-independent. There would, then, be no requirement for a flux term outside the tanh function.

More recent atomistic modeling of dislocation interactions with solute clusters by Bacon and co-workers [46, 47], however, indicates that the Russell-Brown model, although popular in the field of radiation damage, is not always applicable to CEC hardening. Their simulations indicated, while dislocations simply sheared (as assumed in the Russell-Brown model) very small particles, when dislocations passed through larger particles, structural transformations occurred in the particles, leading to a new hardening mechanism. This mechanism appeared to operate for particles of diameter greater than ~2 nm, and again led to the more commonly-observed decrease in hardening from a given volume fraction of precipitates as the precipitate size increases. The predicted trend is shown in Figure 4-2b[5]. If the Bacon model is correct for RPV steels as well as model systems (as supported by the data shown in Figure 3-5) then, whatever the CEC size, the hardening from a given volume fraction of CECs will be affected by cluster size, and there is no theoretical justification for excluding the flux term outside the tanh term. Its absence must be justified on grounds of statistical significance, or parameter confounding.

[5] The data in this Figure are derived from manipulation of information in a Figure in a presentation by Osetsky, Stoller and Bacon. Although the trend is reliable, the precise values of the increase in critical resolved shear stress, (CRSS) may not be.

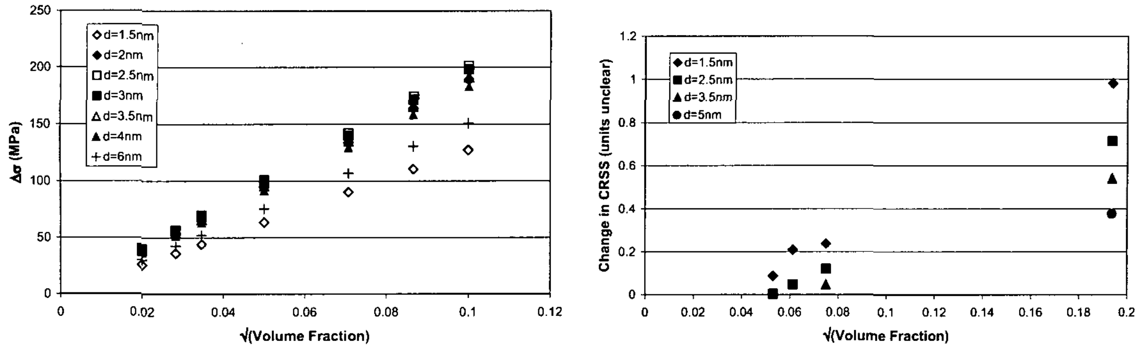

a) b)

Figure 4-2
Effect of particle radius on the hardening produced by a given volume fraction of particles as predicted by a) modulus hardening according to Russell and Brown, and b) transformation hardening according to Bacon and co-workers

The absence of a flux term outside the tanh function could also be the result of parameter confounding. Parameter confounding is possible because the lower flux (typical BWR) samples in the surveillance database are generally exposed to lower irradiation temperatures than remainder of the database (the PWR samples). In addition, the highest-flux samples (BWRa) were exposed at the highest temperatures. Lower-temperature irradiations (in the range 270-310°C) have been shown by the IVAR experiments [48] to produce larger numbers of smaller precipitates. The effect of the low fluxes in encouraging smaller numbers of larger precipitates may, therefore, have been offset by the (slightly) correlated lower temperatures within the TTS8-04R1 database.

During the development of the correlation sNRC2006, a fit was made first to the PWR data [13]. This required no flux term in either the MF or the CRP component. It was only when the BWR data were compared with this, preliminary correlation, that the requirement for a correction became evident. Given its form, and the cut-off at $4.39x10^{10}n/cm^2$-s, introduction of the flux term has no effect on predictions for most of the PWR surveillance samples, and only a minimal effect on the remainder. Thus the flux term accounts for all the differences between the PWR and BWR specimens. Typical BWR surveillance specimens differ from PWR specimens in certain well-defined ways, as described in Table 4-1. The ranges of irradiation temperature, flux and fluence are all narrower, and centred about lower values for the typical BWR samples. Any errors in the trend ascribed to temperature, or in the dependence of hardening on fluence at low fluences, can be offset by the effective flux term, since there is a strong correlation between flux and fluence, and the BWR irradiation temperature range is very narrow. In addition to these obvious differences between BWR and PWR samples, any "hidden" variables between the two types of reactor, such as may be caused by differences in manufacture (as already considered in Section 3.2.2) may also be offset by the optimization of the effective fluence term.

Table 4-1
Comparison between typical BWR and PWR irradiation conditions

Property	Range In LWR Surveillance Database For	
	Typical BWR	PWR
Temperature (F)	527 – 534	522 – 562
Flux (n/cm^2-s)	$1.1x10^9 – 1.9x10^{10}$	$1.9x10^{10} – 8.4x10^{11}$
Fluence (n/cm^2)	$2.3x10^{17} – 2.9x10^{18}$	$5.7x10^{17} – 7.1x10^{19}$

If the flux term in the MF and CRP components is being required to account for non-flux differences between PWR and BWR conditions, then this will affect its usefulness in extrapolation. It will be for the statistical assessment to find out whether any differences between BWR and PWR samples can be accounted for in a more appropriate manner.

4.1.3 Assessment of Overall Form and MF Component

4.1.3.1 General Comments

The overall form of this correlation is as expected, in that it defines two components of hardening embrittlement: a copper-related component (CRP in Equation 4-1) which may be associated with the precipitation of Cu-enriched solute clusters, and another component (MF). The use of two components of this form is common in both the previous U.S. embrittlement correlations, and also in U.K. embrittlement correlations for both CMn steels [28] and MnMoNi [49, 50]. There has been discussion in the literature concerning the use of linear addition of components, root sum of squares (RSS) addition, or a mixture of the two [e.g. 28], and this is also discussed in [13]. Although it is probable that a mixture of the two addition modes would be better justified mechanistically, this is significantly more difficult to apply to data in the form provided by the surveillance databases. It is therefore, justifiable to use either linear addition or RSS addition of components.

The MF component is derived from the hardening of low-Cu steels, with "low" being defined as 0.072wt.% (see Equation 4-5 and Equation 4-6). The derivation of this limit is described in [13], and is both reasonable and in accordance with other work in this area.

A new aspect of this work lies in the interpretation of the component derived from the embrittlement behaviour of low-Cu steels. It is clear from [13], that the MF component is not considered to be due to matrix damage, as defined in Chapter 3, but to the hardening/embrittlement from MNPs and phosphides. If MNPs and phosphides are the major contributors to the MF component, then the behaviour of the MF term will reflect the behaviour of these precipitates rather than that of MDs. This affects the mechanistic expectations of the character of the correlation in several ways:

- It is plausible that the nature of MDs and, hence, the hardening caused by them, are not strongly affected by the presence of Cu, although these properties are known to be affected by the presence of C and N. It is less plausible that the behaviour of MNPs and phosphides will be unaffected by the presence of Cu. The incorporation of Mn, Ni and P into CRPs might be expected to delay or suppress MNP formation, when the steel Cu content is increased, alternatively Cu may assist in nucleating MNPs. Similarly, the effect of P on embrittlement has been found to be more significant in low-Cu steels in the French surveillance program [51]. If the MF component of damage is delayed or reduced in the presence of Cu, then the linear addition of components will overestimate the combined hardening in higher-Cu steels; the use of RSS addition (as in the latest Japanese embrittlement correlation [29]) would be more appropriate.

- If MNPs are the major contributors to the MF component, then the influence of flux in increasing the substitutional solute diffusion rate will be observed in the MF term. If, conversely, MDs are the major contributors to the MF term, then no effect of flux will be expected below the flux threshold for UMD formation. (The effect of flux on P precipitation is likely to be difficult to assess since P can diffuse by both a vacancy and an interstitial mechanism [52].)
- If MNPs are the major contributors to the MF component, then the fluence-dependence of hardening from these solute clusters would be expected to be similar in form to that from CECs i.e. a tanh term. The use of a √fluence term is consistent with dominance by hardening features which increase linearly in number with fluence, as is found for MD. The interpretation of the flux term and the form of the fluence dependence used in the MF component are not readily associable.

The mechanistic plausibility of Equation 4-1 and Equation 4-2 therefore depends on the relative importance assumed for MDs and MNPs as contributors to the MF component. Appendix A therefore examines the IVAR data on low-Cu model steels, and data on Mn-Ni-Si precipitation in the literature in general, to assess the degree of support provided for the inclusion of a flux effect in the MF term for the LWR surveillance database.

4.1.3.2 Occurrence of Mn-Ni-Si Solute Clusters

The examination of data in Appendix A concludes that several possibilities exist concerning the occurrence of Mn-Ni-Si solute clusters, as summarized below:

1. MNP formation is thermodynamically favored above ~0.6Ni, 1.2Mn (as indicated by steels in which MNPs have been observed), but not below these Ni and Mn levels. If this is so, then about half of the low-Cu steels in the U.S. LWR surveillance database could not produce MNPs at any flux/fluence. The data from steels which could produce MNPs come from both BWR and PWR irradiations.
2. MNP formation is thermodynamically possible in all of the low-Cu steels of the U.S. LWR surveillance database, regardless of their Mn and Ni contents (for which there is no experimental evidence either way), but only in the high flux-high fluence range bounded by actual observations of MNPs.
   In this case
   a. MNPs may dominate MF embrittlement in some (~15) PWR surveillance samples,
   b. MNPs will not contribute to MF embrittlement in BWR surveillance samples.

3. Both the composition and flux/fluence limitations hold.
   In this case, then MNPs will contribute to MF embrittlement in 3-4 PWR surveillance samples.

If options 2 and 3 are correct, and MF embrittlement may be dominated by MNP precipitation, then a flux effect should be observed in the MF component of embrittlement of PWR samples, but not in that of BWR samples. In this context it is worth recalling that, during the development of sNRC2006, a flux effect was not observed when only the PWR data were used to form the correlation. It became necessary to introduce the effective flux terms only once the BWR data were included, and the effective fluence is identical with the measured fluence for most PWR surveillance samples. The likelihood that MNPs will be absent is thus greatest in that part of the database which sNRC2006 most requires their presence to explain the postulated flux dependence of matrix damage.

4.1.3.3 Flux

Overall, while MNP dominance of matrix damage is feasible, consistency in the interpretation of the data within the surveillance database, and between these surveillance data and data elsewhere in the literature, indicates that MNPs are not likely to be dominating the MF component of embrittlement in the surveillance database. They are, therefore, not ideal candidates as the source of a flux-dependence in the MF term.

The unstable matrix defects UMDs mentioned in Section 3.2.2 would also produce a flux effect but, as already mentioned, they are currently thought to contribute to hardening only at fluxes $>1\text{-}5\times10^{12}$n/cm^2-s. As shown in Chapter 2, very few of the data points in the U.S. LWR surveillance database were produced at these high flux levels, so UMDs are also not ideal candidates as the cause of a flux effect in the database.

Odette has mentioned that point defect-substitutional solute complexes (of which MNPs may be an extreme form) would develop at a flux-dependent rate. It is difficult to assess the hardening to be associated with such features, not least because, by analogy with strain ageing, the incorporation of substitutional solutes into complexes is likely to be slower, and lead to less hardening than the incorporation of interstitial solutes such as C and N. If C and N combine with point defects in MnMoNi steels to form complexes, as they do CMn steels [53], they will do so very rapidly. The additional hardening associated with the (flux-dependent) diffusion of substitutional solutes to the C/N-point defect complexes is likely to be small.

In summary, it is difficult to identify a microstructural source for a flux-dependent hardening contribution for steels of the compositions of the U.S. surveillance database under the irradiation conditions of the database.

The absence of a flux effect in low-Cu steels is supported by data from Dohi et al [54] who compared the hardening in low-Cu (0.06wt.%) MnMoNi plate (EP2) and forging (EF2) irradiated at different fluxes and moderate fluences (7×10^{10}-10^{12} n/cm^2-s at 10^{18}n/cm^2, or 2×10^{11}-5×10^{12} n/cm^2-s at 10^{19}n/cm^2), and found no flux effect within scatter. These steels had lower Ni (0.59 and 0.73wt.%, respectively) than the IVAR steels, and levels of Mn (1.49 and 1.3wt.%, respectively) between the IVAR medium and high values. The Ni and Mn values of EP2 and

EF2 were thus more representative of the steels in the surveillance database. In addition, Jones et al [55] could also find no effect of flux on the hardening of C-Mn steels (Ni<0.2wt.%, Mn=1-1.4wt.%) irradiated in the flux range $1.7x10^{-12} - 4.6x10^{-8}$ dpa/s at irradiation temperatures of 150°C – 300°C.

If the MF term derived from statistical analysis of the LWR surveillance database is, indeed, more due to MDs than to MNPs, then the use of linear summation of the MF and CRP components is better justified, but the use of the flux-dependent, effective fluence in the MF term is less well justified.

4.1.3.4 Mn and Product Form

The bulk Mn is correlated with product form within the surveillance database in that forgings show the lowest Mn levels, and welds the highest. The range of Mn in plate lies within the range shown by welds. It is, therefore, possible, that Mn effects could appear in the product form dependence in a correlation derived from the LWR surveillance database. Mechanistically, effects both of product form and of Mn on the hardening and embrittlement of low-Cu steels are well-supported by the literature.

Mn has been found to increase the radiation-induced hardening in simple Fe alloys [56, 57], and in CMn steels [58] (i.e. steels with <0.1wt.%Ni). The effect of Mn is reduced as the irradiation temperature increases [56], and when the dissolved ("free") C and N level of the alloy/steel is reduced. In the presence of an explicit Mn term, then, the product form term, A, would not be required to describe Mn effects, but could be required to indicate the ratio of strong carbide/nitride formers (e.g. Cr, Mo, V, Al, Ti) to bulk C and N and, hence the free C and N levels in steels of different forms. (A difference in the hardening of plate and forging was observed in [16, 26]. No unambiguous cause of the difference was determined, but the various observations were consistent with an effect of free C.) It is, therefore reasonable to include both an explicit Mn dependence and a product form dependence within the MF component of the embrittlement correlation.

It was suggested within [13] that there are both product form and explicit Mn terms in the MF component because the ratio of Ni to Mn within the LWR surveillance database correlates with product form, and both Ni and Mn levels contribute to MNP development. Thus there are mechanistic reasons for including the two terms regardless of the assumptions made as to the cause of embrittlement in low-Cu steels.

It should be noted, however, that the Mn levels measured in atom probe (AP) samples are not found to be strongly related to the bulk Mn levels. The two types of measurement are shown in Figure 4-3 for materials examined within the EPRI-CRIEPI program. The relatively low levels of Mn in solution (even in the unirradiated samples) are due to the precipitation of Mn in M_3C carbides and MnS inclusions (in the less clean steels) during heat treatment prior to irradiation.

Overall, then, it is mechanistically plausible that there should be both Mn and product form terms in the MF component of sNRC2006, although the explicit dependence on bulk Mn may not be very strong in the Mo-containing steels of the LWR surveillance database.

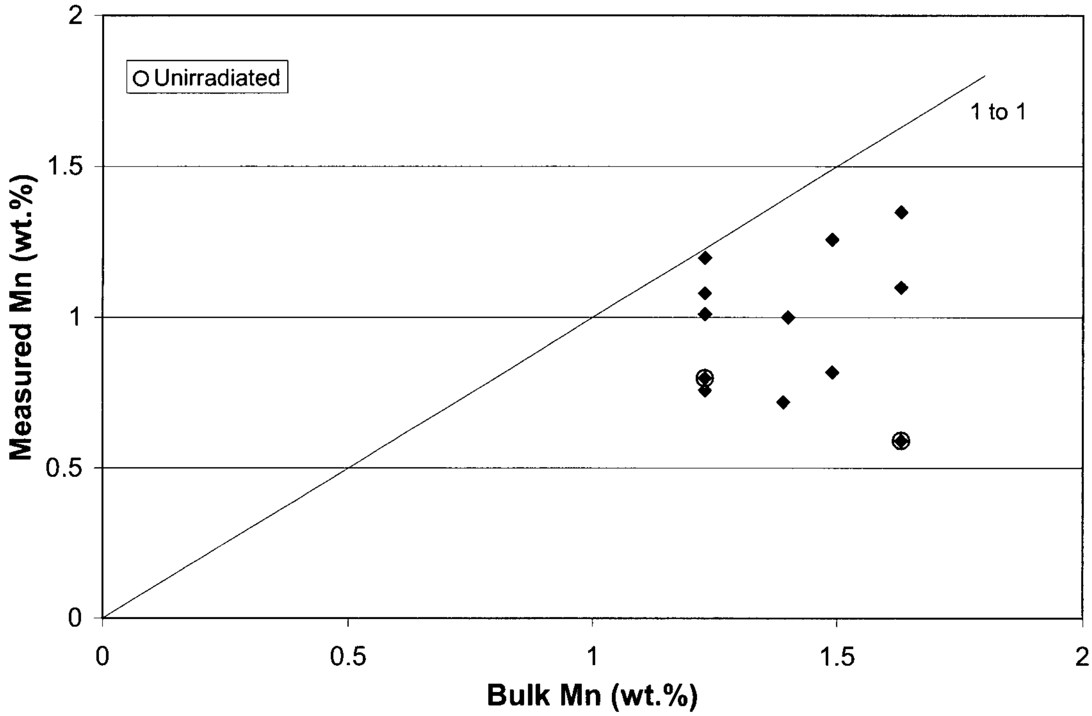

Figure 4-3
Relation between bulk Mn levels and Mn measured in atom probe for plate and weld steels of the EPRI-CRIEPI program

4.1.3.5 Phosphorous (P)

As shown in Figure 4-1, increasing P is well known to increase the radiation hardening in low-Cu steels, and the effect is greater in the presence of Mn. It is, therefore, reasonable that a positive P term should appear in the MF component, and be associated with a Mn term.

It is thermodynamically plausible that Mn_3P precipitates should form in the MnMoNi steels, in which case the cross-product between Mn and P could relate to this reaction. When P clusters have been observed using atom probe (AP), however, these are rarely associated with Mn atoms. It is possible that Fe_3P precipitates are formed. A less direct interaction between Mn and P may also be envisaged, with both elements affecting the size of MD clusters/dislocation loops, and P decoration of the MD features then affecting the resultant hardening. (An equivalent process involving C and N could also be ascribed to the cross-product involving product form.)

4.1.3.6 Temperature

A linear temperature dependence for matrix damage is well supported by the literature on many kinds of steel (CMn, MnMoNi, FeCr, FeCrNi...), as reviewed in [13 and 59]. (There are insufficient data available in the literature to show what sort of temperature-dependence is anticipated for Mn-Ni-Si precipitates and P clusters, but it is plausible that this would resemble the temperature-dependence of CRP hardening more than that of MD hardening.)

4.1.3.7 Other Effects

It has been suggested that the effective fluence term is optimized to incorporate not only flux effects, but also the non-flux differences between BWR and PWR surveillance samples (such as temperature, and unknown heat treatment effects). Although there is no convincing evidence for a flux effect in the low-Cu steels of the LWR surveillance database, the goodness of fit between the typical BWR data, and predictions of their embrittlement when the MF component includes the effective fluence term may be related this compensation for non-flux effects.

4.1.4 Summary of Mechanistic Assessment of sNRC2006

The mechanistic assessment of sNRC2006 indicates that it is largely of a form which is supported by evidence from the literature. The only clear exception is that the P term in the CRP component is positive, which indicates that the effect of P is predicted to be stronger in a Cu>0.072wt.% steel than in a Cu<0.072wt.% steel. This is in contradiction to experimental observations, which would support a negative coefficient for P, or an inverse P term in the CRP component.

The treatment of flux in sNRC2006 is open to question although, given the availability of data in the literature and the nature of the U.S. LWR surveillance database, reasonably credible. Evidence from the IVAR database indicates that it is plausible that the MF component should contain a flux term, but the assessment made in this Chapter and Appendix A indicate that it is more plausible that there should not be a flux term in the MF component. Similarly, the results of the EPRI-CRIEPI program indicate that there should be a flux term in the CRP component both inside the tanh function and outside it. sNRC2006 only contains a flux term inside the tanh function. This, however, may be the result of statistical significance within the surveillance database or parameter confounding. Confounding is most likely to be between flux and temperature. Such confounding would make terms in temperature and flux difficult to identify independently, and could explain the removal of the temperature terms also.

4.2 Mechanistic Assessment of RM-6(2)

4.2.1 Description of Correlation RM-6(2)

The development of an embrittlement correlation to replace Reg. Guide 1.99, Rev. 2 is described in some detail in [14]. The form of the correlation is described as it is taken through a number of revisions. Since [14] is explicitly described as a draft report, the form of the correlation is subject to further revision. The present review uses the last revision described in [14] as the main basis for assessment. This is revision RM-6(2). There have, however, been further revisions made to this correlation, and version RM-9 [60] is considered at the end of this Chapter.

RM-6(2) is in two parts, one applicable to fluences $\leq 3\times10^{19}$n/cm^2, and the other to higher fluences. The higher-fluence part thus applies to ~7% of the PWR points in the LWR surveillance database, to none of the typical BWR points and to ~18% of the atypical BWR data points. Since the aim of the work reported here is to assess the usefulness of the correlations for predicting BWR behaviour, the higher-fluence part of RM-6(2) will be given, but not assessed.

4.2.1.1 Lower-Fluence Form of RM-6(2)

The lower-fluence part of RM-6(2) is as described in Equation 4-8 to Equation 4-16:

$$\Delta T_{30} = \Delta T_{30(MD)} + \Delta T_{30(CRP)}$$ **Equation 4-8**

Where ΔT_{30} = shift in the 30 ft lb (40J transition temperature caused by irradiation, in °F)
$\Delta T_{30(MD)}$ = shift due to matrix damage
$\Delta T_{30(CRP)}$ = shift due to copper-rich precipitates

and

$$\Delta T_{30(MD)} = PF_{MD}(1+35P)\left(\frac{T}{550}\right)^{-14.64}\left\{\log\left(\frac{\phi}{10.7}\right)\right\}^{-3.44}\sqrt{\Phi}$$ **Equation 4-9**

in which P = bulk P content (wt%)
T = irradiation temperature (F)
ϕ = flux (n/cm^2-s)
Φ = fluence (n/cm^2)

$PF_{(MD)}$ = product form coefficient for matrix damage = 6.7×10^{-9} for welds
8.1×10^{-9} for plates
4.75×10^{-9} for forgings.

Equation 4-10

and

$$\Delta T_{30(CRP)} = PF_{CRP}\cdot CF_{CRP}\cdot TF_{CRP}.\Phi F_{CRP}$$ **Equation 4-11**

where PF_{CRP} = product form coefficient for CRPs = 0.301 for welds
0.233 for plates
0.233 for forgings **Equation 4-12**

$$CF_{CRP} = [f(Cu)+2500.3\cdot MIN\{0.32, MAX(0, Cu-0.048)\}\cdot Ni]$$ **Equation 4-13**

$f(Cu) = -116.3 + 530.8\sqrt{Cu}$, subject to 0≤f(Cu)≤118.5 (equivalent to 0.048≤Cu≤0.196)

Equation 4-14

where Ni = bulk Ni content (wt.%)
Cu = bulk Cu content (wt.%)

$$TF_{CRP} = \left(\frac{T}{550}\right)^{-1.74}$$

Equation 4-15

$$\Phi F_{CRP} = 1 - \exp\left[\frac{-\Phi}{2.38x10^{18}}\right]$$

Equation 4-16

4.2.1.2 Higher-Fluence Form of RM-6(2)

The higher-fluence part of RM-6(2) is effectively the correlation developed by Chaouadi et al to describe hardening in their database of hardening under high-flux irradiations (RADAMO) [43, 61, 62]. The correlation is given in Equation 4-17 to Equation 4-24.

$$\Delta T_{30} = \begin{Bmatrix} weld = 1.39 \\ plate = 1.18 \\ Forging = 0.84 \end{Bmatrix} \left\{\Delta YS_{MD} + \sqrt{\Delta YS_{CRP} + \Delta YS_{PRP}}\right\}$$

Equation 4-17

where

$$\Delta YS_{MD} = \begin{Bmatrix} 0 \quad \text{if fluence} < 1x10^{19}\,\text{n/cm}^2\text{, otherwise} \\ \left\{585\exp\left[-1250\exp\left(-\frac{0.345}{kT}\right)\right] + (3880 - 6.3T)\cdot Ni\right\}\sqrt{1 - \exp\left[-0.01(\Phi - 1x10^{19}\right]} \end{Bmatrix}$$

Equation 4-18

in which k = Boltzman's constant, and T is now in Kelvin, and

$$\Delta YS_{CRP} = \Delta_{CRP(Peak)} \cdot f(\phi, t.T, Cu)$$

Equation 4-19

$$\Delta_{CRP(Peak)} = \begin{Bmatrix} 0 \text{ if Cu} \leq 0.03\text{wt.\%, otherwise} \\ 215 \cdot (1 - \exp[2.7(\text{Cu} - 0.03)]) \end{Bmatrix}$$

Equation 4-20

$$f = \begin{cases} 0 & \text{if } t < \dfrac{t_{peak}}{20} \\ \dfrac{1}{Log(20)} \cdot Log\left(20 \dfrac{t}{t_{peak}}\right) & \text{if } \dfrac{t_{peak}}{20} \le t < t_{peak} \\ 1 & \text{if } t \ge t_{peak} \end{cases}$$

Equation 4-21

$$t_{peak} = \frac{10^{\left\{\frac{9677}{T} - \left(15.3 - 0.3/Cu\right)\right\}}}{1 + 6x10^{-20} \exp\left[-\frac{E_0}{kT}\right]} \quad \text{where } E = \begin{cases} E_0 \text{ if flux} < 6x10^{12} 12 \text{ n/cm}^2\text{, otherwise} \\ E_0 + 0.03 Log\left(\dfrac{\phi}{6x10^{12}}\right) \end{cases}$$

Equation 4-22

$$E_0 = -kT \cdot Ln\left\{\frac{6x10^{-20}}{10^{\left\{\frac{9677}{T} - \left(15.3 - 0.3/Cu\right)\right\}} \Big/ t_{peak,\max}}\right\}, \ t_{peak,\max} = t_{peak} \text{ when Cu} = Cu_{max} = 0.425\text{wt.\%}$$

Equation 4-23

$$\Delta YS_{PRP} = (44470.5 - 70T) \cdot (P - 0.012) \ \text{(T in Kelvin)}$$

Equation 4-24

4.2.2 Comparison Between Overall Forms of RM-6(2) and sNRC2006

RM-6(2) is less clearly presented as a mechanistically-supported correlation than sNRC2006, but the low-fluence part has many features which are similar to those in sNRC2006. For the matrix damage component:

- Both correlations contain a dependence on product form, which may incorporate chemistry/heat treatment components difficult to identify explicitly. In both correlations the coefficient for forgings is smaller than that for plates, which is smaller than that for welds. The actual values of the coefficients are smaller in RM-6(2).
- The explicit chemistry dependence for matrix damage in RM-6(2) includes only P, while that for sNRC2006 uses a cross-product between P and Mn. The dependence is generally stronger in RM-6(2), which would be equivalent to the term in sNRC2006 for a Mn level of ~2%.
- Both correlations have a temperature dependence in the matrix damage component, which decreases the embrittlement from matrix damage with increasing temperature. The dependence in RM-6(2) is stronger than in sNRC2006, and does not conform to the known linear temperature-dependence of matrix damage.

- The combination of the product form, chemistry and temperature terms is very similar for Mn levels around 1.0wt.%. (Most low-Cu steels in the surveillance database contain >1.0wt% Mn, see Appendix A Figure A-2).
- In both correlations, the matrix damage is proportional to the square root of fluence, and decreases with increasing flux. The flux dependence is, quantitatively, almost identical in the two correlations (despite the difference in mathematical form), up to 4.39×10^{10}n/cm^2-s. Above this flux the flux term in sNRC2006 is kept at unity while the term in RM-6(2) continues to decrease.

For the CRP component:

- The bulk level of Cu below which CRP embrittlement is negligible is lower in RM-6(2) than in sNRC2006 (0.048 versus 0.072wt.%).
- A maximum effective Cu level is found in both correlations. In sNRC2006, the level is 0.301 for all materials other than Linde 80 welds, for which it is 0.243. In RM-6(2), the maximum effective Cu is the same for all product forms and (in f(Cu)) is lower, at 0.196. There is, however, a term in RM-6(2) which may be either a cross-product between (Cu-0.048) and Ni or 0.32Ni, which suggests that, in the presence of Ni, the maximum effective Cu is 0.368.
- The product form term in RM-6(2) distinguishes between plate/forging and weld, and does not find a difference between CE plates and non-CE plates/forgings. This is consistent with the use of a constant maximum effective Cu (see Section 3.1.2.2). Since an effect of CE *versus* non-CE plate and Linde 80 *versus* other welds is seen in the literature, this may render RM-6(2) less sensitive to product form/manufacturing heat treatment effects than sNRC2006.
- The fluence-dependences in the two correlations are similar, with hardening increasing slowly at low fluences, increasing more rapidly at intermediate fluences, then slowing and reaching a plateau at high fluences. The rate of approach to the plateau is not, however, affected by Cu and Ni levels in RM-6(2).
- At mean levels of Ni and Cu, CRP embrittlement in RM-6(2) starts more slowly, and ultimately approaches the plateau more slowly than sNRC2006; the embrittlement rates w.r.t. fluence are very similar at $\sim 2 \times 10^{18}$n/cm^2.
- The magnitude of the plateau level of embrittlement (the plateau height) is dependent on Cu, Ni, and a cross-product between Cu and Ni in both correlations, although sNRC2006 also includes an effect of P at moderate and high P levels.
- The explicit composition-dependence of the plateau heights is stronger in RM-6(2) than in sNRC2006, while the product form dependence is weaker. The combination of product form and chemistry terms has similar magnitudes in the two correlations for Ni levels ~0.5wt.%. The rate of increase in the plateau height with Cu is more marked in sNRC2006 for higher levels of Ni (and P>0.008wt.%).
- In RM-6(2), the rate of approach to the plateau is not affected by flux.
- In RM-6(2), the hardening from CRPs is temperature dependent. The temperature-dependence of CRPs was removed during the simplification of NRC2006, as being statistically insignificant.

Again, linear addition of $\Delta T_{30(MD)}$ and CRP terms is used.

4.2.3 Assessment of Low-Fluence Form of RM-6(2)

Since the two correlations have many features in common, most of the qualitative assessments made for sNRC2006 also apply to (the lower-fluence form of) RM-6(2).

If the product form term is assumed to contain implicit chemistry and heat treatment effects, then it is plausible that the absence of the Mn dependence in the matrix damage component of RM-6(2) is accounted for within the product form dependence. (The weld and plate values of $PF_{(MD)}$ are higher than the forging value of $PF_{(MD)}$ to a greater degree than the weld and plate values of A are higher than that of forging. This could compensate for the absence of a Mn term, since Mn is higher in plate and weld than it is in forgings.)

As was mentioned in connection with sNRC2006, the presence of a flux-dependence in the matrix damage term of RM-6(2) is not strongly supported by evidence from the literature. The absence of the flux dependence in the CRP term of RM-6(2), where its presence would be supported from the literature, suggests that the partitioning of embrittlement from different mechanisms between the $\Delta T_{30(MD)}$ and $\Delta T_{30(CRP)}$ terms is not precise. The form of the $\Delta T_{30(MD)}$ term may be required to compensate for insufficiencies in the form of the CRP term. In this context, it is worth noting that the initial RM $\Delta T_{30(MD)}$ terms were assumed to contain flux-dependences [14].

The fluence dependence in the $\Delta T_{30(MD)}$ term is of the order expected. The fluence dependence in the CRP term (i.e. the {1-exponential} form) may have been chosen to reflect one of the general functions describing rates of precipitation. It is not clear that the precise variant used here is strictly applicable to the full progress of irradiation-induced precipitation; it is also unclear that hardening is directly related to precipitate volume fraction (as discussed earlier). Thus the exponential function chosen for the fluence dependence of CRP hardening is not much more mechanistically justified than the tanh function used in sNRC2006. Again, a plateau in CRP hardening rather than a maximum is indicated but, as has been discussed previously, this is probably justified by the range of surveillance data and the possibly weak dependence of hardening on precipitate size over the experimentally-observed size ranges.

A comparison between the fluence-dependences in RM-6(2) and sNRC2006, i.e. between ΦF_{MD} and g (for 0.14Cu and 0.57Ni, which are the average levels of Cu and Ni across the surveillance database), is given in Figure 4-4. The RM-6(2) function increases more slowly at low fluences and high fluences, but more rapidly at intermediate fluences. Increasing the Cu level or decreasing the Ni level reduces the difference between the two curves at low fluence, but has little effect at high fluence.

The slight differences in the CRP fluence dependences probably account for the differences in, e.g. the maximum and minimum values for Cu. The choice of a different maximum value for Cu in the cross-product with Ni could relate to the higher degree of hardening per wt.% Cu in the presence of Ni, and to the higher solubility limit for Cu in the presence of Ni.

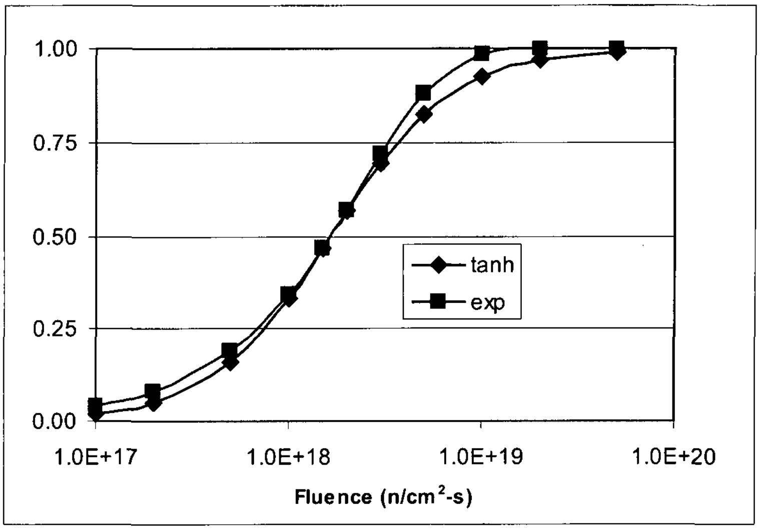

Figure 4-4
Comparison between fluence-dependences of hardening in RM-6(2) ("exponential") and sNRC2006 ("tanh") for average levels of Cu and Ni

The presence of a temperature-dependence in the CRP component is in accordance with observations in the literature [48].

4.3 Comments on RM-9

RM-9 differs from RM-6(2) in the $DT_{30(CRP)}$ term; the $DT_{30(MD)}$ term is unchanged. The new $DT_{30(CRP)}$ term is given in below:

$$\Delta T_{30(CRP)} = PF_{CRP} \cdot CF_{CRP} \cdot TF_{CRP} \cdot \Phi F_{CRP}$$ **Equation 4-25**

where PF_{CRP} = product form coefficient for CRPs = 0.300 for welds
0.233 for plates
0.235 for forgings.
Equation 4-26

$$CF_{CRP} = \left[f(Cu) + 2500.3 \cdot MIN\{0.32, MAX(0, Cu - 0.048)\} \cdot Ni\right]$$ **Equation 4-27**

$f(Cu) = -115.8 + 530.8\sqrt{Cu}$, subject to $0 \le f(Cu) \le 118.5$ (equivalent to $0.048 \le Cu \le 0.196$)
Equation 4-28

where Ni = bulk Ni content (wt.%)

$$TF_{CRP} = \left(\frac{T}{550}\right)^{-1.74}$$ **Equation 4-29**

$$\Phi F_{CRP} = 1 - \exp\left[\frac{-\Phi}{\left(10 + 2.3Ni + 11\log\sqrt{\phi/10.7}\right)\left(10^{17}\right)}\right]$$ **Equation 4-30**

i.e. there are small changes to various coefficients, but the most significant alteration is the introduction of Ni and flux dependences within the exponential fluence function (Equation 4-30).

As has already been mentioned, effects of Ni and flux on the rate at which the maximum in Cu-related hardening is reached, are supported by the literature. The introduction of these terms is, therefore likely to improve the mechanistic justification for the RM correlation, and render it more applicable to data points from steel compositions/irradiation conditions further from the mean of the current LWR surveillance database. There is still, however, no dependence of the rate of CRP embrittlement on Cu, which would be expected on mechanistic grounds.

4.4 Summary

The forms of sNRC2006, RM-6(2) and RM-9 are all generally well-supported by a mechanistic understanding of the processes leading to RPV embrittlement. The smaller number of explicit product forms and chemistry effects in RM-6(2) appear to make the separation of MD and CRP effects into separate $DT_{30(MD)}$ and $DT_{30(CRP)}$ terms less clear than their separation into MF and CRP terms in sNRC2006. The modification which leads to RM-9 is a clear improvement from a mechanistic point of view.

The temperature-dependences of both RM-9 and sNRC2006 are not quite as expected in that there is no CRP temperature-dependence in sNRC2006, while the MD temperature-dependence in RM-9 appears to have been chosen without reference to the literature. Practically, however, the effects may not be statistically significant within the temperature range of the U.S. LWR surveillance database.

The treatment of flux in both RM-9 and sNRC2006 is open to question in that the flux dependence in the MF/MD component is not well supported in the literature, and the flux dependences in the CRP terms do not include the precipitate-size-dependence of embrittlement observed in the EPRI-CRIEPI program and elsewhere in the literature. In the light of the data in the IVAR database it is, however, very reasonable that the effect of introducing a flux term in the MF/MD component should have been investigated. In addition, the flux effect on precipitate size may not be observed with statistical significance within the U.S. LWR surveillance database.

5
COMPARISON BETWEEN PREDICTIONS AND MEASUREMENTS

5.1 Comparison Between Measurements and Predictions by sNRC2006

In Appendix F of [13], the authors of sNRC2006 compared the residuals (predicted DT – measured DT) with a number of individual parameters (considered separately for points with Cu≤0.072wt.% and Cu>0.072wt.%):

- fluence,
- flux,
- irradiation temperature,
- time of irradiation,
- Mn,
- P,
- Ni,
- Cu,
- Si,
- product form[6],

and also a number of composition cross-products:

- for Cu≤0.072wt.%,
  - $P*Mn^{2.47}$,
  - P*Ni,
  - Mn*Ni
- for Cu.0.072wt.%.
  - P*Mn,
  - P*Ni,
  - Mn*Ni,

[6] Plate forging or weld for Cu≤0.072wt.%. Forging, CE and non-CE plates, Linde 80, Linde 1092 and other welds and standard reference materials for Cu>0.072wt.%.

- Cu_e*Ni,
- Cu_e*Mn

In addition, the total predicted shift was compared with the measured shift.

For each plot, a distinction was made between BWR and PWR surveillance data, and between calibration and validation points. Overall, the residuals showed no significant trends. In [10 and 11], however, it was not the overall fit to the data, but the fits to certain sub-sets of the data which raised concerns about the applicability of previous correlations. In addition, the usefulness of the correlation in assessing the condition of operating BWR RPVs is shown better by its fit to the typical BWR surveillance data than to its fit to the atypical BWR data (as defined in Chapter 2). It therefore seems appropriate to examine subsets of the U.S. LWR surveillance database to assess the applicability of sNRC2006, focusing initially on the typical BWR surveillance data.

The comparison between the measured transition temperature shifts and the shifts predicted by sNRC2006 for BWR samples is shown in Figure 5-1. The Figure shows that the fit between measured and predicted DT is fairly good for most typical BWR specimens, but shows a slight tendency towards under prediction, which is most visible at measured shifts DT>75°C. Conversely, the (PWR-like) BWRb measurements are generally over predicted, especially in the DT range 90°C-120°C. The BWRa points (much higher-than-usual temperature and flux) are clearly under-predicted at all DT levels, as was recognized in [13]. If the typical BWR and BWRb points are taken together, the fit between measurement and prediction is very good, as found in [13]. This could be due to the increased number of points reducing the influence of scatter, or to a systematic difference between predictions of the different irradiation conditions.

Figure 5-2 compares the predictions of shifts with the typical BWR measurements for different product forms. The overall fit for the plate data is good, with the best fit line through the data being very close to the one-to-one line. It is possible that the non-CE plates are showing some under-prediction, offset by slight over-predictions for the CE plates, but this is not a marked effect. For the welds, however, the fit is much less accurate. Each weld type is under-predicted and, as is shown by the annotation to Figure 5-2b the overall under-prediction is ~20%, with reasonable significance. The bias in the predictions of the typical BWR data thus appears real. Combining typical BWR data and BWRb data disguises a real effect; it does not merely expand the amount of BWR data available for assessment.

Figure 5-3 investigates the source of the under-prediction by distinguishing between data from steels with Cu<0.072wt.% (for which only the MF component of the correlation contributes to the prediction) and those with Cu>0.072wt.% (for which both the MF and CRP component contribute). The best-fit line through the low-Cu data deviates far more from the one-to-one relationship than the line through the Cu>0.072wt.% data. It thus appears that there is a bias in the MF component which causes under-prediction with increasing shift, and this is offset by an opposing bias in the CRP component. For the compositions and irradiation characteristics represented by the data in Figure 5-3, the bias in the CRP term is weaker than that in the MF term, so the net result remains an under-prediction.

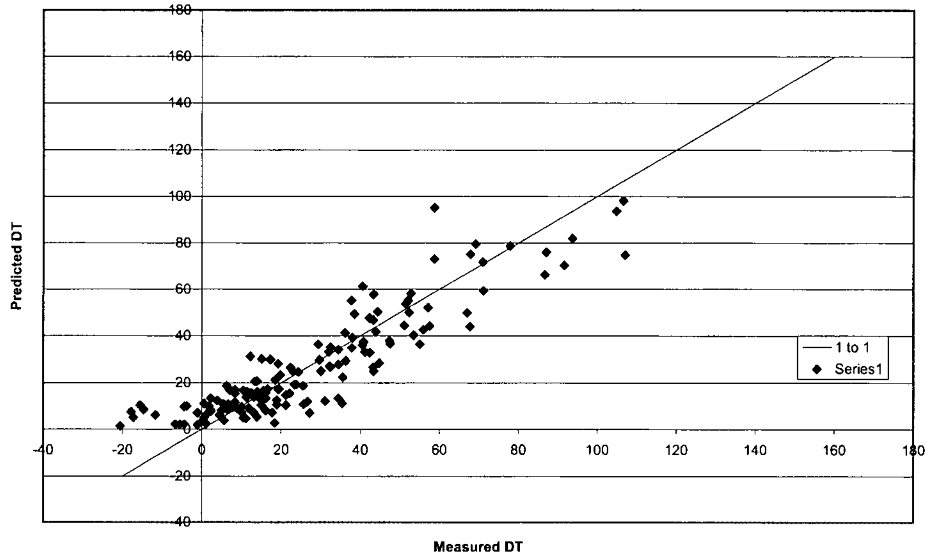

a) typical BWR data

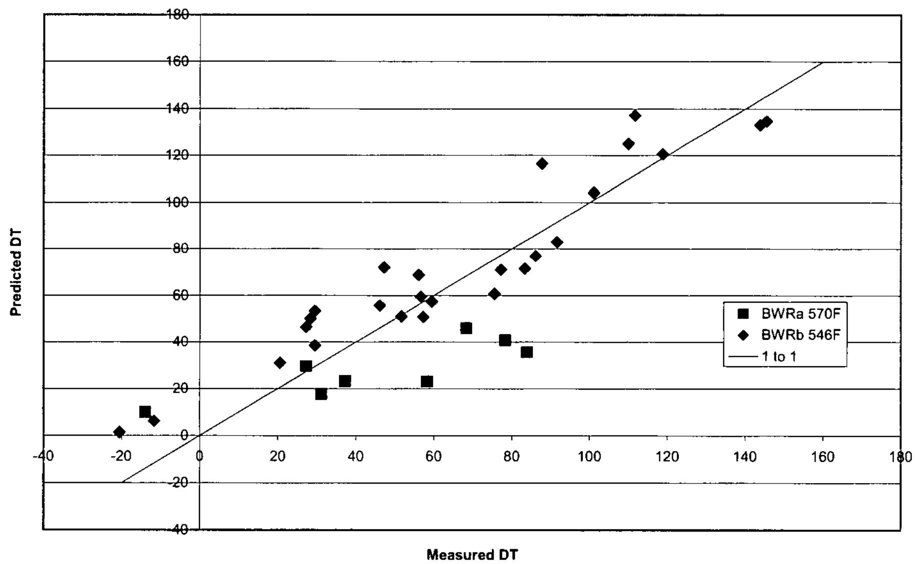

b) atypical BWR data

Figure 5-1
Comparison between measured DT and DT predicted by sNRC2006 for a) typical BWR surveillance data and b) atypical BWR surveillance data

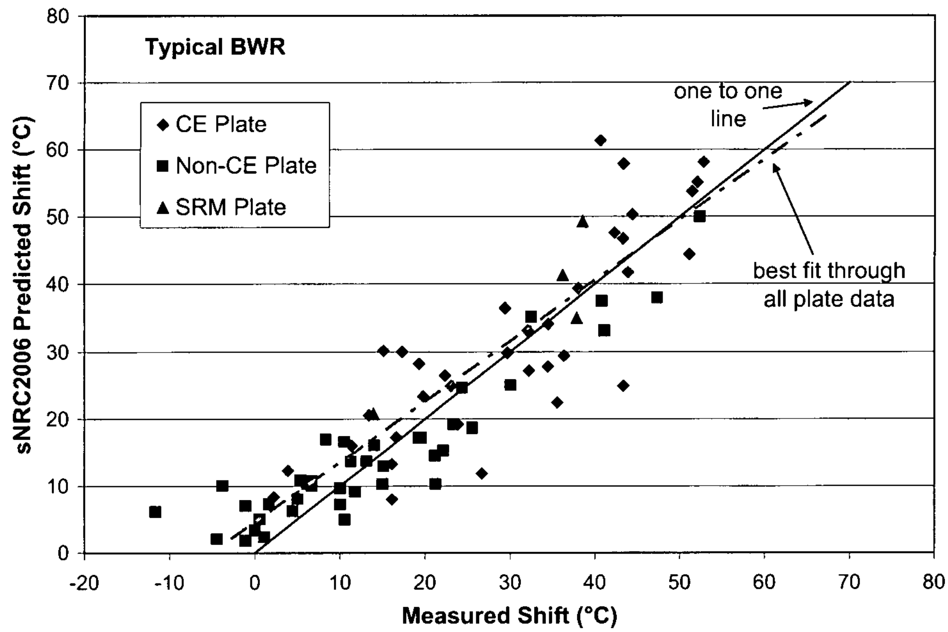

a) Plates

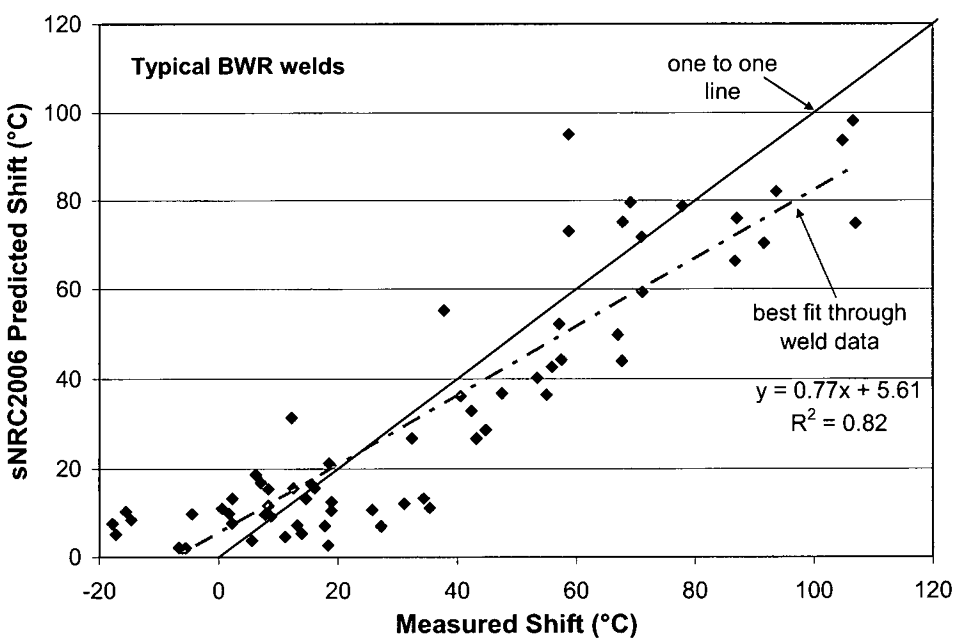

b) Welds

Figure 5-2
Comparison between DT measured in typical BWR specimens and DT predicted by sNRC2006 for a) plates and b) welds

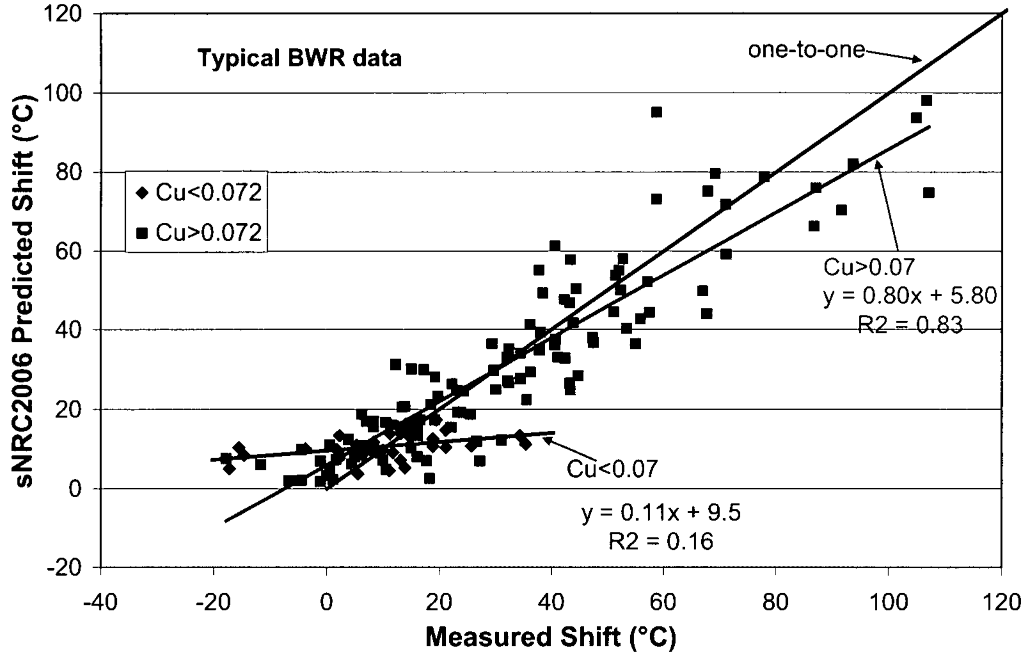

Figure 5-3
The effect of Cu content on the comparison between shifts measured in typical BWR samples and those predicted by sNRC2006

(Colored lines indicate the best fits through the data without constraints)

It is worth noting that the trend in the low-Cu data is affected by the uncertainties in the plotted values. There are uncertainties in the both the predicted and measured shifts. The uncertainties in the predictions come from uncertainties in the input parameters (e.g. fluence, irradiation temperature, P level...). These will combine to produce an uncertainty which cannot exceed the absolute value of the prediction. Thus, to some extent, the uncertainty on the prediction increases with the value of the prediction, and is small when the predicted shift itself is small. The uncertainty on the measured shift, however, is independent of the absolute value of the measured shift, being dependent on the accuracy with which the initial and final values of the DBTT can be measured. At low, DT, therefore, the uncertainty on the measured DT will be greater than that on the predicted DT. This alone will cause a scattering of the data in Figure 5-3 along the x-axis at low DT, and will reduce the slope of a line drawn through data points associated only with small range of DT.

The trends ascribed to Figure 5-3 are, however, likely to be real. This may be shown by limiting the number of Cu>0.072wt.% data points to those with shifts ≤ the highest shift shown by the low Cu points i.e. ~35°C. Even with this limit, it still appears that the best fit line through the higher-Cu points is closer to one-to-one than that through the lower-Cu points. An alternative assessment would consider only those low-Cu data points with measured shifts above ~20°C. At this shift, the mean value (and hence an exact prediction) would be greater than the standard deviation on the measurement (assuming a standard deviation of ~15°C on individual DBTT measurements). A line passing through these data points and the origin would have a slope of ~0.35. Although this is higher than the slope reported in Figure 5-3 (i.e. 0.11), it is still very far from one-to-one, and lower than the best fit line through the Cu>0.072wt.% data. In summary, the distribution of uncertainties may exaggerate the under-prediction of the low-Cu data, but there is still a greater under-prediction of the low-Cu data than of the Cu>0.072wt,% data.

In an early stage in this assessment [63], it appeared that plots of the residuals (measured DT minus predicted DT) versus the measured DT showed the tendency towards under-prediction at moderate-to-high shifts more clearly than the plots of predicted DT versus measured DT, and such plots were used extensively. Some examples are given in Appendix B. It is likely, however, that the uneven distribution of uncertainties affects the observed trends in these plots, without this being as explicitly visible as in simple plots of the predicted DT versus the measured DT. The remainder of this report, therefore, does not include plots of residuals. At that stage, it appeared appropriate to describe the distributions at low DT as exhibiting over-predictions. This may still be the case, but it would be difficult to confirm without a detailed examination of the errors associated with the low-shifting points (or points exhibiting negative shifts). The possibility of over-prediction at low shifts will not, therefore, be discussed further here.

Figure 5-4 shows a plot similar to that in Figure 5-3, but refers to both BWR and PWR samples in the low flux-fluence range. For the purpose of this plot, low-flux-fluence is defined with reference to the tanh fluence function, g in the sNRC2006 correlation. This function lies between 0 and 1 (Equation 4-7), and Figure 5-4 contains data for which g<0.5. The figure shows that both BWR and PWR specimens behave in the same way. There is a small under-prediction of the Cu>0.072wt.% data, and a larger under-prediction of the Cu<0.072wt.% data. This indicates that the under-predictions observed in Figure 5-1 and Figure 5-2 are not due to unspecified differences in the manufacturing history of BWRs and PWRs, but due simply to a poor fit between prediction and data at low fluxes and fluences.

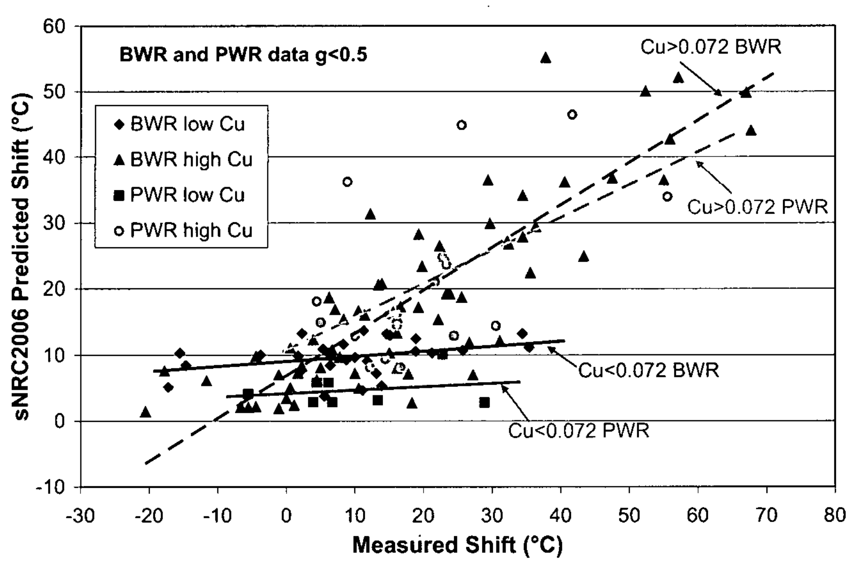

Figure 5-4
The effect of Cu content on the comparison between shifts measured in low-flux-fluence BWR and PWR samples and those predicted by sNRC2006 (Colored lines indicate the best fit lines through the data without constraint)

Figure 5-5 further investigates the source of the under-prediction by distinguishing between the fluxes experienced by low-Cu data in the surveillance database. At the very lowest flux range ($<5x10^9$n/cm^2-s), all the data are from typical BWR samples. The next flux range ($5x10^9$–$5x10^{10}$n/cm^2-s), includes both typical BWR and PWR data, while the higher flux ranges include only PWR data. As can be seen, there is an under-prediction at all fluxes, but it is stronger below $5x10^{10}$n/cm^2-s than at higher fluxes. Since the flux term in the MF component of sNRC2006 only operates below $4.39x10^{10}$n/cm^2-s, the figure indicates that the introduction of the flux term into the MF component does not improve the accuracy of the predictions of embrittlement in steels with Cu<0.072wt.%.

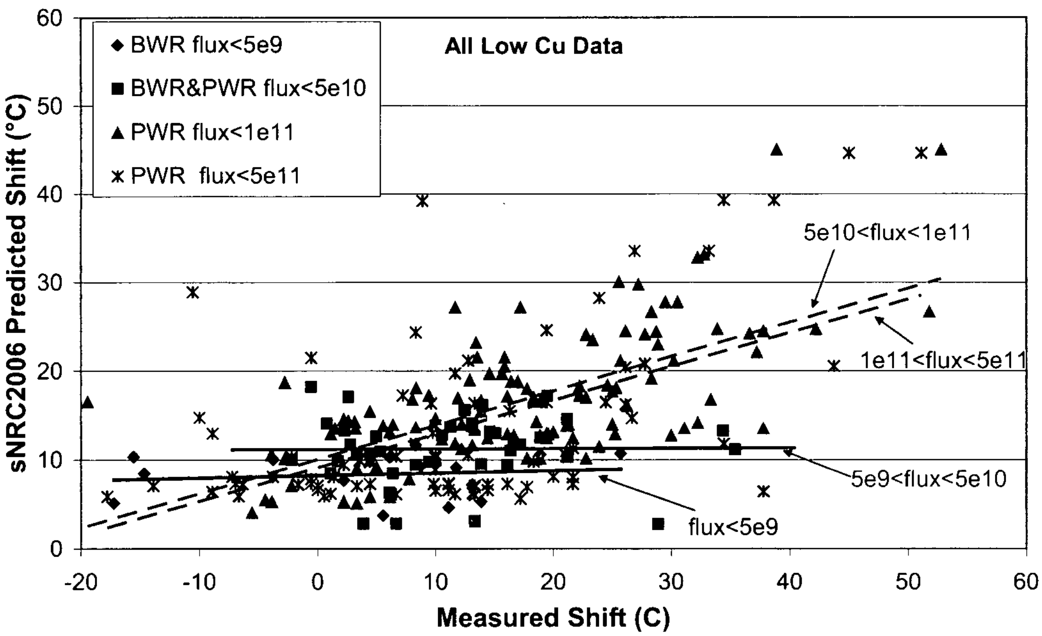

Figure 5-5
Effect of flux on comparison between measured DT and DT predicted by sNRC2006 for all the low-Cu steels of the U.S. LWR surveillance database (Colored lines indicate the best fits through the data without constraints)

Figure 5-6 shows an equivalent plot for the steels with Cu>0.072wt.%. Here it can be seen that the under-prediction of the MF component at fluxes $<5x10^{10}$n/cm^2-s does not lead to an overall under-prediction when both the MF and CRP components operate. There is no obvious change in the accuracy of the predictions with the onset of the effective fluence (i.e. the flux) term. This indicates that the under-prediction of the MF component (caused by the introduction of the effective fluence term) is balanced by an over-prediction of the CRP component at fluxes $< 5x10^{10}$n/cm^2-s. At fluxes between $5x10^{10}$n/cm^2-s and $5x10^{11}$n/cm^2-s, the predictions of embrittlement in the Cu>0.072wt.% steels are extremely good. Apart from aspects associated with the onset of the effective fluence term, Figure 5-6 does show that, overall, there is a slight under-prediction at the lowest fluxes ($<5x10^9$n/cm^2-s) and a slight over-prediction at the highest fluxes (flux $>5x10^{11}$n/cm^2-s). This may indicate that there may be a small continuous flux effect on the fit. Since there is no continuous flux term in sNRC2006, this could identify a requirement for a small, continuous flux term.

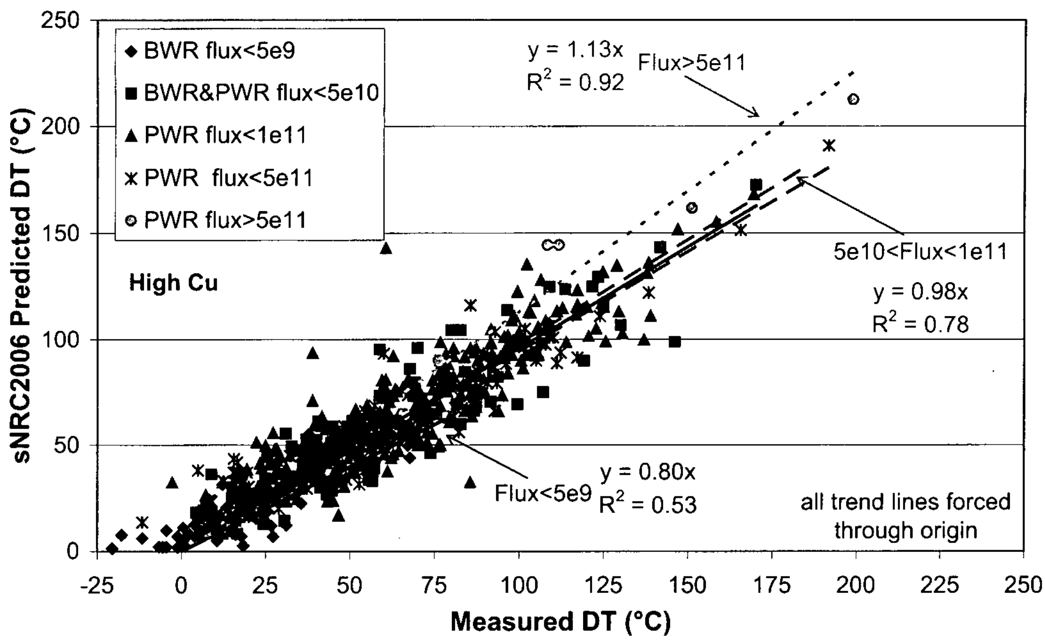

Figure 5-6
Effect of flux on comparison between measured DT and DT predicted by sNRC2006 for all the steels of the U.S. LWR surveillance database with Cu>0.072wt.%

(Colored lines indicate the best fits through the data without constraints)

Figure 5-7 attempts to discriminate between the effects of flux and fluence by plotting the predicted versus measured values of DT in terms of the CRP tanh fluence function, g (see Equation 4-7).[7] At g<0.5, for example, Cu precipitation is at less than a half the maximum level, regardless of the individual values of the flux, fluence, Cu and Ni contributions to g. The unconstrained best fits through BWR and PWR data are also drawn on the plots.

The figure shows that, as g increases, the fit between the measured and predicted values improves. Some of this will be the result of the decreasing influence of the points with negative measured shifts. Figure 5-7 shows an attempt to allow for this factor by constraining the best fit line through the BWR data to pass through the origin. The slopes of the best fit lines (free or constrained), and the associated R^2 values are given in Table 5-1. Forcing the lines to pass through the origin increases their slopes, as expected, with the effect being greater for g<0.5 than for higher levels of g. With or without constraint, however, Table 5-1 shows that (apart from BWRa specimens) specimens from BWR and PWR surveillance schemes behave in a similar way, and also that the deviation from one-to-one is greatest at lowest g levels.

[7] Note that the tanh function, g, has a finite value even when Cu<0.072. In steels with Cu<0.072, g is affected by fluence, flux and Ni content. Since the f-term in the CRP component goes to zero when Cu ≤0.072, the entire CRP component also goes to zero. For steels with Cu<0.072, therefore, the values of both g and the predicted DT are affected by flux and fluence, but g itself does not affect the predicted value of DT.

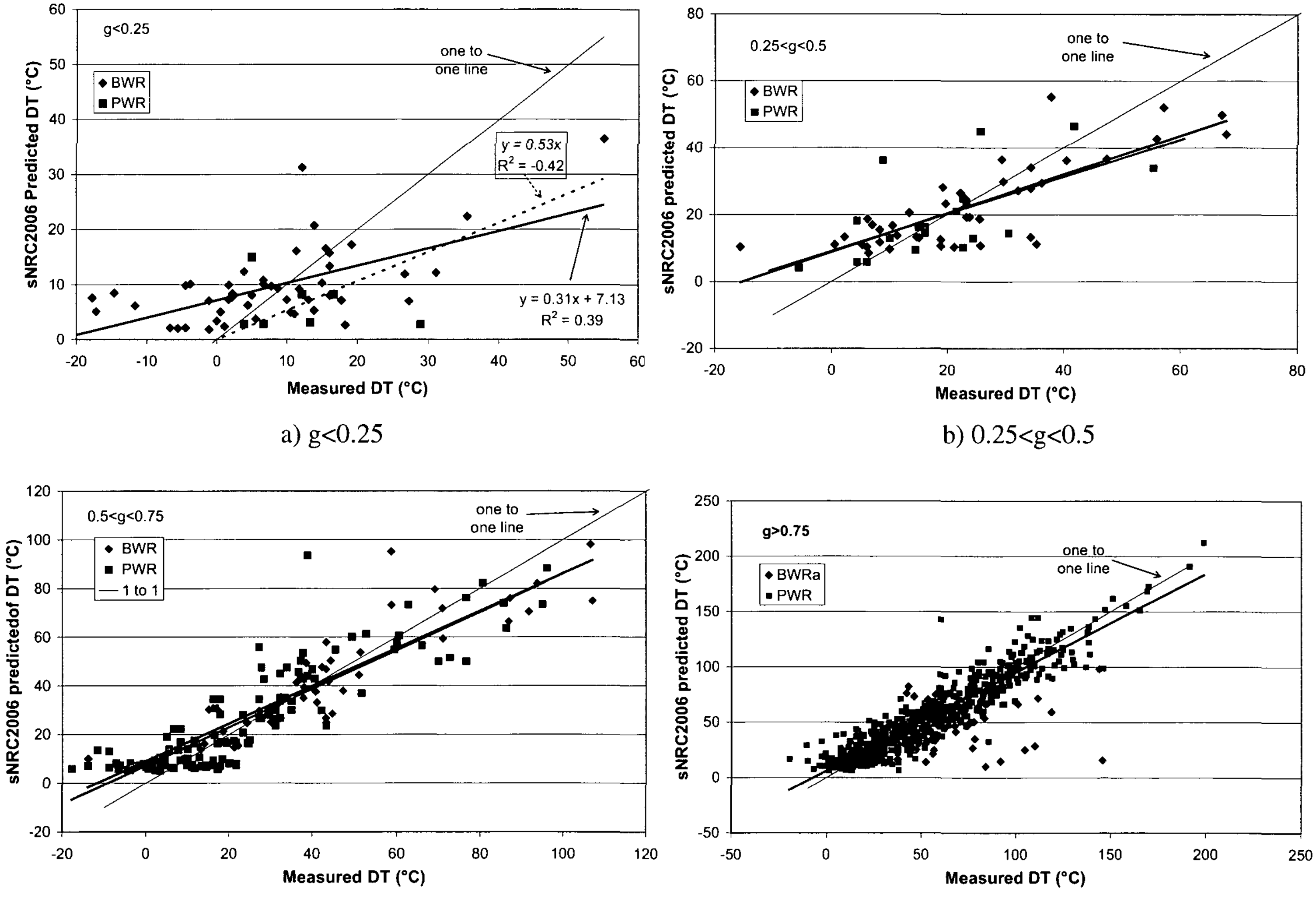

a) g<0.25

b) 0.25<g<0.5

c) 0.5<g<0.75

d) g>0.75

Figure 5-7
Comparison between measured shifts and shifts predicted by sNRC2006 at different levels of the CRP fluence function, g

Table 5-1
Properties of best fit lines through plots of measured shift vs. shift predicted by sNRC2006

Data Range	Reactor/Specimen Type	Properties of Best Fit Lines			
		Unconstrained		Forced Through Origin	
		Slope	R^2	Slope	R^2
g<0.25	Typical BWR	0.31	0.39	0.53	0.42
0.25<g<0.5	Typical BWR	0.58	0.66	0.82	0.48
	PWR	0.56	0.38	0.87	0.19
0.5<g<0.75	BWRb	0.79	0.77	0.94	0.71
	PWR	0.77	0.79	0.92	0.75
g>0.75	PWR	0.89	0.87	0.97	0.86

Figure 5-8 illustrates the distributions of samples at different g levels in the surveillance database. It shows that the distribution is heavily skewed towards high values of g. This is due to the distribution of the PWR, BWRa and BWRb specimens. Taken together the BWR data are fairly evenly distributed, since the reduction in typical BWR samples at g>0.8 is offset by the presence of BWRa and BWRb samples in this range. The typical BWR data provide most of the information on the fit of the tanh function at g values up to 0.6.

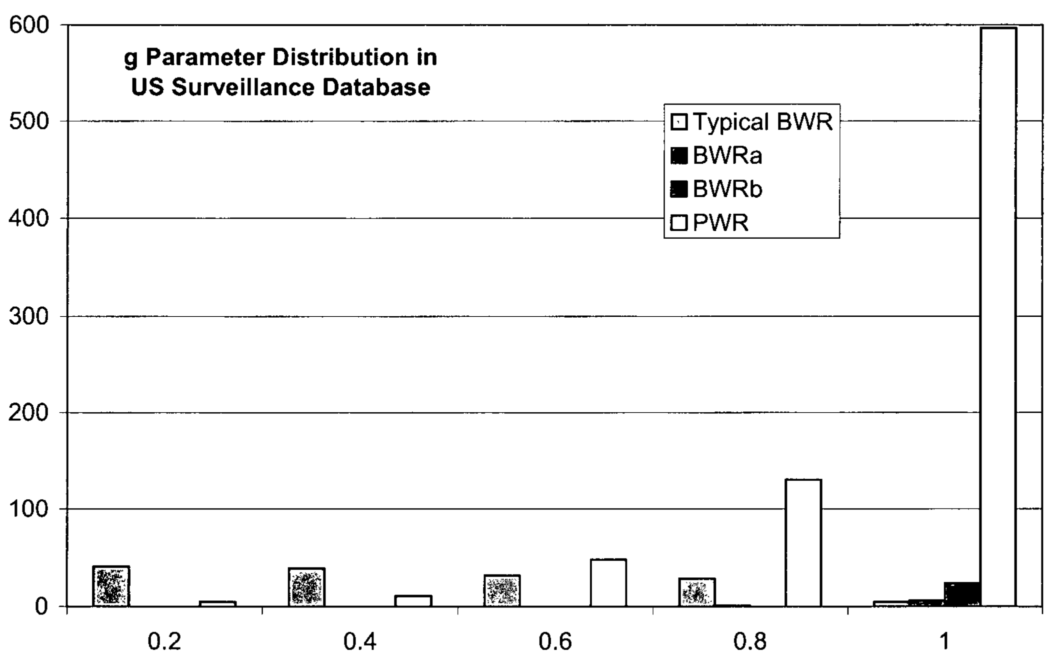

Figure 5-8
Distribution of sample types at different levels of the fluence function, g, in sNRC2006

Given this distribution of data, it is possible that the trends shown in Figure 5-7 and Table 5-1 could indicate that, in addition to the flux effects already described, the fluence functions are a poorer fit to the data at low levels of precipitation than at high levels. If this is so, then it would explain the more significant under-prediction of the welds. At any g level, the welds exhibit greater shifts than the plates. Any discrepancy between the fluence function and the actual trend in the data will, therefore, be most easily visible in the weld data.

5.1.1 Summary of Trends Observed in sNRC2006 Predictions

1. sNRC2006 provides a good overall fit to the data in the U.S. LWR surveillance database as of 2004. This is the database described in Chapter 2 as TTS8-04R1.
2. Both TTS8-04R1 and the database used for the present assessment are dominated by data acquired under higher-flux, -fluence, and -temperature conditions than are seen by typical BWR surveillance samples.
3. Comparison between measured and predicted shifts shows that sNRC2006 is not optimal as an embrittlement correlation for typical BWR surveillance samples. There is a tendency towards under prediction, especially for welds.
4. There is no intrinsic difference in the fit to PWR and BWR data, at a given flux or level of precipitation. The difference between the overall fit and the fit to the typical BWR data occurs because:

   The typical BWR data are dominated by points with low levels of precipitation or low fluxes/fluences;

   The PWR data are dominated by higher-g and higher fluxes/fluences.

   The good overall fit is caused by both the dominance of PWR data and the compensating effects of combining data from low and high levels of g.
5. Investigation of the cause of the poor fit indicates that it is most strongly related to the inclusion of a flux dependence (i.e. the effective fluence) in the MF component. In samples for which this effect dominates the prediction (Cu<0.072wt.%, flux<4.39×10^{10}n/cm^2-s), this results in under-predictions of the shift. The association of poor fit with the MF flux term is understandable on a mechanistic basis, since there is no evidence that matrix damage, as traditionally understood (MD) is flux dependent. A flux dependence of the MF component can be justified mechanistically on the assumption that MNPs dominate the MF component of hardening/embrittlement in the surveillance database. As discussed in Chapter 4, however, MNPs are unlikely to form in more than a few samples within the surveillance database. Other microstructural features may result in a flux-dependence but they are either unlikely to form under the conditions of the database (e.g. UMDs) or difficult to describe or measure (unspecified complexes between point defects and substitutional solutes).
6. The introduction of the flux dependence leads to an over-prediction in the CRP term. In steels with Cu>0.072wt.%, therefore the overall under-prediction at low fluxes is small. At intermediate fluxes, the fit between measurement and prediction for steels with Cu>0.072wt.% is good, although there may be some over-prediction at fluxes >5×10^{11} n/cm^2-s. This might indicate that a small continuous flux term should be introduced. On the basis of the insights into radiation-induced precipitation hardening acquired in EPRI-CRIEPI jointly-

funded research program, it would be worth investigating the introduction of a flux term outside the g term in the CRP component.

7. It would also be worth considering the possibility of using other fluence functions. It is possible that the fluence exponent in the MF term need not be fixed at precisely 0.5. In addition, although hardening is likely to begin slowly, proceed at an increasing rate, and then slow down as the hardening maximum is approached, the shape of the hardening curve is not precisely characterized. It is possible that the tanh function is not the best of the available descriptions of the actual hardening process. It may be worth considering the use of other, similar functions.

5.2 Comparison Between Measurements and Predictions by RM-9

Figure 5-9 compares the measured shifts for the BWR data within the U.S. LWR surveillance database with the predictions by RM-9. As was found for sNRC2006, the typical BWR data appear generally under-predicted but, with RM-9, the degree to which the BWRb data offset this under-prediction is weaker.

Concentrating again on the typical BWR data, Figure 5-10 compares the measured shifts for typical BWR plates and welds with the predictions made by RM-9. As with sNRC2006, the welds are under-predicted, and less well predicted than the plates although now, the plates appear slightly under-predicted also. Since the best fit lines in Figure 5-10 have been constrained to pass through the origin, the under-prediction of the welds by RM-9 is actually greater than by sNRC2006.

It is possible to make an analysis of the source of the under-prediction similar to that made for sNRC2006. Figure 5-11a divides the typical BWR data into low-and high-Cu groups, with the predictions of the low-Cu points involving only the $\Delta T_{30(MD)}$ component, and the predictions of the high-Cu points involving both the $\Delta T_{30(MD)}$ and $\Delta T_{30(CRP)}$ components. Figure 5-11b shows a similar analysis for the BWR and PWR data for which the RM-9 exponential fluence function, ΦF, is <0.5.

There are fewer low-Cu points in Figure 5-11 than in Figure 5-3 because, in RM-9, the $\Delta T_{30(CRP)}$ component operates at Cu>0.048wt.%, rather than 0.072wt.%, and only about half the points in the U.S. LWR surveillance database with Cu<0.072wt.% refer to samples with Cu<0.048wt.%.

Inspection of in Figure 5-11 indicates that, again, BWR and PWR samples are behaving in a similar manner. It is possible that the under-predictions of the BWR and low-flux/fluence PWR data are greater in the Cu<0.048wt.% specimens than in the Cu>0.048wt.% specimens, but the influence of measurement uncertainties within the small number of low-shifting data points will be great.

The data are divided up according to flux level, as well as Cu in Figure 5-12. Figure 5-12a confirms that the low-Cu data are significantly under-predicted but, within the small dataset, it is not possible to observe any effect of flux on the degree of under-prediction. Figure 5-12b shows the effect of flux on the overall predictions of shift in the samples with Cu>0.048wt.%. Here, it is possible to pick out an effect of flux. The deviation from one-to-one decreases as the flux level increases. With the RM-9 correlation, there is no over-prediction, even at fluxes $>5x10^{11}$n/cm^2-s.

The comparison between measurement and prediction as a function of the precipitation term ΦF, is given in Figure 5-13. Comparing Figure 5-13 with Figure 5-7 indicates that, although the exponential form of the fluence dependence in RM-9 (i.e. ΦF_{MD}) differs slightly from the tanh function in sNRC2006 (i.e. $g(\phi t_e, Cu_e, Ni)$), the fit between data and approximating trend curve is still not good in the early stages of CRP precipitation (i.e. at low ΦF_{MD} or low g). This is not very important for a description of the PWR surveillance data, but it is significant when describing the BWR surveillance data.

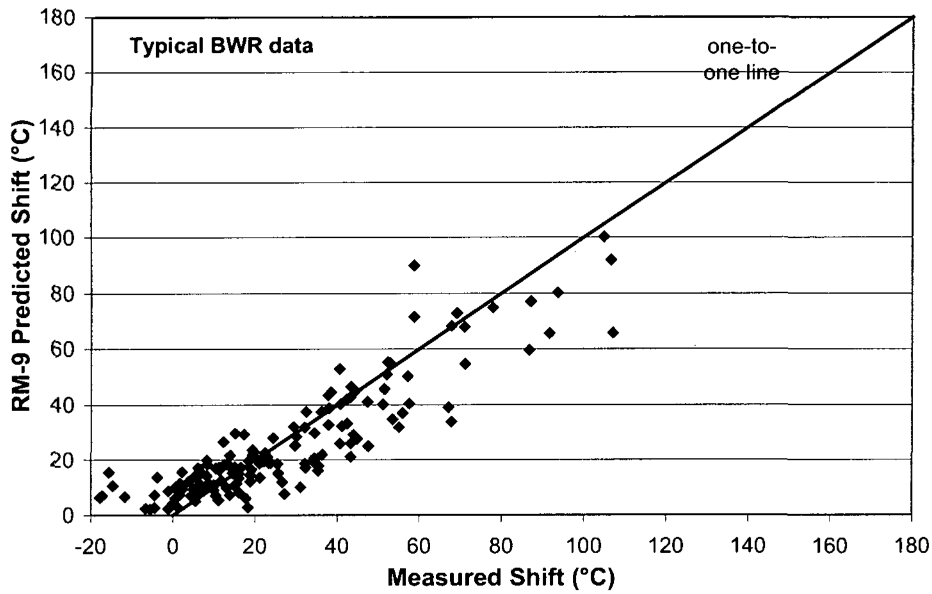

a) Typical BWR data

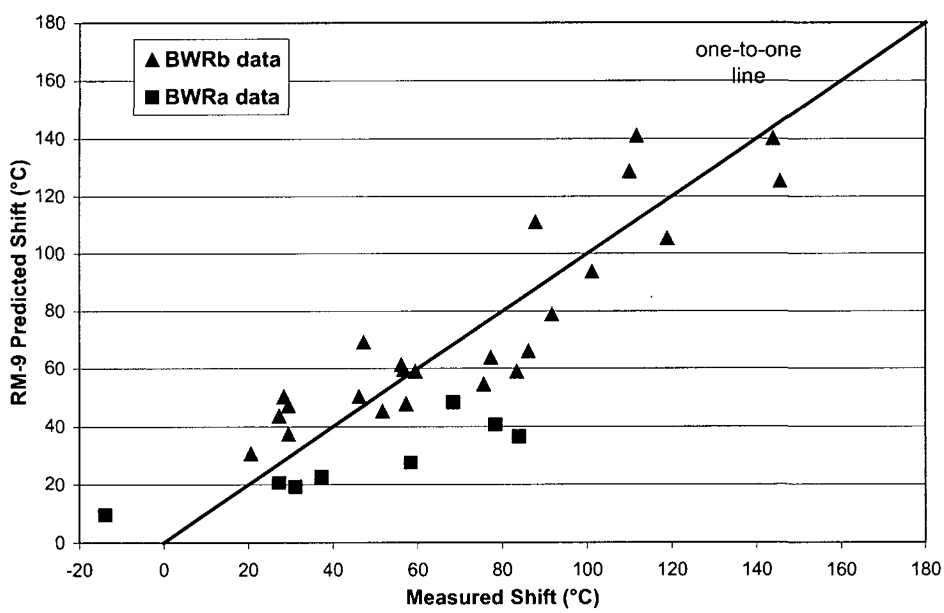

b) Atypical BWR data

Figure 5-9
Comparison between measured DT and DT predicted by sNRC2006 for a) typical BWR surveillance data and b) atypical BWR surveillance data

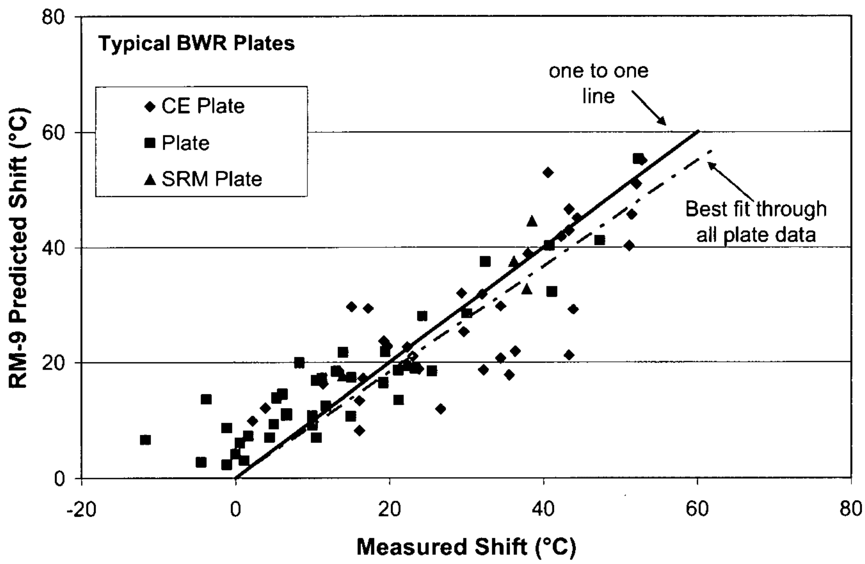

a) Plates

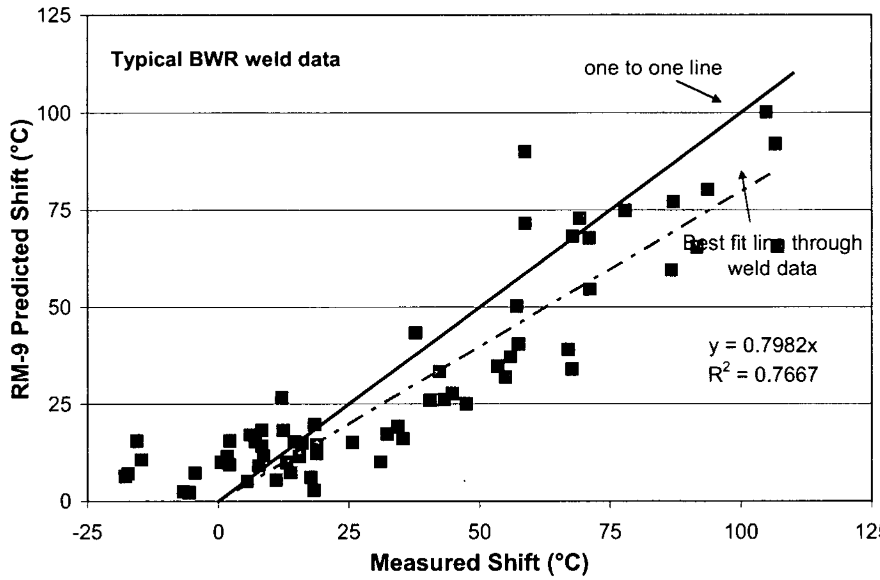

b) Welds

Figure 5-10
Comparison between measured shifts and shifts predicted by RM-9 for typical BWR a) plates and b) welds

(Best fit lines constrained to pass through origin)

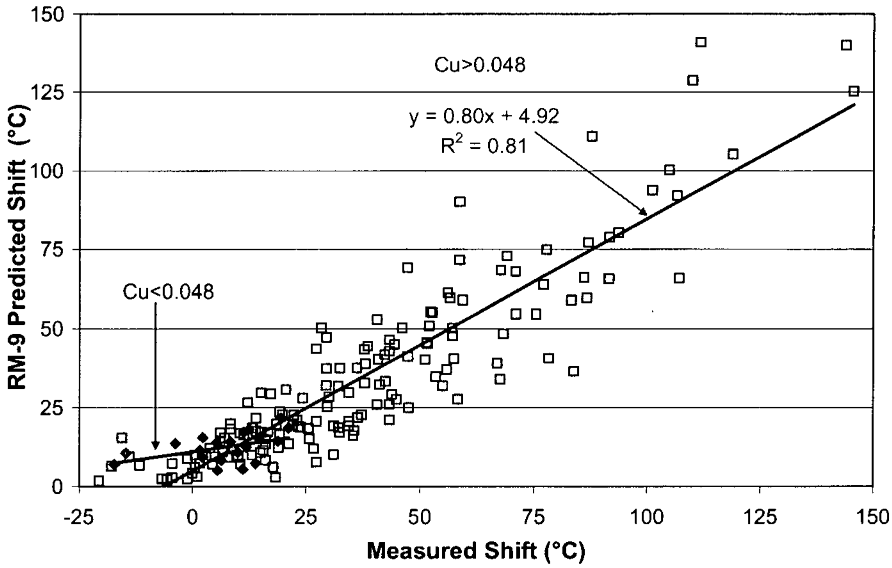

a) Typical BWR samples

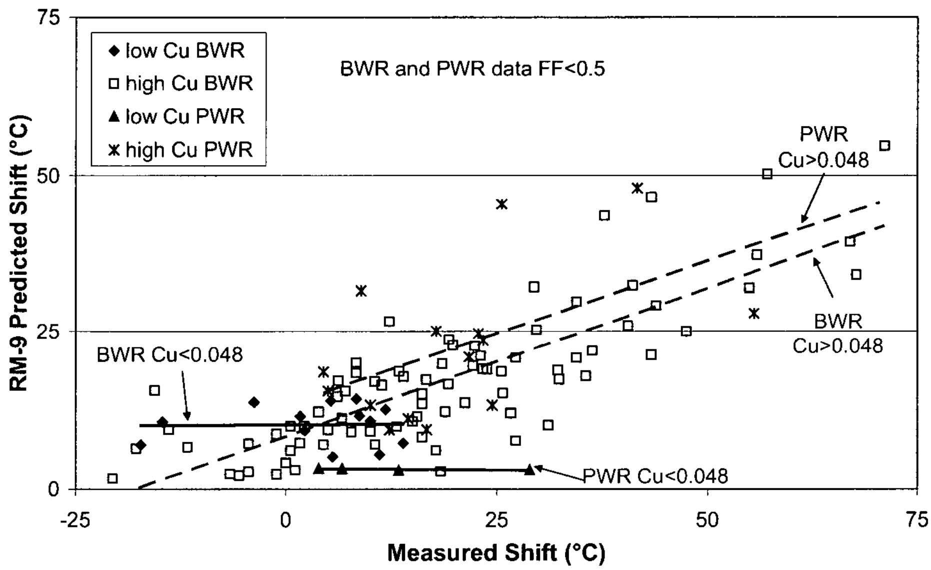

b) Typical BWR and PWR samples with ΦF<0.5

Figure 5-11
The effect of Cu content on the comparison between shifts measured in low-flux-fluence BWR and PWR samples and those predicted by RM-9

(Colored lines indicate the best fits through the data without constraints)

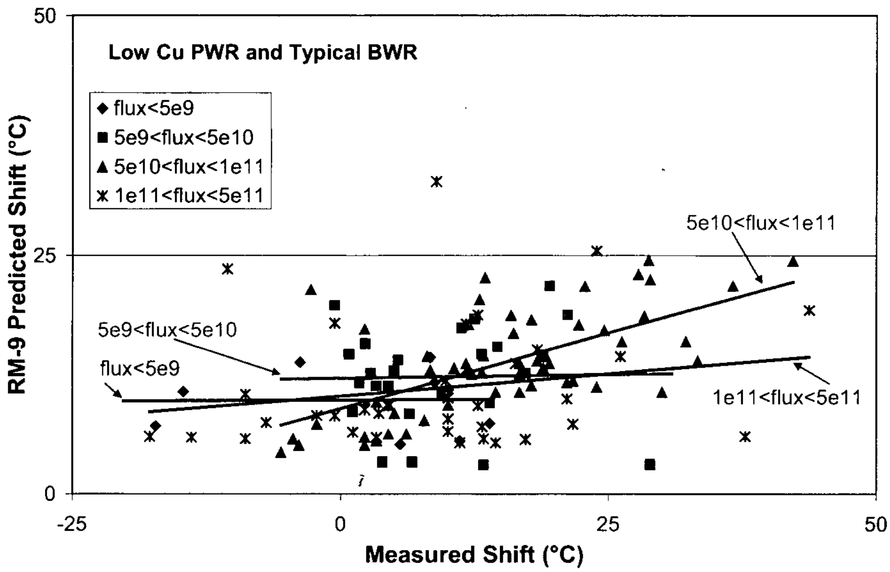

a) Cu>0.048wt.%

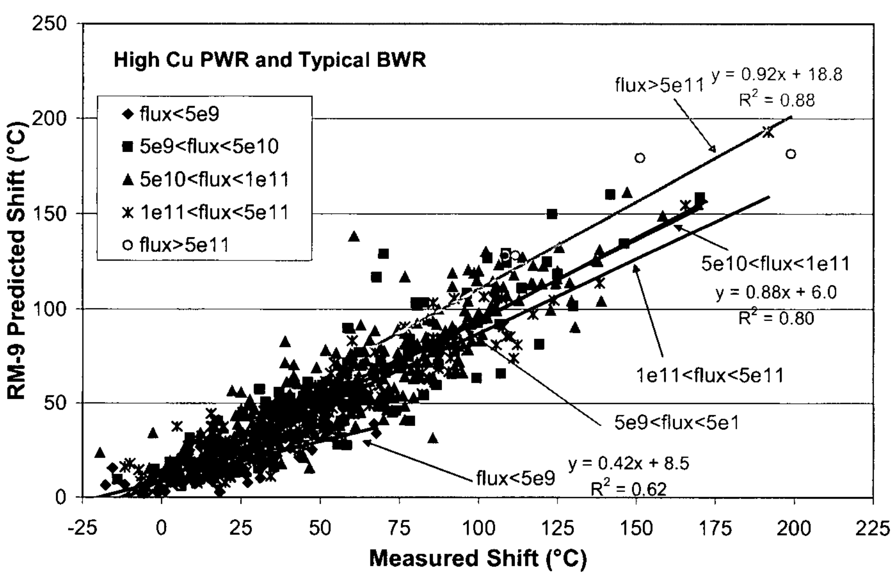

b) Cu>0.048wt.%

Figure 5-12
Effect of flux on comparison between measured DT and DT predicted by RM-9 for (a) all the low-Cu steels and (b) all the high-Cu steels of the U.S. LWR surveillance database

(Colored lines indicate the best fits through the data without constraints)

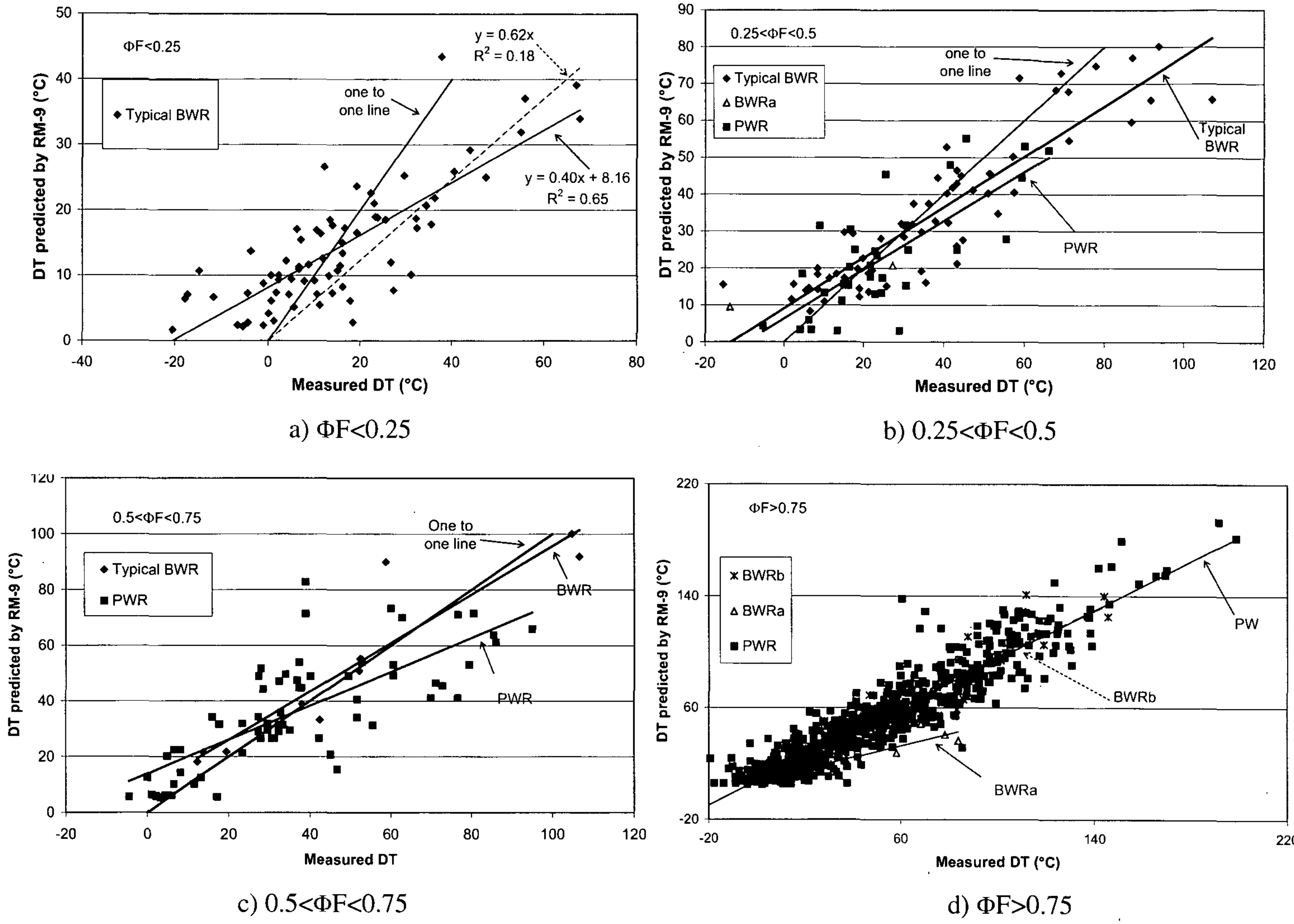

Figure 5-13
Comparison between measured shifts and shifts predicted by RM-9 at different levels of the CRP fluence function, ΦF

Table 5-2 shows that, as for the sNRC2006 predictions, the RM-9 predictions are closer to the measured values at higher levels of the (flux-and composition-moderated) fluence function. The higher the level of precipitation, the more likely it is that the under-prediction in the $\Delta T_{30(MD)}$ part of the correlation will be offset by the contribution of the $\Delta T_{30(CRP)}$ component.

Table 5-2
Properties of best fit lines through plots of measured shift versus shift predicted by RM-9

Data Range	Reactor/Specimen Type	Properties of Best Fit Lines			
		Unconstrained		Forced Through Origin	
		Slope	R^2	Slope	R^2
ΦF<0.25	Typical BWR	0.40	0.65	0.62	0.18
0.5<ΦF<0.5	Typical BWR	0.68	0.81	0.85	0.74
	PWR	0.66	0.57	0.84	0.51
0.5<ΦF<0.75	BWR	0.87	0.86	0.99	0.84
	PWR	0.61	0.58	0.87	0.42
ΦF>0.75	BWRb	0.83	0.80	0.98	0.78
	PWR	0.87	0.86	0.97	0.85
	BWRa	0.43	0.67	0.53	0.62

The distribution of samples at different levels of the RM-9 fluence function ΦF is shown in Figure 5-14. The PWR data (and, hence, the data overall) are even more heavily skewed towards high ΦF levels than was found for the g function in sNRC2006. The fit to the typical BWR data is thus even more important in showing the fit of the fluence function.

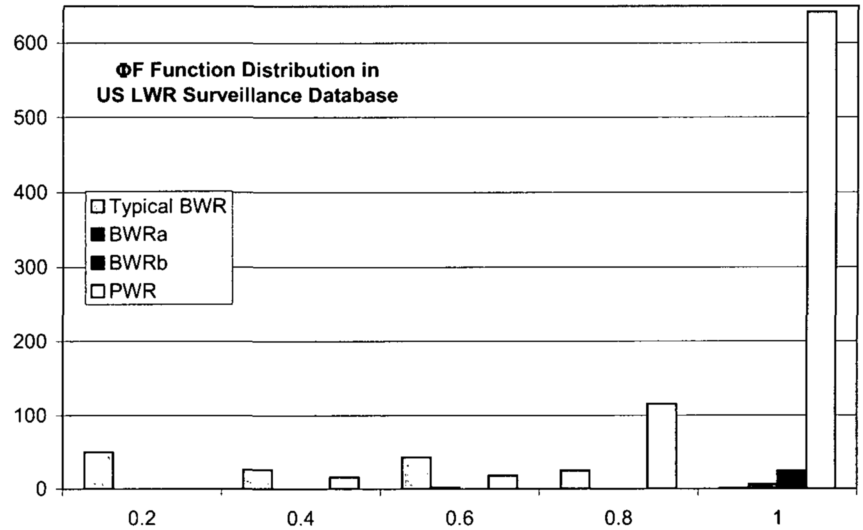

Figure 5-14
Distribution of sample types at different levels of the fluence function, ΦF, in RM-9

5.2.1 Summary of Trends Observed in RM-9 Predictions

1. RM-9 provides a good overall fit to the data in the U.S. LWR surveillance database.
2. Comparison between measured and predicted shifts shows that RM-9 is not optimal as an embrittlement correlation for typical BWRs. As with sNRC2006, there is a tendency towards under prediction at high shifts.
3. In general, the fit to data with low fluxes and fluences is not as good as the fit to data with high fluxes and fluences. Since typical BWR data are predominantly low flux-fluence data, they are less well predicted than the PWR data, which are dominated by high flux-fluence combinations.
4. Investigation of the source of the poor fit indicates that the $\Delta T_{30(MD)}$ component tends to under-predict the embrittlement of low-Cu samples. When both the $\Delta T_{30(MD)}$ and the $\Delta T_{30(CRP)}$ components contribute to the prediction, the under-prediction is smaller, and is reduced as the flux increases. This suggests that the flux terms are not optimal.
5. It is probable that (as in sNRC2006) the predictions improve at higher levels of the fluence function. This may be because, at low values of ΦF, precipitation levels are low, and the MF/MD terms are of similar magnitudes to the CRP terms. The under-prediction from the MD term is then less fully offset by the CRP term. Alternatively, this may offer some insight into the functional form which will better describe the low-precipitation CRP data.
6. The presence of the flux term in $\Delta T_{30(MD)}$ could have arisen because the initial optimization of $\Delta T_{30(MD)}$ was made with a flux term, and against data with Cu<0.07wt.%, while the $\Delta T_{30(CRP)}$ term actually becomes finite at Cu>0.048 wt.%. Only a little over half of the data with Cu<0.07wt.% contain <0.048wt.%Cu.

5.3 Comments on RM-6(2)

RM-6(2) also shows the under-predictions exhibited by RM-9. Some graphs illustrating the behavior seen in RM-6(2) are provided in Appendix B.

5.4 Comments on Behavior of Predictions

Both of the correlations examined provide good fits to the LWR database as a whole. This is not surprising as they have all undergone extensive examination by their authors and other reviewers. Because of the record of these examinations, it was not necessary for the authors of the present report to repeat the standard assessments of residuals as a function of individual parameters (fluence, Cu, etc).

The present assessment differed from those carried out by the authors of the correlations in that it was required to consider the BWR sub-set specifically, and was able to focus on this sub-set in detail rather than on the LWR data as a whole. In addition, because of the additional low-flux-fluence-temperature BWR data acquired within the BWR ISP VIP program, it was possible to focus on the behaviour of the typical BWR samples without including contributions from the atypical samples irradiated at higher than usual fluxes and temperatures (the BWRa and BWRb sub-sets).

Because of particular focus of this assessment, the study was able to reveal that both of the correlations exhibit a bias. Data at low fluxes and fluences are under-predicted.

In particular, the MF/MD components of the predictions under-predict the shifts in low-Cu materials. The precise extent of the under-prediction is difficult to assess because of the influence of the error distributions, but it is a real effect. In the case of sNRC2006, the under-prediction is more marked when the effective fluence term is introduced (for fluxes below 4.39×10^{10}n/cm^2-s). There are insufficient data to make an equivalent assessment of flux effects on the RM-9 predictions. Given the lack of independent support for the inclusion of a flux effect in the MF/MD components, it may be best to remove the MD/MF flux terms in both correlations, and re-optimize the flux dependence in the CRP components.

When the predictions include the CRP components of the correlations, the under-predictions in general are weaker. This indicates that the CRP terms over-predict the Cu-related aspects of the hardening. This was particularly evident when considering the sNRC2006 predictions at low fluxes. In the case of RM-9, the over-prediction of the CRP component appears to grow more gradually with flux. With both correlations, there appears to be a remnant overall flux effect in that there is slightly more under-prediction at lowest fluxes; there is possibly some over-prediction at very high fluxes with sNRC2006.

Given the relation between flux and fluence in the surveillance database, it is not simple to determine whether the remnant under-predictions (or over-prediction at high flux in sNRC2006) would be better treated by the introduction of a continuous flux effect in the part of the CRP component describing maximum embrittlement, or by modifying the fluence function. Examination of the distributions of the data in the database in terms of the fluence functions indicate that most of the data sit in the top 20% (RM-9) to 40% (sNRC2006) of the functions' ranges. It is plausible that it has not been possible to obtain accurate estimates of the behavior of the functions in their low ranges, and it may have been necessary to assume that the functions will be symmetric. More accurate estimates of the functions in their low ranges will be assisted by the increased amount of typical BWR data, which provides most of the information at these ranges.

The large number of negative measured shift values affects the embrittlement trends shown by the low-Cu specimens. It would be worth investigating these measurements to determine whether they may be treated in a consistent manner to reduce the importance of the negative shifts. For example, the use of a plant-specific offset term could be applied [29]. Reducing the influence of measurements errors at low shifts would render trends more evident, and assist in the production of a more accurate MD term.

6 STATISTICAL ASSESSMENT OF CORRELATIONS

The two correlations, sNRC2006 and RM-6(2), were assessed using the statistical procedures described in the following sections.

6.1 Data Description

The U.S. LWR surveillance database contains 948 measurements, 795 PWR, 152 BWR (119 normal, 33 identified as unusual – 8 BWRa, 25 BWRb) One sample was irradiated in both BWR and PWR reactors.

The BWR database contains 177 measurements (including 8 BWRa and 26 BWRb).

Information in the surveillance database includes type of test piece (weld, forging plate, etc), irradiation temperature, neutron flux and fluence, manufacturer, and chemical composition in addition to the measured temperature shift.

The U.S. LWR surveillance database used here is similar, but not identical to that used to derive the sNRC2006 correlation (TTS8-04R1). The BWR part of the database is an augmented version of the BWR content in TTS8-04R1.

6.2 Data Analysis Method

Two basic analysis methods have been used:

- Assessment of the goodness of fit of the competing correlations for each of the datasets (Full U.S. LWR surveillance database, all BWR, BWR excluding unusual values);
- Refit of the correlations to the BWR database(s) using the same correlation form, but allowing all parameters to vary, to assess the degree of improvement that can be obtained from a BWR-specific correlation.

Refitting was carried out using the non-linear solver capacity of the Mathcad calculation package to optimize the parameters. The default solution method selected by Mathcad is Quasi-Newton; the Levenberg-Marquardt method was also used [64, 65].

6.3 Assessment of sNRC2006

6.3.1 Description

The numerical constants in the sNRC2006 correlation described in Equation 4-1 – Equation 4-7 are translated into parameters to be fitted as shown in Table 6-1. Parameters not included in the Table are treated as fixed. These parameters are the cut points between different regimes, and the flux/fluence exponents:

- Cu_{min} = 0.072 wt.%,
- the onset flux for the flux correction of the fluence = 4.39×10^{10} n/cm^2-s
- the effective fluence exponent in the MF term = 0.5
- the flux exponent in the effective fluence = 0.259 or 0

Table 6-1
Parameter definition for sNRC2006

Fitting Parameter	Value	Description		
		Component	**Term**	**Comment**
F_0	1.14e-7	MF	A	Forging coefficient
F_1	1.561e-7	MF	A	Plate coefficient
F_2	1.417e-7	MF	A	Weld coefficient
F_3	1.718e-3	MP		Temperature coefficient
F_4	6.13	MF		P.Mn coefficient
F_5	2.47	MF		Mn exponent
F_6	0.243	CRP	Cu_{max}	Linde 80 welds
F_7	0.301	CRP	Cu_{max}	Other materials
F_8	0.668	CRP	$f(Cu_e, P)$	Cu_e, P exponent
F_9	1.359	CRP	$f(Cu_e, P)$	P coefficient
F_{10}	1.139	CRP	g	Cu_e coefficient
F_{11}	0.448	CRP	g	Ni coefficient
F_{12}	18.12	CRP	g	offset
F_{13}	0.629	CRP	g	denominator
F_{14}	102.3	CRP	B	Forging coefficient
F_{15}	155	CRP	B	Weld coefficient
F_{16}	128.2	CRP	B	SRM coefficient
F_{17}	135.2	CRP	B	CE plate coefficient
F_{18}	102.5	CRP	B	Non-CE plate coefficient
F_{19}	3.77	CRP		Ni coefficient
F_{20}	1.191	CRP		Ni exponent

The effect of including flux-dependence in the correlation was assessed by refitting the parameters in Table 6-1 with the flux exponent fixed at 0.259 (as in the original correlation) or set to zero. With the exponent set to zero, the flux term becomes unity. Three options were examined:

- Flux exponent = 0.259 in MF and in CRP components (flux-dependence in both components)
- Flux exponent = 0 in MF and 0.259 in CRP (no MF flux-dependence, flux dependence in CRP)
- Flux exponent = 0 in MF and CRP (no flux dependence in either component).

6.3.2 Application to Full U.S. LWR Surveillance Database

Table 6-2 shows the measures of fit between sNRC2006 and the full surveillance database (i.e. TTS8-04R1 plus recent extra BWR information). Given that there was some uncertainty as to the usefulness of the flux term in the MF component of sNRC2006, assessments were carried out using the form as given in Equation 4-1 to Equation 4-7 ("Original"), and a similar form, which used the actual rather than the effective fluence in the MF component, but left the flux term in the CRP component ("CRP flux term only"), and a form which used the actual rather than the effective fluence at all points ("without the flux term"). The parameters were then revised using Mathcad for both the original expression, and for the expressions without the flux terms.

The adjusted R^2 attempts to compensate for the number of terms in a regression model, and hence avoid over-fitting; the conventional R^2 will always increase (or stay the same) if additional terms are added to a model. For datasets with large numbers of observations however, the effect is small, and hence caution is still required.

Table 6-2
sNRC2006 fit to the U.S. LWR surveillance data

Parameter	Expression		
	Without Flux Term	CRP Flux Term Only	Original
Residual sum of squares	$5.208\text{x}10^5$	$4.955\text{x}10^5$	$4.940\text{x}10^5$
Residual root mean square	23.464	22.886	22.853
R^2	0.863	0.870	0.870
Adjusted R^2	0.860	0.867	0.867

Number of points 946, Number of parameters 22.

Table 6-2 shows that the presence of the flux term in the MF component does not affect the fit very much (comparing columns 3 and 4). The residual sum of squares is slightly lower when the flux term is present in both components, but the adjusted R^2 value is unchanged at the 3rd significant figure. The flux term in the CRP component, however, clearly affects the overall goodness of fit (comparing column 2 with columns 3 or 4).

Table 6-3 shows the changes in the various parameters caused by refitting against the entire database (i.e. the database expanded by 2-3% from the one used to fit the original correlation).

Table 6-3
Changes in sNRC2006 parameters with refit against full U.S. LWR surveillance database

Parameter	Original Model	Refitted Parameter Values		
		Without Flux Terms	CRP Flux Term Only[8]	With Flux Terms
F_0	1.14e-7	4.276e-7	4.148e-7	4.218e-7
F_1	1.561e-7	5.598e-7	5.427e-7	5.561e-7
F_2	1.417e-7	4.055e-7	4.016e-7	4.057e-7
F_3	1.718e-3	1.663e-3	1.657e-3	1.661e-3
F_4	6.13	19.318	19.356	19.356
F_5	2.47	-0.163	-0.152	-0.164
F_6	0.243	0.259	0.258	0.259
F_7	0.301	0.29	0.289	0.289
F_8	0.668	0.947	0.949	0.962
F_9	1.359	-4.437	-4.668	-4.449
F_{10}	1.139	1.395	1.55	1.183
F_{11}	0.448	0.19	0.237	0.259
F_{12}	18.12	18.174	18.342	18.225
F_{13}	0.629	0.964	0.583	0.614
F_{14}	102.3	133.881	127.621	131.288
F_{15}	155	275.956	255.675	266.381
F_{16}	128.2	204.809	190.797	198.357
F_{17}	135.2	236.654	218.922	228.337
F_{18}	102.5	170.279	157.339	164.412
F_{19}	3.77	2.933	3.05	2.988
F_{20}	1.191	1.286	1.271	1.289

The new expressions are very similar to each other, regardless of where the effective fluence term is used, but all differ more markedly from the original expression. In order to discuss the changes more conveniently, the original correlations (from Chapter 4) are outlined below:

$$MF = A(1-0.001718T_i)(1+6.13PMn^{2.47})\sqrt{(\phi t_e)}$$ **Equation 6-1**

[8] The exponent in the expression for effective fluence is not included in the fitted parameters.

$$CRP = B\left(1 + 3.77Ni^{1.191}\right)f(Cu_e, P)g(Cu_e, Ni.\phi t_e)$$ **Equation 6-2**

$$f(Cu_e, P) = \begin{Bmatrix} 0 \text{ for Cu} \le 0.072 \\ [\text{Cu}_e - 0.072]^{0.668} \text{ for Cu} > 0.072 \text{ and P} \le 0.008 \\ [\text{Cu} - 0.072 + 1.359(\text{P} - 0.008)]^{0.668} \text{ for Cu} > 0.072 \text{ and P} > 0.008 \end{Bmatrix}$$ **Equation 6-3**

$$g(Cu_e, Ni, \phi t_e) = \frac{1}{2} + \frac{1}{2}\tanh\left[\frac{\log_{10}(\phi t)_e + 1.139Cu_e - 0.448Ni - 18.120}{0.629}\right]$$ **Equation 6-4**

Table 6-3 shows that both sets of product form terms, F_0 to F_2 (corresponding to A in the MF component in Equation 6-1) and F_{14} to F_{18} (corresponding to B in the CRP component in Equation 6-2) are increased. Within the MF term (Equation 6-1), the multiplying factor on the phosphorous/manganese cross-term in the matrix damage component (F_4) is increased, while the exponent on the manganese percentage (F_5) is reduced and, more importantly, changes sign. Mechanistically, the negative Mn exponent (F_5) in the revised fit is not as well supported as the positive coefficient in the original fit. The much reduced magnitude of the exponent suggests, however, that the strength of the Mn term is very small. Taking these changes together, it appears that the P/Mn cross term is changing to a term more dominated by P, and the effects of Mn are being subsumed in the product form terms.

In the CRP component the refit results in the phosphorous term (F_9, corresponding to the P coefficient in Equation 6-3) also changing sign, and significantly increasing in magnitude. The negative P coefficient in the CRP term is better justified mechanistically than the original positive term. The improved description of the P effect may be in response to the more explicit P-dependence developed in the MF component.

Table 6-4 shows the results of these parameter changes on the goodness of fit between data and predictions. In all three flux-related variants, the fit is slightly improved by the refit. Once again, removing the flux term from the MF term has a minimal effect, but removing it from both the MF and CRP terms renders the fit slightly worse.

Table 6-4
Fit of re-parameterized versions of sNRC2006 to the full surveillance database

Parameter	Expression		
	Without Flux Term	CRP Flux Term Only	Both Flux Terms
Residual sum of squares	4.981×10^5	4.861×10^5	4.834×10^5
Residual root mean square	22.947	22.669	22.606
R^2	0.869	0.872	0.873
Adjusted R^2	0.866	0.869	0.870

Number of points 946, Number of parameters 22.

6.3.3 Application to Full BWR Database

The full BWR data set comprises both the typical and atypical (BWRa and BWRb) data.

Table 6-5 shows the goodness of fit of the original model to the BWR only data. The level of fit to the BWR data alone is not as good as for the full (PWR+BWR) expanded database, particularly if the flux terms are omitted.

Table 6-5
sNRC2006 fit to BWR data only (typical BWR, BWRa and BWRb)

Parameter	Expression		
	Without Flux Term	CRP Flux Term Only	Original
Residual sum of squares	1.46×10^5	9.882×10^4	9.523×10^4
Residual root mean square	28.722	23.628	23.196
R^2	0.750	0.831	0.837
Adjusted R^2	0.716	0.808	0.815

Number of points 177, Number of parameters 22.

Table 6-6 shows the effect on the parameters in sNRC2006 of fitting against only the BWR data. There is a roughly similar pattern of changes to that seen in refitting to the entire surveillance data set. However there is now more variation between models with different flux terms.

Table 6-6
Changes in sNRC2006 parameters with refit against BWR data only

Parameter	Original Model	Refitted Parameter Values		
		Without Flux Terms	CRP Flux Term Only[9]	With Flux Terms
F_0	1.14e-7	4.276e-7	4.148e-7	4.218e-7
F_1	1.561e-7	5.598e-7	5.427e-7	5.561e-7
F_2	1.417e-7	4.055e-7	4.016e-7	4.057e-7
F_3	1.718e-3	1.663e-3	1.657e-3	1.661e-3
F_4	6.13	19.318	19.356	19.356
F_5	2.47	-0.163	-0.152	-0.164
F_6	0.243	0.259	0.258	0.259
F_7	0.301	0.29	0.289	0.289
F_8	0.668	0.947	0.949	0.962
F_9	1.359	-4.437	-4.668	-4.449

[9] The exponent in the expression for effective fluence is not included in the fitted parameters.

Table 6-6
Changes in sNRC2006 parameters with refit against BWR data only (continued)

Parameter	Original Model	Refitted Parameter Values		
		Without Flux Terms	CRP Flux Term Only[9]	With Flux Terms
F_{10}	1.139	1.395	1.55	1.183
F_{11}	0.448	0.19	0.237	0.259
F_{12}	18.12	18.174	18.342	18.225
F_{13}	0.629	0.964	0.583	0.614
F_{14}	102.3	133.881	127.621	131.288
F_{15}	155	275.956	255.675	266.381
F_{16}	128.2	204.809	190.797	198.357
F_{17}	135.2	236.654	218.922	228.337
F_{18}	102.5	170.279	157.339	164.412
F_{19}	3.77	2.933	3.05	2.988
F_{20}	1.191	1.286	1.271	1.289

For the fits to the BWR data, the manganese exponent in the matrix damage expression (F_5) is again reduced so that the P/Mn cross term becomes more dominated by P. The Mn exponent (F_5) no longer changes sign, however, (as it did for the full dataset) possibly showing that the absolute value of this exponent is not easily defined. In response to this, the P coefficient in the CRP component (F_9) again changes sign.

Refitting the correlations against only the BWR data results in improved fits (Table 6-7) to the BWR data, surpassing both the original correlation and its refit to the full database. For this subset of the data, removing the MF flux term reduces the goodness of fit, while removing both flux terms has less of an effect.

Table 6-7
Effect on goodness of fit to BWR data of reparameterizing sNRC2006 against BWR data only (typical BWR, BWRa and BWRb)

Parameter	Expression		
	Without Flux Terms	CRP Flux Term Only	With Flux Terms
Residual sum of squares	6.518×10^4	6.918×10^4	6.403×10^4
Residual root mean square	19.190	19.769	19.019
R^2	0.888	0.881	0.890
Adjusted R^2	0.873	0.866	0.876

Number of points 177, Number of parameters 22.

6.3.4 Application to Typical BWR Data Only

Table 6-8 shows the goodness of fit of the original model to the typical BWR only data. As expected from the investigation of residuals in Chapter 4, the level of fit of the original sNRC2006 to the typical BWR data alone is not as good as for the full BWR dataset or the (PWR+BWR) set, particularly if the flux terms are omitted.

Table 6-8
sNRC2006 fit to typical BWR data only

Parameter	Expression		
	Without Flux Term	CRP Flux Term Only	Original
Residual sum of squares	1.089×10^5	6.165×10^4	5.806×10^4
Residual root mean square	27.494	20.692	20.079
R^2	0.657	0.806	0.817
Adjusted R^2	0.599	0.773	0.786

Number of points 144, Number of parameters 22.

Refitting the parameters against only the typical BWR data results in the parameter values shown in Table 6-9.

Table 6-9
Changes in sNRC2006 parameters with refit against typical BWR data only

Parameter	Original Model	Refitted Parameter Values		
		Without Flux Terms	CRP Flux Term Only[10]	With Flux Terms
F_0	1.14e-7	1.14e-7	1.14e-7	1.14e-7
F_1	1.561e-7	1.322e-6	1.332e-6	9.686e-7
F_2	1.417e-7	1.267e-6	1.245e-6	8.644e-7
F_3	1.718e-3	1.839e-3	1.841e-3	1.815e-3
F_4	6.13	56.797	60.144	38.403
F_5	2.47	0.328	0.269	0.391
F_6	0.243	0.252	0.253	0.245
F_7	0.301	0.301	0.301	0.301
F_8	0.668	1.501	1.446	1.177
F_9	1.359	-8.36	-8.34	-8.461
F_{10}	1.139	1.987	1.523	2.401
F_{11}	0.448	-0.014	0.017	0.056
F_{12}	18.12	17.913	18.229	18.437
F_{13}	0.629	0.53	0.447	0.406

[10] The exponent in the expression for effective fluence is not included in the fitted parameters.

Table 6-9
Changes in sNRC2006 parameters with refit against typical BWR data only (continued)

Parameter	Original Model	Refitted Parameter Values		
		Without Flux Terms	CRP Flux Term Only[10]	With Flux Terms
F_{14}	102.3	102.3	102.3	102.3
F_{15}	155	677.558	647.77	371.076
F_{16}	128.2	128.2	128.2	128.2
F_{17}	135.2	570.963	528.385	276.998
F_{18}	102.5	455.799	430.557	228.823
F_{19}	3.77	2.034	2.062	2.403
F_{20}	1.191	1.178	1.169	0.764

As with the other re-fitting procedures, refitting to the typical BWR sub-set affects the Mn dependence in the MF term. The Mn exponent in the P/Mn cross term (F_5) is again reduced, (remaining positive in this instance), while the product form terms, F_1 and F_2[11] are increased, subsuming the explicit Mn effect into the product form terms. The P/Mn coefficient (F_4) again increases (more so than when the entire data set was considered), resulting in a strong P-dependence in the MF component. Again, in response, the P coefficient in the CRP term (F_9) is more easily defined, and becomes negative, as anticipated from mechanistic understanding.

In addition to these changes observed in the fits to the other data sets, there are also changes in the Ni terms in the CRP component when only the typical BWR data are considered. The Ni term outside g (affecting the maximum embrittlement level, see Equation 6-2)) contains the expression $F_{19}Ni^{F20}$. The refit reduces both F_{19} and F_{20}, reducing the effect of Ni on the maximum embrittlement. In addition the Ni-dependence of the rate of CRP embrittlement (within the g term, see Equation 6-4), F_{11}, and the Cu-dependence of the rate of CRP embrittlement, F_{10}, also change. The effect of Ni is reduced, while that of Cu is increased.

It is possible that these changes are simply the result of parameter distributions within the database. There is a slight correlation between Cu and Ni when the entire surveillance database is considered, as shown in Figure 6-1, and this is stronger in the BWR and typical BWR sub-sets. The slightly stronger correlation between Cu and Ni in the typical BWR samples may have made the Ni dependence more difficult to identify. Alternatively, the changes in F_{10}, F_{11}, F_{19} and F_{20} may indicate that CRP embrittlement depends differently on Cu and Ni at different stages in the precipitation process. As shown in Figure 5-8, most of the information on the fluence function at $g<0.6$ must come from the typical BWR data, since the rest of the data are heavily biased towards $g>0.6$. This possibility is supported by the change in the parameter F_{13}. F_{13} is the denominator in the fluence function, g (see Equation 6-4). For all of the refitting procedures, this parameter is changed when the flux dependences are removed. This is understandable as the flux term is in the numerator of the g function, and some compensation for its removal will be required. Only when refit is to the typical BWR sub-set, however, does F_{13} change significantly even with the flux exponents unchanged. The changes in the Cu and Ni-dependences and in F_{13} suggest that the fluence function may differ at high and low values.

[11] F0 is the product form term for forgings. It has been left unchanged as there is only one typical BWR forging point.

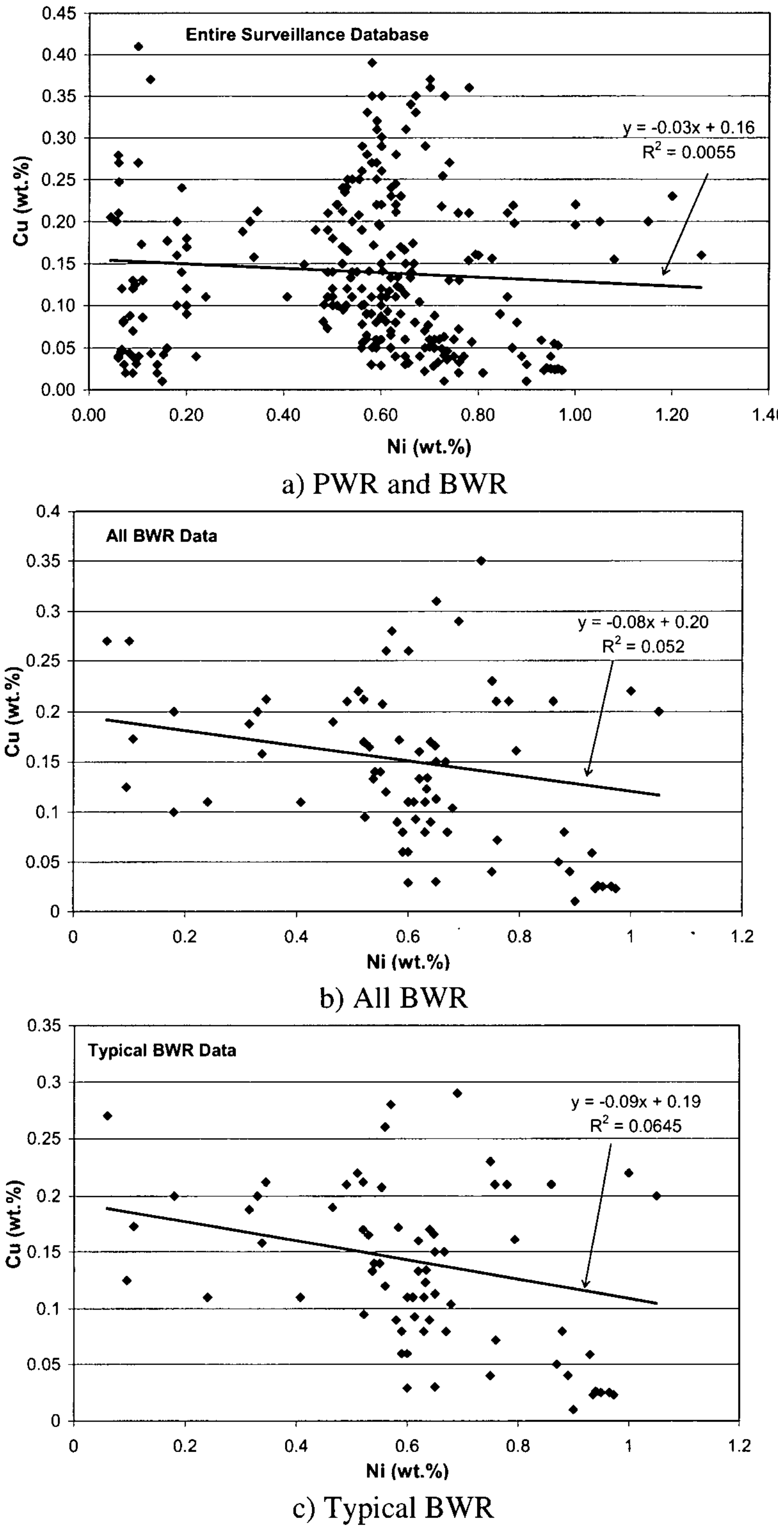

Figure 6-1
Correlation between Cu and Mn in a) the entire surveillance database, b) among all the BWR data and c) within the typical BWR sub-set

It is worth noting that F_3, the temperature dependence in the MF component, is very stable both to changes in the data set used and to the presence/absence of the flux terms. This supports the use of a linear form for the MF temperature dependence. It also suggests that the under-predictions of the atypical BWRa data (see Figure 5-1b) are unrelated to the high irradiation temperature. The under-predictions are more likely to be related to the high fluxes and fluences seen by the specimens.

The re-parameterization shown in Table 6-9 affects the fit as shown in Table 6-10. The fit is improved, but it is still not as good as the optimized fits to all BWR data or all BWR + PWR data. In this case, the versions of the model without the flux term in the MF component are slightly better than the model with the flux term in the MF component.

Table 6-10
Goodness of fit to typical BWR data of sNRC2006 after re-parameterization against typical BWR data

Parameter	Expression		
	Without Flux Term	CRP Flux Term Only[12]	With Flux Terms
Residual sum of squares	4.376×10^4	4.356×10^4	4.444×10^4
Residual root mean square	17.432	17.393	17.567
R^2	0.862	0.863	0.860
Adjusted R^2	0.839	0.839	0.836

Number of points 144, Number of parameters 22.

Comparisons between the predicted and measured shifts for typical BWR data are given in Figure 6-2. The relevant re-parameterized fit is slightly better for the full BWR dataset, and clearly better for predicting the typical BWR data. Conversely, Figure 6-3 shows that the original version of sNRC2006 is much better at predicting PWR shifts than the version of sNRC2006 optimized to predict typical BWR shifts.

[12] This solution required the inclusion of an additional constraint on parameter F_9 to prevent the prediction of complex residuals and summary measures of fit.

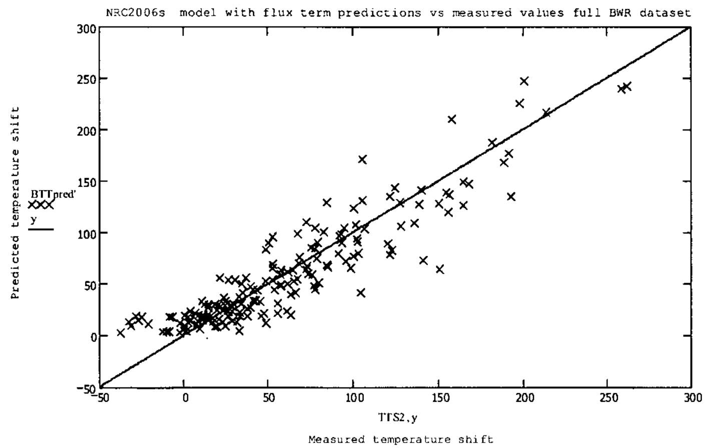

a) original sNRC2006, all BWR data

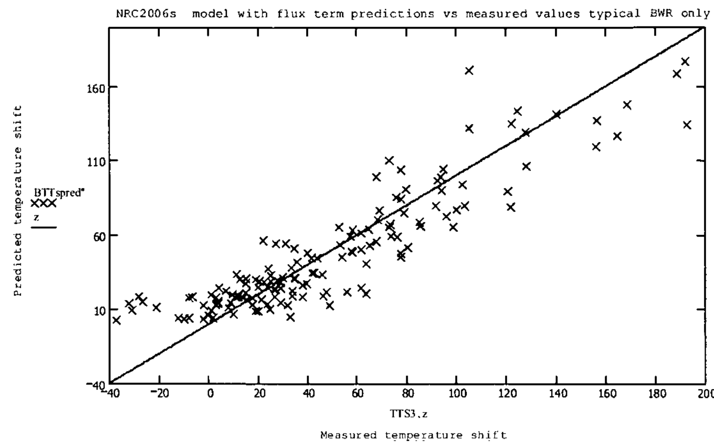

b) original sNRC2006, typical BWR data

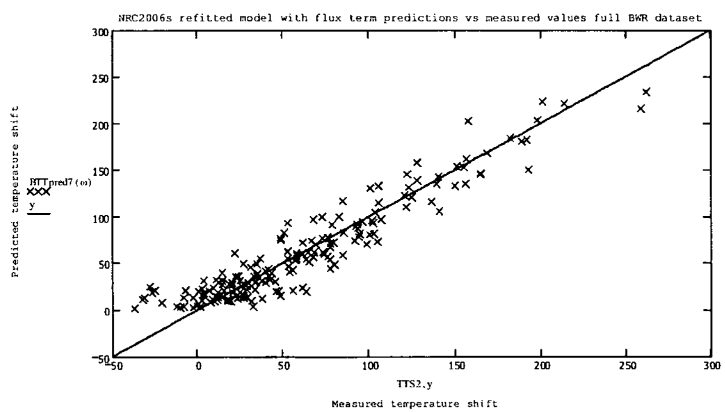

c) refitted sNRC2006 all BWR data

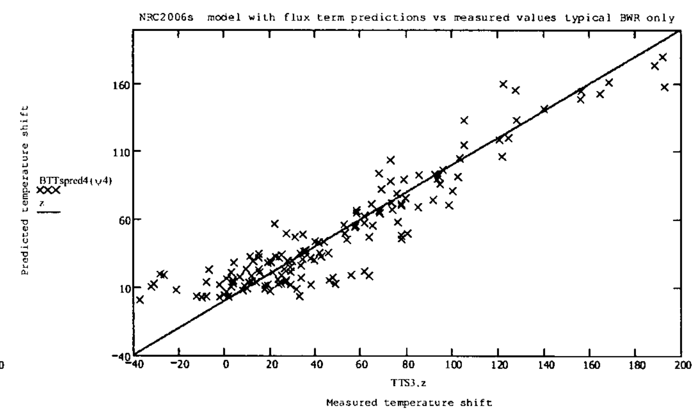

d) refitted sNRC2006, typical BWR data

Figure 6-2
Predicted versus measured shifts for full and typical BWR datasets with the original and re-fitted sNRC2006 models
(In each case, the model with all flux terms is used)

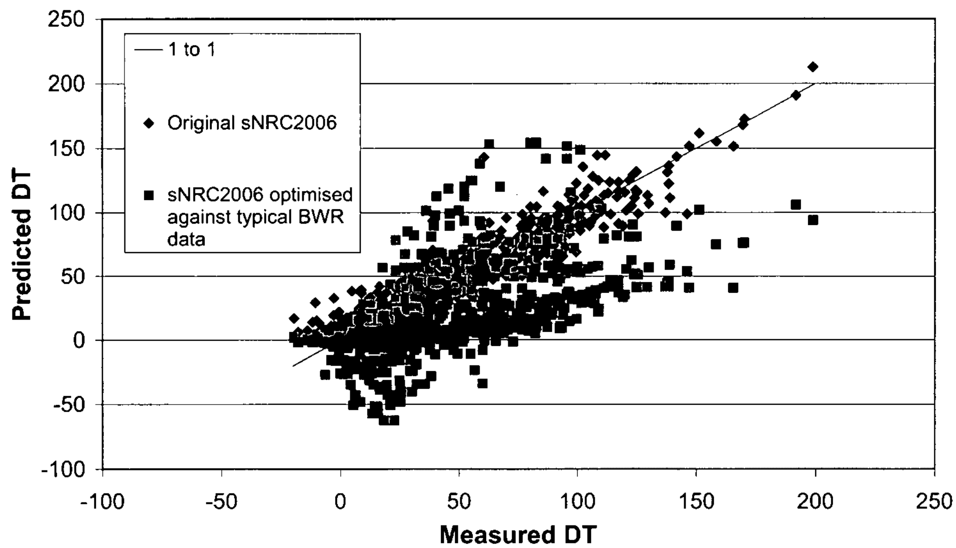

Figure 6-3
Prediction of PWR shifts using original sNRC2006 correlation, and correlation re-parameterized against typical BWR data

6.4 Model RM-6(2)

6.4.1 Description

The numerical constants in the RM-6(2) correlation are translated into parameters to be fitted as shown in Table 6-11. Parameters not included in the Table (i.e. the cut point between different regimes, Cu_{min} = 0.048wt.%, and the fluence exponent in the MF term of 0.5) are treated as fixed.

Table 6-11
Parameter definition for RM-6(2)

Fitting Parameter	Value	Description		
		Component	Term	Comment
R_0	-14.64	MD	TF_{MD}	Temperature exponent
R_1	-3.44	MD	ϕF_{MD}	Flux exponent
R_2	35	MD	CF_{MD}	P coefficient
R_3	6.7	MD	PF_{MD}	Weld coefficient
R_4	8.1	MD	PF_{MD}	Plate coefficient
R_5	4.75	MD	PF_{MD}	Forging coefficient
R_6	-1.74	CRP	TF_{CRP}	Temperature exponent
R_7	-116.3	CRP	f(Cu)	Offset
R_8	530.8	CRP	f(Cu)	Cu coefficient
R_9	2500.3	CRP	CF_{CRP}	Cu.Ni coefficient
R_{10}	0.301	CRP	PF_{CRP}	Weld coefficient
R_{11}	0.233	CRP	PF_{CRP}	Plate/Forging coefficient

6.4.2 Application to Full BWR dataset

The fit of the original RM-6(2) model to the full BWR data set (typical BWR data, BWRa and BWRb) is shown in Table 6-12. It is not as good as the fit of the original sNRC2006 model to this data set (Table 6-5). The fit is improved by the re-parameterization described in Table 6-13, but is still not as good as the equivalent re-parameterized sNRC2006 model (Table 6-7).

Table 6-12
Assessment of fit of original and re-fitted RM-6(2) model on full BWR dataset

Parameter	Original Model	After Re-Fitting
Residual sum of squares	4.107×10^4	2.687×10^4
Residual root mean square	15.232	12.322
R^2	0.772	0.851
Adjusted R^2	0.755	0.840

Table 6-13
Original and refitted parameter values for RM-6(2) with full BWR dataset

Parameter	Description	Original Model	After Re-Fitting
F_0	Temperature exponent (MD term)	-14.64	5.285
F_1	(Log) Flux exponent	-3.44	-5.307
F_2	Phosphorous factor	35	43.944
F_3	Product type factors (MD term)	6.7	12.416
F_4		8.1	10.629
F_5		4.75	6.725
F_6	Temperature exponent (CRP term)	-1.74	-14.288
F_7	Copper function offset (intercept)	-116.3	-64.86
F_8	Copper function factor (slope)	530.8	321.143
F_9	Copper-nickel interaction factor	2500	746.867
F_{10}	Product type factors (CRP term)	0.301	0.551
F_{11}		0.233	0.415

The most significant changes produced by fitting to the BWR data only are to the temperature exponents in both the matrix damage and CRP components. Both change significantly in magnitude, and the temperature exponent in the matrix damage component changes sign. This is not mechanistically supported, and may reflect the use of a power-law form for the temperature-dependence instead of the well-known linear temperature dependence. In this context, it is worth noting that the linear MF temperature dependence in sNRC2006 was extremely stable during refitting to different databases.

The effect of phosphorus is increased while that of copper and the copper-nickel interaction is decreased.

6.4.3 Application to Typical BWR Data Only

The fit of the original RM-6(2) model to only the typical BWR data set is shown in Table 6-14. It is not as good as the fit to all the BWR data (typical and atypical data, Table 6-12), and it is not as good as the original sNRC2006 fit to the typical BWR data (Table 6-8).

The fit is considerably improved by the re-parameterization described in Table 6-15, but is still not as good as the equivalent re-parameterized sNRC2006 model (Table 6-10).

Table 6-14
Assessment of fit of original and re-fitted RM-6(2) model on typical BWR data

Parameter	Original Model	After Re-Fitting
Residual sum of squares	$2.806x10^4$	$1.621x10^4$
Residual root mean square	13.959	10.611
R^2	0.714	0.835
Adjusted R^2	0.688	0.820

Table 6-15
Original and refitted parameter values for RM-6(2) with typical BWR data only

Parameter	Description	Original Model	After Re-Fitting
F_0	Temperature exponent (MD term)	-14.64	12.217
F_1	(Log) Flux exponent	-3.44	-3.701
F_2	Phosphorous factor	35	-10.542
F_3	Product type factors (MD term)	6.7	17.932
F_4		8.1	28.124
F_5		4.75	4.75
F_6	Temperature exponent (CRP term)	-1.74	-143.606
F_7	Copper function offset (intercept)	-116.3	-34.237
F_8	Copper function factor (slope)	530.8	232.944
F_9	Copper-nickel interaction factor	2500	631.763
F_{10}	Product type factors (CRP term)	0.301	5.384e-3
F_{11}		0.233	4.345e-3

As with the full BWR dataset, the temperature terms show the most significant change, though the product factors in the CRP term decrease correspondingly. This is due to the limited range of temperatures in the reduced dataset, and is an example of both over-fitting and collinearity between predictors (in this case between temperature and the constant term). With such a limited range of temperature in the BWR database, it is probably unreasonable to try to fit the power law temperature terms. If a fit to the entire database (i.e. PWR + BWR) can be justified, then it would be sensible to leave the temperature terms fixed if further re-fitting to the BWR-only sub-set is required.

6.5 Discussion

All of the correlations provide a reasonable fit to the data after refitting. The sNRC2006 model is slightly the better, though it has more free parameters.

The method used to refit the correlations is a brute force approach, solving for all parameters simultaneously, without constraints. While this is simple to implement, it may not give the best results.

As mentioned earlier, the default solution method selected by Mathcad is Quasi-Newton. When this method is used, however, the results appears sensitive to the initial guess values, and do not converge to an optimum value in a single operation. It is necessary to use the output values as inputs for a subsequent operation, sometimes more than once, before convergence is achieved. The Levenberg-Marquardt method does appear to converge in a single operation, but can sometimes produce infeasible results, i.e. producing predictions which are complex numbers (though the parameter values remain real).

Methods are available to minimize the effect of these fitting problems, by constraining the range of the parameters, though this moves away from the simple least squares methodology.

This behavior may indicate that:

- There may be multiple local optima, which trap the solution, distant from the global optimum;
- Portions of the error surface may be (nearly) flat, which can also trap the solution.

Due to this possibility the results above must be tentative, until we can resolve the uncertainty and prove that we converge to the global optimum in each case. This could be assisted by examination of the error norm surface, for various combinations of the parameters. Fitting by Markov Chain Monte Carlo methods should ensure that the global optimum is reached, though this would require programming (possibly using an alternative software platform).

It is also worth considering possible alternatives to the tanh or exponential functions. The tanh function by itself gives values between ±1, for arguments between ±∞, though it reaches ±0.995 for arguments of ±3. The formulation used scales the output value to the range 0 to 1. The function is symmetric, and in this formulation the slope and spread is fixed. It is completely equivalent to a (cumulative) logistic distribution with location parameter of zero and scale parameter of ½.

Any other cumulative probability distribution could be used and there are several families of distributions which are flexible enough to fit a range of shapes. (e.g. the 2 parameter beta distribution takes values between 0 and 1and returns values in the same range, but allows a variety of curve types, including the basic sigmoid, within this range.)

The tanh function is unbounded, in the sense that it only approaches its limits of zero and one as the argument tends to $\pm\infty$. We have a choice of alternative distributions that can be bounded on one or both sides, or unbounded as most appropriate for the pattern of the data.

Variation in the variables included within the function can have only a limited effect if the argument is near the edge of its range. In this case the fluence is the controlling term (whether or not the flux term is included), with the copper and nickel terms being relatively minor modifiers.

7
CONCLUSIONS

The applicability of the embrittlement correlations produced by Eason et al [13] and EricksonKirk [14] to BWR data prediction has been investigated by considering:

- The mechanistic basis for the form of each correlation;
- Comparisons between predicted and measured transition temperature shifts for different sub-sets of the U.S. LWR surveillance database;
- The effects of changing the database (by increasing the amount of BWR data, or by consideration of data sub-sets) on the values of the parameters selected as optimal by different statistical analysis techniques.

This investigation has led to conclusions outlined below.

7.1 Overall Behavior of Correlations

All the correlations examined in this report and the preliminary assessment [63], sNRC2006, RM-6(2) and RM-9 appear good descriptions of the U.S. LWR surveillance database, when the database is considered as a whole. When the database is broken down into sub-sets, however, deviations appear in the relation between prediction and measurement:

- If the database is broken down according to flux, then at low fluxes ($<\sim 10^{10}$n/cm^2-s) the data are under-predicted. The under-predictions are smaller at medium and high fluxes in RM-9, while in sNRC2006 there may even be some over-prediction at the very highest fluxes ($>5\times10^{11}$n/cm^2-s).
- If the data are broken down according to the fraction of CRPs precipitated (i.e. the values of g in sNRC2006 or ΦF in RM-9), then at low levels of precipitation (g or $\Phi F<0.5$) the data are under-predicted. The data are well predicted at high levels of precipitation (g or $\Phi F>0.75$).

Within the entire surveillance database, the majority of data are found at medium-to-high fluxes ($>5\times10^{10}$n/cm^2-s). In terms of the precipitation parameters, most data are found at g or $\Phi F>0.8$. This is due to the dominance of the PWR data, although the atypical BWR data also fall in this range. The typical BWR data lie within the low-flux and mid-to low-g or -ΦF ranges.

7.2 Predictability of BWR Data

It is only recently that sufficient typical BWR data have been accumulated that it has become possible to assess the applicability of the correlations to BWR data without including atypical data in the assessment.

Since the typical BWR surveillance data correspond to low g or ΦF levels, the under-predictions become evident when this sub-set is examined. For all of the correlations considered the predictions do not bear a one-to-one relation to the data. In addition, welds are less well predicted than plates. Under-predictions of the order ~20% become clear at the higher shifts. As a result, none of the correlations are optimal for assessing the condition of BWR RPVs.

7.3 Source of BWR Data Under-Prediction

It is important to recognize that there is little intrinsic difference between BWR and PWR surveillance data in the applicability of the correlations. Where PWR and BWR data fall in the same g or ΦF ranges, the bias tends to be similar for the two reactor types. There are no "hidden" variables, associated with differences in BWR and PWR manufacturing processes, which have major effects on the predictions of transition temperature shift in the two kinds of reactor. (There is a slight effect of reactor type in the RM-6(2) predictions, but this is more likely to be due to the deliberate reduction in the number of product form terms incorporated, rather than to any "hidden" factors.)

Examination of the source of the under-prediction indicates that it derives mostly from the MF or $DT_{30(MD)}$ terms. Over-predictions in the CRP terms compensate for these under-predictions. The extent of the compensation depends on the relative sizes of the MF and CRP terms for each prediction. Only the MF or $DT_{30(MD)}$ terms are involved in predictions of shift in low-Cu steels (where low is <0.072wt.% for sNRC2006 and <0.048wt.% in RM-6(2) or RM-9). In predictions to which the CRP term also contributes, the MF/$DT_{30(MD)}$ term is relatively more important at lower g or ΦF (lower flux-and composition-compensated fluences), since the CRP terms increase only slowly with fluence at low fluences.

In sNRC2006, it is possible to associate the under-prediction in the MF term mostly with the onset of the flux dependence (i.e. the use of the effective fluence) as the bias is strongest when this term operates. Even when the effective fluence ≡ actual fluence, however, there is some bias in the MF term, for which the CRP term is required to compensate. At high g levels, the compensation in the CRP term is sufficient for the overall bias in the predictions of shifts in Cu>0.072wt.% steels to be ~nil.

The bias in the CRP term in sNRC2006 does not turn on at the onset of the effective fluence term (i.e. only at fluxes <4.39×10^{10}n/cm^2-s). It increases continuously with increasing flux. This has two implications. Most simply, it suggests the possibility that, at high fluxes there is a possibility of overcompensation. More importantly, it suggests that there is a continuous flux-dependence in the CRP term which is currently not described in sNRC2006. A continuous flux term in the CRP component would be mechanistically justifiable on the basis that CEC sizes (at a given volume fraction) are flux-dependent, and the hardening from CECs is, in fact, size-dependent.

The limiting value of Cu at which the CRP term is introduced is lower for RM-6(2) and RM-9 than for sNRC2006. This means that the LWR database contains fewer points for which only the $DT_{30(MD)}$ term is involved in the prediction of shift. In addition, the flux dependence in the $DT_{30(MD)}$ term does not turn on at a particular flux. Thus it is harder to identify the source of the bias in the $DT_{30(MD)}$ term in RM-9. It is likely, however, that this is also affected by the incorporation of a flux dependence in the $DT_{30(MD)}$ term in RM-9.

The mechanistic justification for the inclusion of a flux dependence within the $MF/DT_{30(MD)}$ term is that Mn-Ni-Si clusters (or MNPs) induce hardening with this characteristic. There is, however, no direct evidence that Mn-Ni-Si clusters dominate the non-Cu component of hardening at the Mn-Ni-flux-fluence combinations of the U.S. LWR surveillance database. Given the presence of a flux effect in the IVAR database, however, it was necessary to investigate whether a flux dependence of this nature was present in the surveillance database also.

7.4 The Role of Statistical Analysis in Optimizing the Correlations

Statistical analysis shows that both sNRC2006 and RM-6(2) are equations with complex distributions of errors. The error surface may contain many local minima or regions of minimal slope, so that reaching the global minimum in error space is difficult. The local minimum to which a statistical analysis tends depends strongly on the starting values chosen for different parameters and functions, and on the algorithms used to minimize the errors. If an inappropriate term is introduced, then the depth of the local minimum may be such that it is not straightforward to remove the term. This highlights the importance of using the most up-to-date microstructural understanding to provide the starting conditions, and the most suitable statistical techniques to optimize the embrittlement correlations.

7.5 Implications of Using these Correlations

The extent of embrittlement in BWR surveillance samples and vessels will be under-predicted.

If there are not many data points within the U.S. LWR database which correspond to situations in which MNPs dominate the size of the $MF/DT_{30(MD)}$ term, then neither sNRC2006 nor RM-6(2)/RM-9 are describing hardening from these microstructural features. Extrapolation of correlations derived from the LWR database will not be able to characterize the onset of hardening from MNPs. This is important when considering the use of these correlations to predict behaviour at high fluences.

7.6 Possible Ways Forward

The BWR database has been expanded in recent years, and it has proved possible to optimize the parameters within sNRC2006 and RM-6(2) against this enlarged database. The BWR-optimized correlations are not, however, good fits to the PWR data in the LWR surveillance database. Since there is no evidence to suggest that BWRs and PWRs are intrinsically different, this indicates that it would be better overall to produce a new correlation for the combined BWR+PWR database without the biases observed in this report. The terms which it appears most useful to investigate are the flux and fluence dependences.

It is possible that a correlation which predicts both the low-and mid-fluence data well could identify where MNPs begin to affect embrittlement and, thus, be of more use at high fluences than the current correlations.

8 RECOMMENDATIONS

Based on the assessment of the current candidate embrittlement correlations describing the U.S. LWR database and additional BWR data, we recommend that modifications be made to improve the predictability of typical BWR data, while retaining the current good fit to PWR data. We recommend that a modification program should include:

- Consideration of the forms of the equations, with special reference to the location of the flux-dependence, and the form of the fluence-dependence;
- Consideration of Monte Carlo methods for fitting candidate functions;
- Examination of error norms to check for multiple minima and/or plateau regions;
- Consideration of the need for constraints on parameters (e.g. non-negative least squares);
- Consideration of methods of minimizing the influence of negative shift measurements.

9
REFERENCES

1. *Radiation Embrittlement of Reactor Vessel Materials, Regulatory Guide 1.99, Revision 2*, Office of Nuclear Regulatory Research, U.S. Nuclear Regulatory Commission, Washington, DC 1988.
2. ASTM E900-87(1994) Standard Guide for Predicting Neutron Radiation Damage to Reactor Vessel Materials, E 706 (IIF).
3. E. D. Eason, J. E. Wright and G. R. Odette, "Improved Embrittlement Correlations for Reactor Pressure Vessel Steels", NRC Report NUREG/CR-6551, pub. U.S. Nuclear Regulatory Commission, Washington, DC, USA (1998).
4. M. Kirk, C. Santos, E. Eason, J. Wright and G. R. Odette, "Updated Embrittlement Trend Curve for Reactor Pressure Vessel Steels" in *Transactions of the 17th International Conference on Structural Mechanics In Reactor Technology (SMiRT 17)*, held Prague, Czech Republic, August 2003 (2003).
5. W. Server, C. English, D. Naiman, and S. Rosinski, "Charpy Embrittlement Correlations – Status of Combined Mechanistic and Statistical Bases for U.S. Pressure Vessel Steels (MRP-45)". EPRI Report 1000705, published EPRI, Palo Alto, CA, USA (2001).
6. ASTM International "Standard Guide For Predicting Neutron Radiation Damage To Reactor Pressure Vessel Materials" E706 (IIF), E900-02, in *Annual Book of ASTM Standards*, pub. ASTM International (2002).
7. C. English, W. Server, and R. Lott, "Materials Reliability Program: Validation and Use of ASTM E 900-02 for Reactor Pressure Vessel Integrity (MRP-86)". EPRI Report 1003537, pub. EPRI, Palo Alto, CA, USA (2003).
8. R. G. Carter, T. J. Griesbach, and T. C. Hardin, "The BWRVIP Integrated Surveillance Program" presented at the 2004 ASME Pressure Vessels and Piping Conference, ASME, New York, to be published in 2004.
9. R. G. Carter, N. Soneda, K. Dohi, J. M. Hyde, C. A. English, and W. L. Server, "Microstructural Characterization of Irradiation-Induced Cu-enriched Clusters in Reactor Pressure Vessel Steels," Journal of Nuclear Materials, *298*, 211 (2001).
10. W. L. Server, R. G, Lott, S. T. Rosinski and C. A. English, "Recent Surveillance Data and a Revised Embrittlement Correlation", J. ASTM International, *2* (7) (July 2005).
11. R. Carter, W. Server, and C. English, "Predictions of Neutron Irradiation Embrittlement in BWR Vessel Steels," Proceedings of Fontevraud 6, France (2006).
12. W. Server and R. G. Carter, "BWR Surveillance Data and Predictions of Irradiation Embrittlement in BWR Vessel Steels: Assessment of Supplemental Surveillance Program Capsules. Interim Report". EPRI Report 1015506, Palo Alto, CA, USA (2007).

13. E. Eason, G. R. Odette, R. K. Nanstad and T. Yamamoto, "A Physically Based Correlation of Irradiation-Induced Transition Temperature Shifts for RPV Steels" ORNL Report ORNL/TM-2006/530 (November 2007).

14. M. EricksonKirk, "Technical Basis For Revision Of Regulatory Guide 1.99: NRC Guidance on Methods to Estimate the Effects of Radiation Embrittlement on the Charpy V-Notch Impact Toughness of Reactor Vessel Materials" Draft NUREG Report as of August 2007.

15. J.M.Hyde, C.A.English and W.J.Phythian, *Microstructural Characterization of RPV Steels – Phase 1*. EPRI Report TR-107535, CRIEPI T989601, December 1996.

16. J.M.Hyde, C.A.English and M.T.Hutchings, *Microstructural Characterization of RPV Steels – Phase 2: Evolution Of Matrix Damage.* EPRI Report TR-107965, CRIEPI T989701, March 1998.

17. J.M.Hyde, C.A.English, M.T.Hutchings and W.J.Phythian, *Microstructural Characterization Of RPV Steels – Summary Of Phases I and II and Program Plan for 1999-2004*. EPRI, Palo Alto, CA: 1998. TR-110086.

18. F.J.Loss, S.M.Graham, B.H.Menke and W.L.Server, *Fracture Toughness Characterization of Japanese Reactor Pressure Vessel Steels: Joint EPRI-CRIEPI RPV Embrittlement Studies.* EPRI Report TR-102409, CRIEPI T989203, May 1993.

19. T.Hardin, W.Server, R.Lott and J.Perock, *Evaluation of Capsule PWR5: EPRI-CRIEPI Integrated Reactor Vessel Surveillance Program (IRVSP) Capsule Irradiated in Davis Besse (PWRMRP-08).* EPRI, Palo Alto CA: 1999. TR-113891.

20. D.Bream, C.A.English, J.Hyde, J.Mace and R.Thomas, *Microstructural Characterization of RPV Steels – Series 3, Interim Report 1: Joint EPRI-CRIEPI RPV Embrittlement Studies (1999-2004).* EPRI, Palo Alto CA: 2000. 1001015 and CRIEPI, Tokyo, Japan: T00909.

21. C.A.English, R.G.Carter, N.Soneda, S.Ortner and W.L.Server, "A Review of Dose Rate Effects" in Proc. EPRI/CRIEPI Workshop on Dose Rate Effects In Reactor Pressure Vessel Materials held Squaw Creek, California, U.S.A. November 2001.

22. J.M.Hyde, "Further Analysis of Atom Probe Data" AEA Technology Report AEAT/R/NS/0639 Issue 2 April 2003.

23. R.M.Boothby, J.Carrol, M.T.Hutchings, T.L.Shaw and J.Hyde, "SANS Examination of BWR Irradiated RPV Steels" BNFL Report NSTS (03) 4520 December 2003.

24. S.Ortner and S.Dumbill, "FEGSTEM Analysis of BWR Irradiated RPV Steels" BNFL Report NSTS (04) 4927 May 2004.

25. S.R.Ortner, J.M.Hyde and C.A.English, *Microstructural Characterization of RPV Steels – Series 3, Interim Report 2: Joint EPRI-CRIEPI RPV Embrittlement Studies (1999-2004).* EPRI, Palo Alto, CA: 2002, 1003530, and CRIEPI, Tokyo, Japan: T980206, December 2002.

26. S.R.Ortner, *Microstructural Characterization of RPV Steels: Post-Irradiation Annealing Experiments: Joint EPRI-CRIEPI RPV Embrittlement Studies (1999-2004).* EPRI, Palo Alto CA: 2004. 1003531 and CRIEPI, Tokyo, Japan: Q980401.

27. J. T. Buswell and R. B. Jones, "The Modelling of Radiation Hardening and Embrittlement in Magnox Mild Steel Submerged-Arc Welds" in *Effects of Radiation on Materials: 16th International Symposium, ASTM STP 1175*, p424, 1994.

28. S. B. Fisher, J. E. Harbottle and N. Aldridge, "Radiation Hardening in Magnox Pressure Vessel Steels", Phil. Trans. Roy. Soc. Lond. A, 315, 301-332 (1985).

29. N. Soneda, K. Dohi, A. Nomoto, K. Nishida and S. Ishino, "Microstructural Analysis of RPV Materials and Development of Mechanism-Guided Embrittlement Correlation Method" in Proc Int. Symp. on *Research for Aging Management of Light Water Reactors* held October 2007, Fukui City, Japan.

30. E. A. Little and D. R. Harries, "Radiation-Hardening and Recovery in Mild Steels and the Effects of Interstitial Nitrogen", Metal Sci. J., *4*, 195-200 (1970).

31. G. R. Odette, E. V. Mader, G. E. Lucas, W. J. Phythian and C. A. English, "The Effect of Flux on the Irradiation Hardening of Pressure Vessel Steels" in *Effects of Radiation on Materials: 16th International Symposium, ASTM STP 1175*. Eds. D. S. Gelles, R. K. Nanstad, and E. A. Little, pub ASTM, Pennsylvania, USA 1993. p373.

32. C. A. English, R. G. Carter, N. Soneda, S. Ortner and W. L. Server, "A Review of Dose Rate Effects" in *Proc. EPRI/CRIEPI Workshop on Dose Rate Effects in Reactor Pressure Vessel Materials* held Squaw Creek, California, U.S.A. November 2001.

33. G. R. Odette, G. E. Lucas and D. Klingensmith, "Anomalous Hardening in Model Alloys and Steels Thermally Aged at 290°C and 350°C: Implications to Low Flux Irradiation Embrittlement", in *Effects of Radiation on Materials: 18th International Symposium, ASTM STP 1325*. Eds. R. K. Nanstad, M. L. Hamilton, F. A. Garner and A. S. Kumar, pub ASTM, Pennsylvania, USA 1996. p88.

34. G. R. Odette, T. Yamamoto and D. Klingensmith, "On the Effect of Dose Rate on Irradiation Hardening of RPV Steels", Philos. Mag., *85* (4-7) 779-797 (2005).

35. T. J. Williams and W. J. Phythian, "Electron Microscopy and Small Angle Neutron Scattering Study of Precipitation in Low Alloy Steel Submerged-Arc Welds" in *Effects of Radiation on Materials: 17th Int. Symp., ASTM STP 1270*. Eds. D. S. Gelles et al, pub. ASTM, West Conshohocken, USA (1996), pp191-205.

36. J. M. Hyde, D. E. Ellis, C. A. English and T. J. Williams, "Microstructural Evolution in High-Nickel Submerged Arc Welds" in *Effects of Radiation on Materials: 20th Int. Symp. ASTM STP 1405*. Eds. S.T.Rosinski et al pub ASTM, 2001.pp 262-288.

37. R. B. Jones and C. J. Bolton, "Neutron Radiation Embrittlement Studies in Support of Continued Operation, and Validation by Sampling of Magnox Reactor Steel Pressure Vessel and Components" in Proc 24th NRC Water Reactor Safety Meeting held October 1996.

38. P. Auger, P. Auger, S. Welzel and J.-C. Van Duysen, "Synthesis of Atom Probe Experiments on Irradiation-Induced Solute Segregation in French Ferritic Pressure Vessel Steels", J. Nuclear Mater., *280*, 331-344 (2000).

39. W. Server, C. A. English, D. Naimon and S. Rosinski, "Charpy Embrittlement Correlations – Status of Combined Mechanistic and Statistical Bases for U.S. RPV Steels – MRP-45" PWR Materials Reliability Program (PWRMRP). EPRI, Palo Alto, CA: 2001. 1000705.

40. R. J. McElroy and A. L. Lowe, "Irradiation Embrittlement Modelling of Linde 80 Weld Metals" in *Effects of Radiation on Materials: 17th Int. Symp., ASTM STP 1270*. Eds. D. S. Gelles et al, pub. ASTM, West Conshohocken, USA (1996), pp68-85.

41. M. Miller and M. G. Burke, "Fine-Scale Microstructural Characterisation of Pressure Vessel Steels and Related Materials Using APFIM", in *Effects of Radiation on Materials: 14th Int. Symp., ASTM STP 1064*. Eds. N. H. Packen, R. E. Stoller and A. S. Kumar, pub. ASTM, Philadelphia, USA (1990), pp 107-126.

42. R. B. Jones, and J. T. Buswell, "The Interactive Roles of Phophorus, Tin and Copper in the Irradiation Embrittlement of PWR Pressure Vessel Steels" in Proc. 3rd Int. Symp. on Environmental Degradation of Reactor Materials – Water Reactors, pub. Met. Soc. Inc., Warrendale, Pa, USA (1998), pp.111-120.

43. R. Chaouadi, "An Engineering Radiation Hardening Model for RPV Materials" SCK-CEN report R-4235 (September 2005).

44. R. J. McElroy, T. J. Williams, F. M. D. Boydon and B. Hemsworth, "Low Temperature Embrittlement of LWR RPV Support Structures", Int. J. Press. Vess. & Piping, *54*, 171-211 (1993).

45. K. C. Russell and L. M. Brown, "A Dispersion Strengthening Model Based on Differing Elastic Moduli Applied to the Iron-Copper System", Acta Metall., *20*, 969 (1972).

46. T. Harry and D. J. Bacon, "Computer Simulation of the Core Structure of the <111> Screw Dislocation in α-Iron Containing Copper Precipitates: I. Structure in the Matrix and a Precipitate", Acta Mater., 50, 195-208 (2002).

47. D. J. Bacon and Yu. Osetsky, "Hardening Due to Copper Precipitates in α-Iron Studied By Atomic-Scale Modelling", J. Nuclear Mater., 329-333, 1233-1237 (2004).

48. S. C. Glade, B. D. Wirth, G. R. Odette and P. Asoka-Kumar, "Positron Annihilation Spectroscopy and Small Angle Neutron Scattering Characterization of Nanostructural Features in High-Nickel Model Reactor Pressure Vessel Steels", J. Nuclear Materials, *377* (3), 409-528 (2008).

49. S. B. Fisher and J. T. Buswell, "A Model for PWR Pressure Vessel Embrittlement", Int. J. Press. Vess. Piping, *27*, 91-135 (1988).

50. T. J. Williams and D. Ellis, "A Mechanistically-Based Model of Irradiation Damage in Low Alloy Steel Submerged Arc Welds" in Effects of Radiation on Materials: 20th Int. Symp., ASTM STP 1405. Eds. S.T. Rosinski et al, pub. ASTM, West Conshohocken, USA (2001), pp8-27.

51. J. R. Hawthorne, "Significance of Selected Residual Elements to the Radiation Sensitivity of A302-B Steels," Nuclear Technology, 59, 440, 1982.

52. A. V. Barashev, "Segregation of Phosphorus Atoms to Grain Boundaries in Ferritic Steels Under Neutron Irradiation" Philos. Mag. Letters, *82* (6) 323-332 (2002).

53. E. A. Little and D. R. Harries, "The Correlation Of Radaition Hardening With Interstitial Nitrogen Content In Mild Steels", Metal Science J., 4, 195-200 (1970).

54. K. Dohi, N. Soneda, T. Onchi, S. Ishino, G. R. Odette and G. E. Lucas, Dose Rate Effect in Low-Copper Steels Irradiated in FNR in *Proc. EPRI/CRIEPI Workshop on Dose Rate Effects in Reactor Pressure Vessel Materials*, held Squaw Creek, CA, USA (November 2001).

55. R. B. Jones, J. T. Buswell and M. R. Wootton, "Assessment of Dose Rate Effects on the Mechanical Properties of Low-Copper C-Mn Steels" in *Proc. EPRI/CRIEPI Workshop on Dose Rate Effects in Reactor Pressure Vessel Materials*, held Squaw Creek, CA, USA (November 2001).

56. V. I. Badanin and V. A. Nikolaev, "The Effect of Alloying Elements on the Radiation Embrittlement of Ferritic-Pearlitic Steel Being Tempered", Physics of Metals and Metallography, *9*, 21-22 (1979). (Electricity Association Translation No 50/4967).

57. T. Takeyama, S. Ohnuki and H. Takahashi, "Effect of Neutron and Electron Irradiation on Low Manganese Steels", Transaction of the Japanese Iron and Steel Institute, *21*, 326-331 (1981).

58. M. Grounes, "Irradiation Effects in 2103/R3 Steel – Comparison Between Different Heats and Different Fabrication Procedures", Report S386 Aktiebolaget Atomenergi, Studsvik, Sweden 1968 (presented at ANS Annual Meeting, Toronto, Canada, June 9-13, 1968).

59. R. B. Jones, "Review of Irradiation Effects in Ferritic Alloy Steels" in International Atomic Energy Agency Technical Meeting on *Irradiation Effects and Mitigation In Reactor Pressure Vessel and Reactor Internals*, held Gus Khrustalny, Russia, May 2004.

60. W. S. Server, private communication May 2008.

61. R. Chaouadi, "Status Report on Radiation Damage Modelling of Reactor Pressure Vessel Steels" SCK-CEN report, R-3538 (June 2001).

62. R. Chaouadi and R. Gérard, "Copper Precipitation Hardening of Irradiated RPV Materials and Implications on the Superposition Law and Re-Irradiation Kinetics" J. Nuclear Mater., *345*, 65-74 (2005).

63. S. R. Ortner, C. A. English, A. Fellerman and W. L. Server, "BWR Embrittlement Correlation Studies" UK National Nuclear Laboratory Report NNL (08) 9105 Issue 1 (August 2008).

64. J. J. More, B. S. Garbow and K. E. Hillstrom, *User's Guide to Minpack I.*, Argonne National Laboratory publication ANL-80-74, 1980.

65. W. H. Press, W. T. Flannery, S. A. Teukolsky, and B. P. Vetterling, *Numerical Recipes in C*, Cambridge University Press, New York: 1992.

66. R. Gerard, private communication (IGRDM-14 P006) 2008.

67. P. Auger, P. Pareige, M. Akamatsu and J.-C Van Duysen, "Microstructural Characterisation of Atom Clusters in Irradiated Pressure Vessel Steels and Model Alloys", J. Nuclear Materials, *211* (3), 194-201 (1994).

A

APPENDIX: OCCURRENCE OF MN-NI-SI SOLUTE CLUSTERS

Mn-Ni-Si solute clusters have been observed directly using the Local Electrode Atom Probe (LEAP). Some of these observations have suggested that the clusters are more dilute than CRPs [38], and there is a possibility that the Mn-Ni-Si clusters are associated with dislocation loops. These observations might suggest that the clusters are closer to solute clouds around dislocations than actual precipitates. In this case, it would be hard to predict the additional hardening to be associated with the development of a substitutional solute cloud around MDs which are already associated with interstitial solutes. Other observations have, however, indicated that the Mn-Ni-Si solute clusters are no more dilute than CRPs [29]. In this case, the Mn-Ni-Si solute clusters would harden in a similar manner to CRPs, independent of the hardening provided by MDs. Under these circumstances, it is reasonable to refer to the Mn-Ni-Si solute clusters as MNPs. (Within the IVAR database, the features are analyzed predominantly by Small Angle Neutron Scattering (SANS) and Resistivity/Seebeck coefficient measurements (RSC), and thereby predetermined to be precipitates.) If, further, the growth of MNPs is controlled by vacancy diffusion, then the response of MNP hardening to flux and fluence will be similar to that of CRPs, and it is reasonable to use the effective fluence term.

Considering the IVAR data used to support the inclusion of the effective fluence term in the MF component of sNRC2006, a flux dependence of hardening in low-Cu steels is clearly visible when data from the high-Ni, high-Mn steel CM6 (0.02Cu, 1.68Ni, 1.50Mn, 0.05Cr, 0.54Mo, 0.007P, 0.15C, 0.17Si in wt.%), are examined, as shown in Figure A-1a. (The IVAR fluxes are given in units of 10^{12}n/cm^2-sec in the legends.[13])

In FigureA-1a, the high-flux data from CM6 definitely show slower hardening (w.r.t. fluence) than the low-flux data. It is even possible that the hardening of this model steel is following the tanh/peaking form expected for precipitation (rather than just solute cloud enhancement of the hardening of pre-existing MDs). This is in accordance with the expectation that the hardening is dominated by the precipitation of elements which diffuse substitutionally.

A similar flux effect may be seen in the medium-Ni, high-Mn, high-P model steels CM4 (0.02Cu, 0.86Ni, 1.53Mn, 0.05Cr, 0.55Mo, 0.031P, 0.16C, 0.16Si), and CM5 (0.02Cu, 0.86Ni, 1.61Mn, 0.04Cr, 0.53Mo, 0.035P, 0.15C, 0.16Si), as shown in Figure A-1b. In this Figure, the extent of the data scatter is illustrated by comparing the data from the two alloys. Equivalent data points from the slightly higher-P CM5 steel sometimes fall above those from CM4, and sometimes below them (and it is not obvious that this is strictly fluence-related). This

[13] For comparison, about one third of the TTS8-04 data were acquired at fluxes above 8x10^{10}n/cm^2-sec, and three points at fluxes above 8x10^{11}n/cm^2-sec.

interchangeability of the two sets of data suggests that, despite their slight differences in composition, the two steels could be treated as a single data set. If this is done, however, the flux effect is no longer apparent.

It is possible that there is still a flux effect on the hardening of the medium-Ni, high-Mn, low-P steels CM3 (0.02Cu, 0.85Ni, 1.60Mn, 0Cr, 0.49Mo, 0.006P, 0.13C, 0.16Si) and CM10 (0.02Cu, 0.88Ni, 1.66Mn, 0.05Cr, 0.53Mo, 0.008P, 0.16C, 0.17Si), as shown in Figure A-1c, but any effect is much less clear than in the high-Ni or high-P steels and, again, is completely lost if data from the two, similar steels are combined.

No flux effect is evident in the hardening of the medium-Ni, medium-Mn, low-P steel CM9 (0.02Cu, 0.86Ni, 0.85Mn, 0.04Cr, 0.55Mo, 0.003P, 0.15C, 0.15Si) shown in Figure A-1d.

Considering the IVAR data, then, it appears that the hardening in low-Cu steels is flux-dependent in the same way as in high-Cu steels if both the Mn and the Ni are high (~1.6wt.%) or, possibly, if both the Mn and P are high, when the Ni is at moderate (~0.85wt.%) levels. In medium-Mn, medium-Ni steels, there is no such flux dependence over the range of fluences shown.

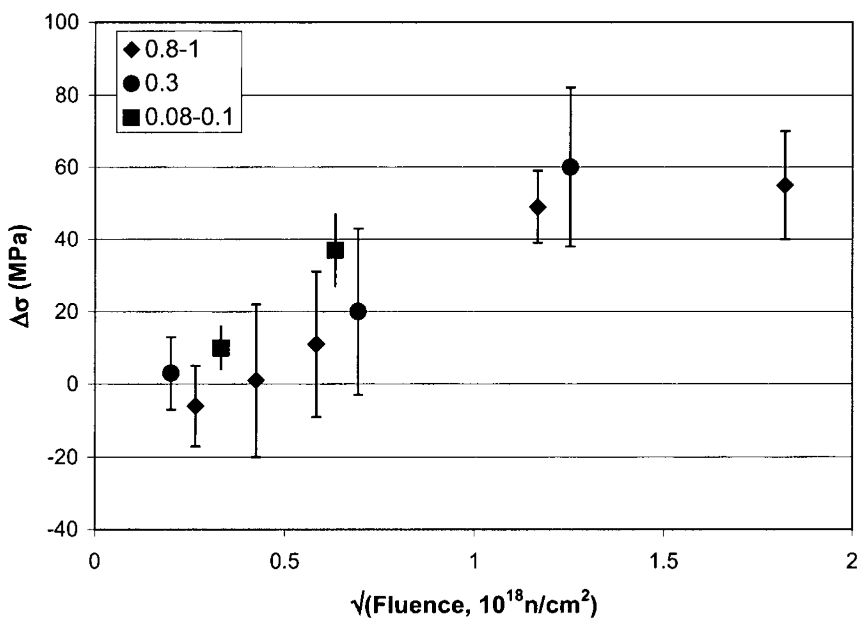

a) CM6 (1.68Ni, 1.86Mn, 0.007P)

Figure A-1
Effect of flux and fluence on the irradiation-induced yield stress increment in IVAR model steels a) high-Ni, high-Mn CM6, b) medium-Ni, high-Mn, high-P CM4 and CM5, c) medium-Ni, high-Mn, low-P CM3 and CM10, and d) medium-Ni, medium-Mn CM9

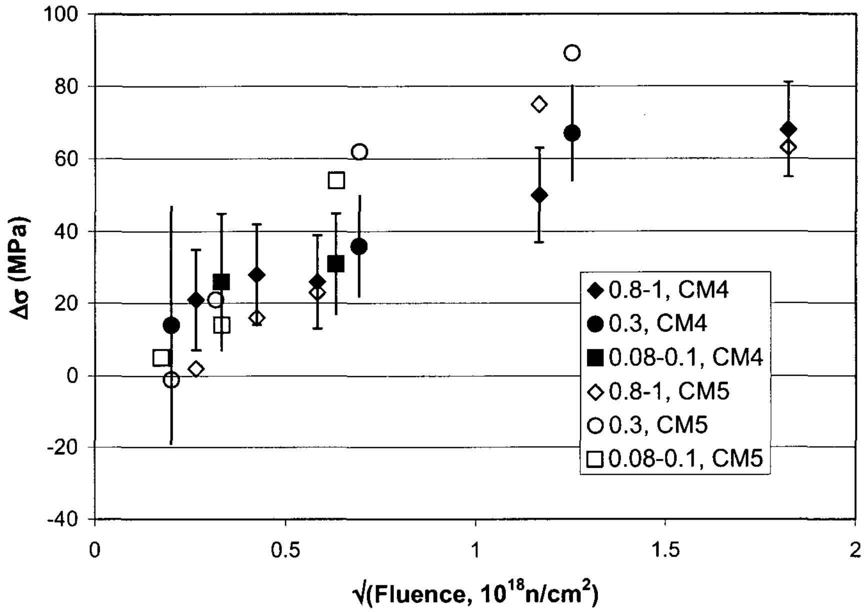

b) CM4 (0.86Ni, 1.53Mn, 0.031P) and CM5 (0.86Ni, 1.61Mn, 0.035P)

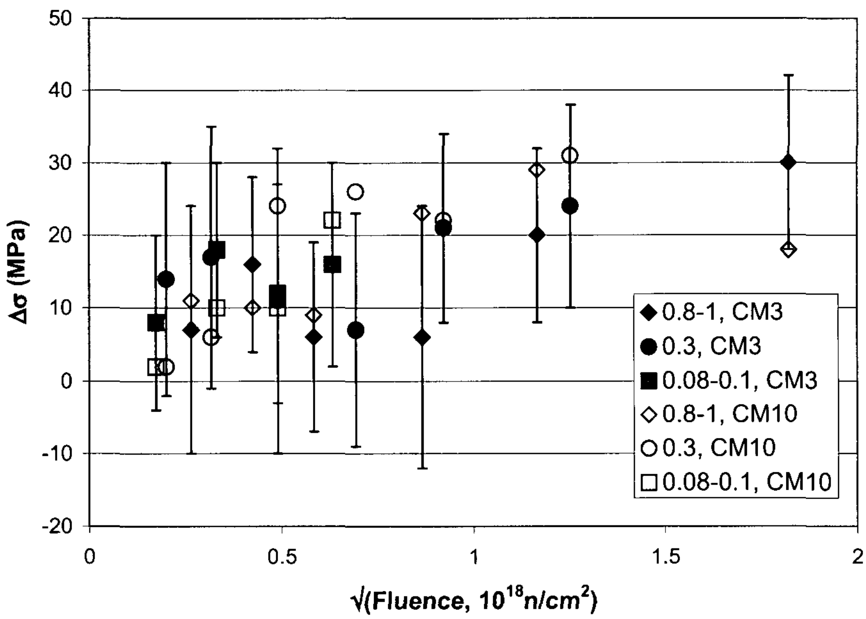

c) CM3 (0.85Ni, 1.6Mn, 0.006P) and CM10 (0.88Ni, 1.66Mn, 0.008P)

Figure A-1 (continued)
Effect of flux and fluence on the irradiation-induced yield stress increment in IVAR model steels a) high-Ni, high-Mn CM6, b) medium-Ni, high-Mn, high-P CM4 and CM5, c) medium-Ni, high-Mn, low-P CM3 and CM10, and d) medium-Ni, medium-Mn CM9 (continued)

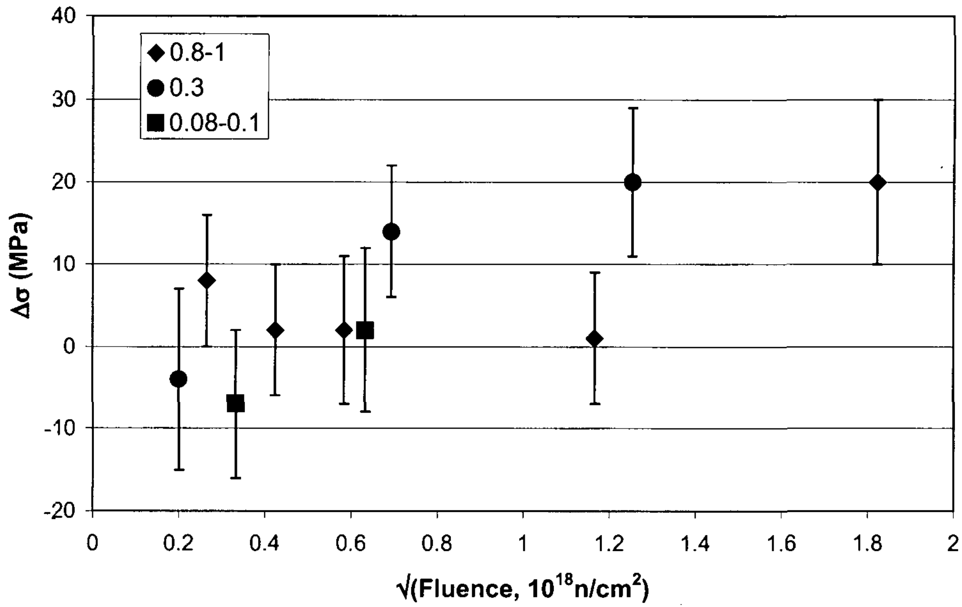

d) CM9 (0.86Ni, 0.85Mn, 0.003P)

Figure A-1 (continued)
Effect of flux and fluence on the irradiation-induced yield stress increment in IVAR model steels a) high-Ni, high-Mn CM6, b) medium-Ni, high-Mn, high-P CM4 and CM5, c) medium-Ni, high-Mn, low-P CM3 and CM10, and d) medium-Ni, medium-Mn CM9 (continued)

Figure A-2 shows the Mn and Ni levels of the steels within the LWR surveillance database, Figure A-2a shows that, within the low-Cu part of the database, there are no high-Ni, high-Mn points (in the sense of the definitions used in the IVAR data i.e. Mn and Ni>~1.6wt.%). There are a number of high-Mn specimens, with Ni levels close to the moderate IVAR level (Ni not far below 0.85wt.%), of which 3 points could fall into the high-P (P>0.01) range. There are more points in the database from steels which contain less Mn and Ni than those IVAR steels which showed no flux effect (Mn, Ni<0.85wt.%). Most surveillance data, however, fall in the composition range in which Mn is between 0.85-1.6wt.%, and Ni is <0.85wt.%, and it is unclear from the IVAR data whether hardening will be flux-dependent in this composition range. Overall, then, it does not appear that the IVAR database provides direct support for the MNP-dominance of the MF term in LWR surveillance data. It does, however, indicate that the possibility should be investigated.

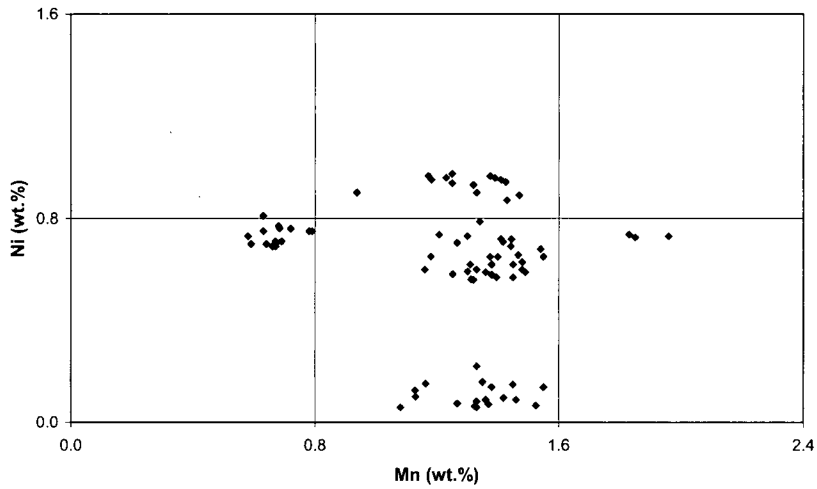

a) Samples with Cu<0.072wt.%

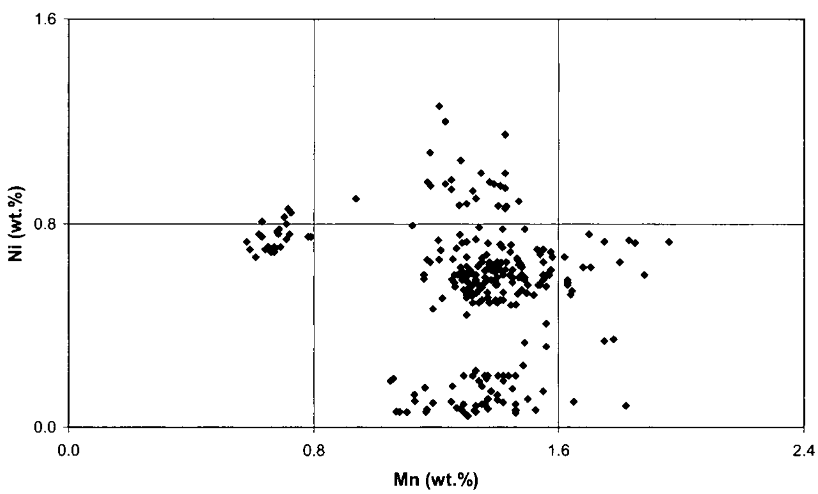

b) All Cu levels

Figure A-2
Levels of Mn and Ni found in LWR surveillance samples compared with requirements for MNP precipitation in thermally-aged Fe-Mn-Ni

The absence of evidence that hardening is dominated by MNP precipitation in the IVAR medium-Mn, medium-Ni steels may be due to energetic or kinetic effects. Possibly the levels of Mn and Ni are thermodynamically insufficient to cause precipitation at all. In this case, MNP precipitation will not be expected in the PWR or BWR surveillance samples. Under these circumstances, the lack of observation of precipitation of any kind in 0.05Cu-0.75Ni-1.43Mn-0.008P-0.28Si (wt. %) A533B plate irradiated for 25 years in a surveillance position in the Doel-4 reactor [66], or in 16MND5 (0.07Cu-0.74Ni-1.25Mn-0.24Si-0.008P) irradiated in Dampierre 2 for 9 years [67] would be explicable. Mn-Ni-Si precipitates were, however, observed in ferritic-bainitic 0.09Cu-0.57Ni-1.26Mn-0.32Si (wt.%) 16MND5 steel from the Chooz A surveillance scheme [67].

Ni-Mn-Si clusters have also been observed in a number of low-Cu (0.01-0.07wt.%) A533B plates and related welds containing around 0.6wt.% Ni irradiated to relatively high fluences and fluxes [29]. The bulk Mn levels for these steels are not always recorded but, if the steels are all A533B type, then the Mn is likely to be in the range 1.2-1.6wt.%.

From this small survey, about half of the low-Cu data points in TTS8-04R1 come from steels with Mn and Ni levels higher than those of steels in which Mn-Ni-Si clusters have been observed.

If it is assumed that the precipitation of MNPs is thermodynamically favored throughout the IVAR and LWR surveillance databases, then the absence of an obvious flux effect in Figure A-1c and Figure A-1d could be due to the slower rate of MNP precipitation in the lower-Mn, lower-Ni IVAR steels. A kinetic effect implies that there will be flux-fluence combinations under which Mn-Ni-Si clustering may be the dominant contributor to MF for medium-Ni-Mn RPV steels. This is investigated in Figure A-3.

Figure A-3 shows the fluences at which Mn-Ni-Si clusters were observed during atom probe analyses of A533B-type steels with Cu<0.072wt.%, and compares them with the fluxes and fluences of samples with Cu<0.072wt.% in the LWR surveillance database. The samples of Soneda et al [29] are described as having been irradiated at PWR or MTR fluxes. The data from these samples are plotted at nominal fluxes of 10^{10}n/cm^2-s, 10^{11}n/cm^2-s or 10^{13}n/cm^2-s, respectively. The solid points refer to LEAP analyses, while the open points refer to atom probe experiments using machines (e.g. OPoSAP) which measure smaller sample sizes and, therefore are less accurate in measuring low number densities of clusters. The two solid points marked as "low number density" refer to samples in which the number densities were $<10^{23}$m^{-3}, at which levels they could have been overlooked by non-LEAP measurements. (When CRPs are observed at these densities, they produce minimal hardening.)

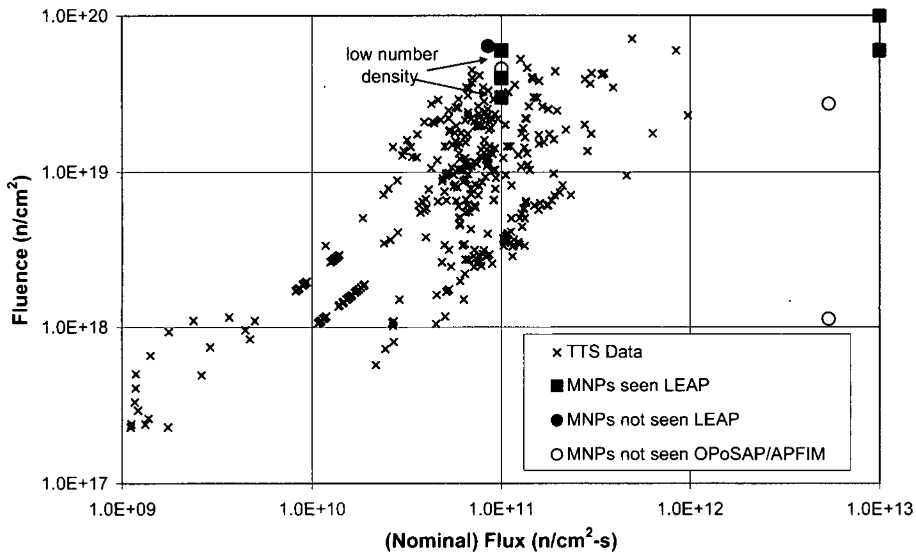

Figure A-3
Comparison between fluxes and fluences of the low-Cu samples in the LWR surveillance database, and the conditions under which Mn-Ni-Si clusters have/have not been observed in 0.6wt.%Ni A533B steels AP [29, 38, 66, 67]

Figure A-3 shows that, in low-Cu 0.6Ni MnMoNi steels MNPs are observed at high fluxes and fluences. There are ~15 surveillance data points with fluxes/fluences bounded by the conditions under which MNPs have definitely been seen.

To summarize:

1. If MNP formation is thermodynamically favored above ~0.6Ni, 1.2Mn (as indicated by steels in which MNPs have been observed), but not below these Ni and Mn levels, then about half of the low-Cu steels in the U.S. LWR surveillance database could not produce MNPs at any flux/fluence. The data from steels which could produce MNPs come from both BWR and PWR irradiations.

2. If MNP formation is thermodynamically possible in all of the low-Cu steels of the U.S. LWR surveillance database, regardless of their Mn and Ni contents (for which there is no experimental evidence either way), but only in the flux-fluence range bounded by the observations in Figure A-3, then

    a. MNPs may dominate MF embrittlement in some (~15) PWR surveillance samples,

    b. MNPs will not contribute to MF embrittlement in BWR surveillance samples.

3. If both the composition and flux/fluence requirements hold, then MNPs will contribute to MF embrittlement in 3-4 PWR surveillance samples.

If options 2/3 are correct, and MF embrittlement may be dominated by MNP precipitation, then a flux effect should be observed in the MF component of embrittlement of PWR samples, but not in that of BWR samples. In this context it is worth recalling that, during the development of sNRC2006, a flux effect was not observed when only the PWR data were used to form the correlation. It became necessary to introduce the effective flux terms only once the BWR data were included, and the effective fluence is identical with the measured fluence for most PWR surveillance samples. The likelihood that MNPs will be absent is thus greatest in that part of the database which sNRC2006 most requires their presence to explain the postulated flux dependence of matrix damage.

B

APPENDIX: EXAMPLES OF THE BEHAVIOR OF RESIDUALS IN RM-6(2)

This Appendix shows the effects observed using the residuals i.e. measured shift – shift predicted when they are plotted in terms of the measured transition temperature shift. Similar effects are observed with both expressions by EricksonKirk. Since the main body of the report concentrates on RM-9, this Appendix considers only the data from RM-6(2).

Figure B-1 shows the residuals associated with specimens from BWR and PWR surveillance schemes. There is no significant trend in the residuals for the PWR data, but there is a clear trend in the smaller number of BWR residuals. The predicted value of the irradiation-induced shift in the transition temperature is greater than the measured value at small shifts (<~20°C), but is progressively smaller than the measured value with increasing shift. At the highest measured shifts in BWR samples, the predicted shift is ~30°C lower than the average measured shift. Note that in this representation, it is not clear how many of the over-predictions at low DT are associated with negative measured shift. Thus although the apparent trend is clear, the significance of the trend is less easy to determine than when simple plots of predicted DT versus measured DT are used.

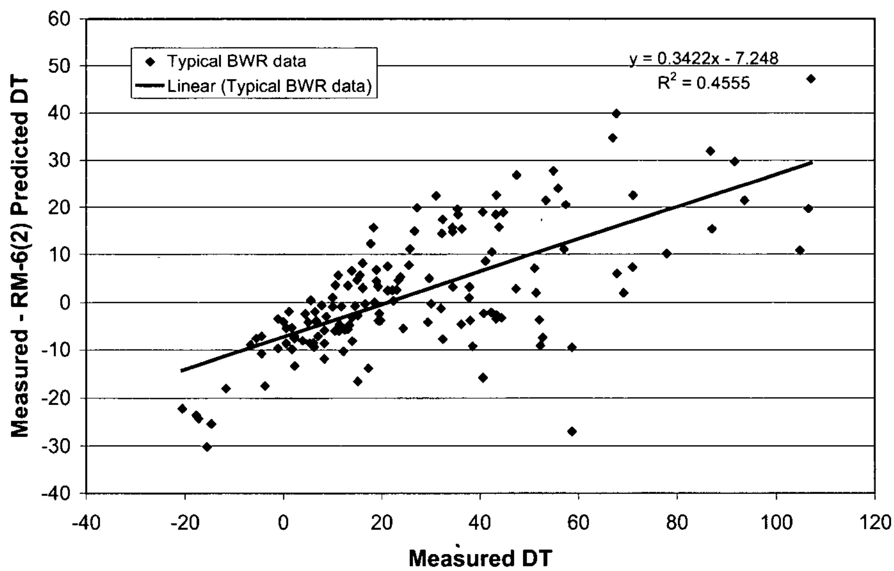

a) Typical BWRs

Figure B-1
Residuals (measured DT-prediction of DT by RM-6(2)) for BWR and PWR data

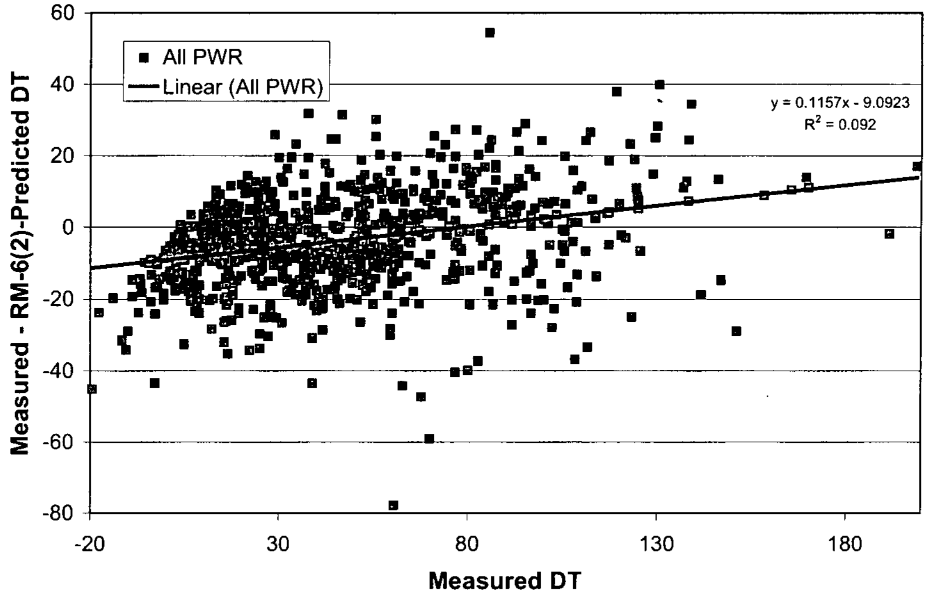

b) PWRs

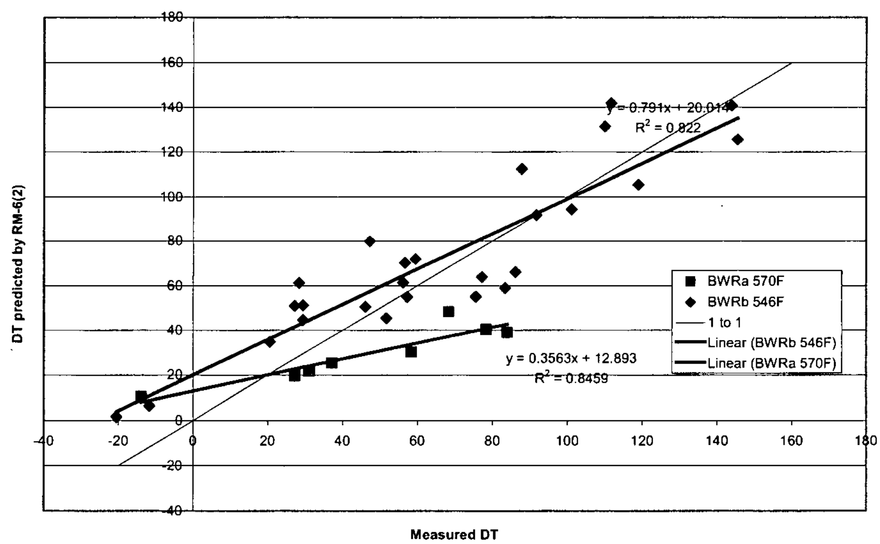

c) Atypical BWRs

Figure B-1 (continued)
Residuals (measured DT-prediction of DT by RM-6(2)) for BWR and PWR data (continued)

Despite the influence of the error distributions on the trend lines, it is clear that, for RM-6(2), as for RM-9 and sNRC2006, the typical BWR data do show under-predictions when the measured DT is above ~20°C. The situation is less clear for the PWR or BWRb data.

Examining this in more detail, Figure B-2 shows the trends in the residuals at different levels of the fluence function. At low fluences, as defined by $\Phi F_{MD}<0.25$, (Figure B-2a) there is a marked trend in the residuals. The best fit trend line indicates that over-predictions are associated with measured DT values of <~12°C, with under-predictions of increasing magnitude occurring at higher measured DT. Again, it is not simple to assess what significance to ascribe to the under-predictions because of the influence of the negative shifts. Even if all the points for measured DT<20°C are ignored, however (to limit the effect of DT values smaller than measurement uncertainties), the under-predictions at higher DT are clear. In this ΦF_{MD} range, most of the data points come from typical BWR surveillance samples.

The slope and significance of the best fit line are both slightly lower in the fluence range $0.25<\Phi F_{MD}<0.5$ (Figure B-2b). In this range, there are sufficient data from the different reactor types to show that the trends are similar in PWR and BWR surveillance data. The transition from possible over- to under-prediction occurs at ~20°C (PWR data) – 30°C (BWR data) in this ΦF_{MD} range. Excluding the DT<20°C data would lead to a trend line with lower slope than that shown, in Figure B-2b, and of lower slope than the equivalent fit to the $\Phi F<0.25$, DT<20°C data.

In the range $0.5<\Phi F_{MD}<0.75$ (Figure B-2c), there are too few BWR data to make comparisons between the reactor types, but the PWR trend is of similar slope and significance to that seen in the $0.25<\Phi F_{MD}<0.5$ range, though with a transition now at ~40°C.

At the highest fluence range $\Phi F_{MD}>0.75$ (Figure B-2d) the trend in the PWR residuals is much shallower, of weaker significance, and with a transition around 85°C. Excluding the points with DT<20°C would render the slope minimal. The atypical BWRa surveillance data points still show under-predictions in this range.

The differences between the different graphs in Figure B-2, explain why the trend in the residuals was so much clearer in the BWR data than in the PWR data of Figure B-1. The BWR data fall mostly in the $\Phi F_{MD}<0.5$ range, in which the trend is marked, while the PWR data lie mostly in the $\Phi F_{MD}>0.75$ range where the trend is weak. Mixing data from different ΦF_{MD} ranges, which have transitions from over-to under-prediction at different $DT_{measured}$ values, makes the trend more difficult to discern.

Further investigation of RM-6(2) shows that, as with RM-9 the bias is stronger in the $\Delta T_{30(MD)}$ component than in the $\Delta T_{30(CRP)}$ component, and stronger at low fluxes and fluences. The definition of low flux appears to be higher in the PWR samples than in the BWR samples. This is difficult to understand, but may be related to the deliberate reduction in the number of product forms used by EricksonKirk, and the different product form distributions in the two surveillance schemes.

In summary, the tendencies to under-prediction seen in RM-9 are also present in RM-6(2). Using the plots of residuals, it appears that the under-predictions occur only at high shifts, with over-predictions occurring at low shifts. This may be consistent with the assessment made in the main body of the report, that the fluence functions may not be optimal, and asymmetric functions should be considered. It is also likely, however, that the extent of the apparent over-predictions is strongly influenced by the distribution of uncertainties in the measurements – most particularly the negative measured shift. Even so, the conclusions reached from an assessment of the residuals during the early stages of this program [63] still hold. The flux effects are not optimal and it may be worthwhile to consider the use of an asymmetric fluence function.

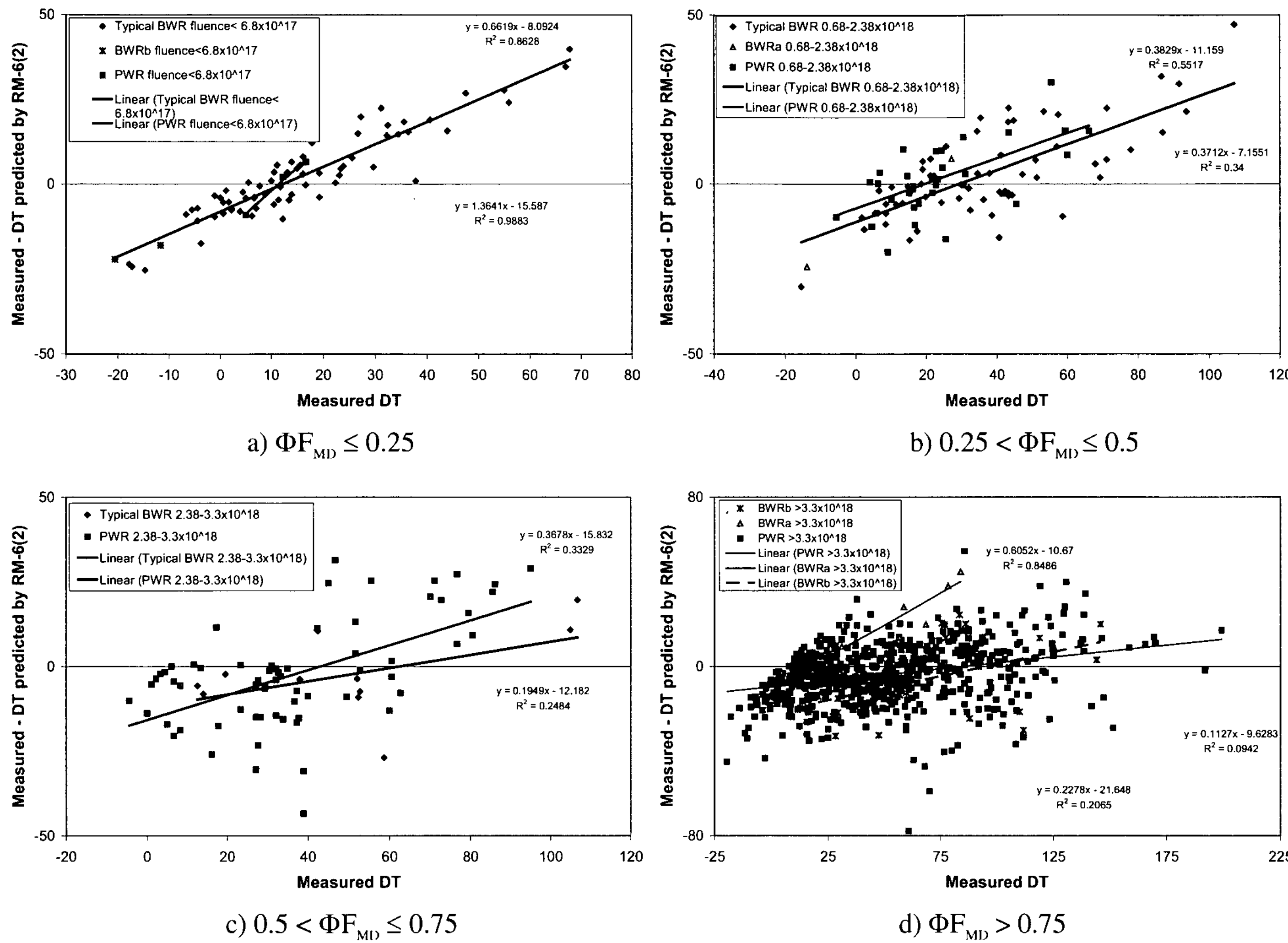

Figure B-2
RM-6(2) residuals in different fluence function ranges (Legends indicate fluence ranges in units of n/cm²)

The Electric Power Research Institute Inc., (EPRI, www.epri.com) conducts research and development relating to the generation, delivery and use of electricity for the benefit of the public. An independent, nonprofit organization, EPRI brings together its scientists and engineers as well as experts from academia and industry to help address challenges in electricity, including reliability, efficiency, health, safety and the environment. EPRI also provides technology, policy and economic analyses to drive long-range research and development planning, and supports research in emerging technologies. EPRI's members represent more than 90 percent of the electricity generated and delivered in the United States, and international participation extends to 40 countries. EPRI's principal offices and laboratories are located in Palo Alto, Calif.; Charlotte, N.C.; Knoxville, Tenn.; and Lenox, Mass.

Together...Shaping the Future of Electricity

Program:

BWRVIP

Printed on recycled paper in the United States of America

1019056

Electric Power Research Institute
3420 Hillview Avenue, Palo Alto, California 94304-1338 • PO Box 10412, Palo Alto, California 94303-0813 USA
800.313.3774 • 650.855.2121 • askepri@epri.com • www.epri.com